Think Energy

Rio Pipeline & Logistics 2025

Adobe Express

ibp
INSTITUTO BRASILEIRO DE PETRÓLEO, GÁS E BIOCOMBUSTÍVEIS

RIO PIPELINE & LOGISTICS

Think Energy

Rio Pipeline & Logistics 2025

Editora

I59 **Instituto Brasileiro de Petróleo e Gás e Biocombustíveis (IBP).**

Think Energy: Rio Pipeline & Logistics 2025 / Instituto Brasileiro de Petróleo e Gás e Biocombustíveis. – n. 4, (dez. 2025). – Rio de Janeiro: IBP, 2025.

23 p. : il. color. ; formato digital (PDF).

Publicação contínua a partir de 2025
Modo de acesso: https://www.ibp.org.br/hub-de-conhecimento/biblioteca/revista-think-energy/
Disponível apenas online em formato PDF

1. Petróleo – Transporte. 2 .Petróleo – Derivados - Transporte. 3. Energia - Transporte. 4. Oleodutos de petróleo. 4. Gasodutos. I. Instituto Brasileiro de Petróleo, Gás e Biocombustíveis. II. Título.

CDD: 338.5

Sumário

Editorial

Tendo em vista a evolução da atividade dutoviária ao longo dos anos, é possível observar marcos de grande relevância para o setor, desde os avanços em materiais e tecnologias de inspeção até o fortalecimento de uma cultura voltada à integridade, segurança, gestão de riscos e sustentabilidade. Dentro desse percurso, a Rio Pipeline & Logistics, a partir da sua primeira edição, sempre se destacou como um evento de grande relevância a nível internacional. Mais do que um congresso técnico, é um ponto de encontro que inspira, conecta e impulsiona a evolução do modal dutoviário.

Participar da Rio Pipeline, seja como palestrante, ouvinte, moderador ou colaborador em comissões técnicas, é estar inserido no centro do debate mais qualificado sobre o transporte dutoviário no Brasil e no mundo. Aqui, os desafios operacionais encontram soluções criativas, as experiências de campo se transformam em conhecimento compartilhado, e as inovações ganham espaço para florescer. A cada edição, a conferência reafirma o papel estratégico dos dutos como infraestrutura essencial para o desenvolvimento tecnológico, energético, econômico e social.

Em um momento em que o setor de óleo e gás enfrenta crescentes demandas por eficiência, descarbonização e segurança operacional, os dutos se consolidam como uma alternativa robusta e confiável de transporte. E é justamente nesse contexto que o Rio Pipeline se torna ainda mais relevante: como catalisador de avanços técnicos, como plataforma de networking qualificado e como ambiente de construção coletiva de soluções para o futuro.

Por trás da força do Rio Pipeline está o trabalho contínuo e articulador do Instituto Brasileiro de Petróleo, Gás e Biocombustíveis (IBP) em conjunto com a Comunidade Brasileira de Dutos. Com uma trajetória de mais de seis décadas, o IBP atua como elo entre operadores, fornecedores, academia, reguladores e sociedade, promovendo conhecimento técnico, defendendo boas práticas e estimulando a inovação. Através de seus comitês técnicos, grupos de trabalho e eventos, o IBP tem sido fundamental para a formação de consensos e para a elevação da maturidade técnica e regulatória do setor. Ao reunir especialistas de diferentes segmentos, o IBP fomenta o diálogo transparente, qualificado e construtivo — um ativo essencial para um setor que lida diariamente com riscos complexos, exigências técnicas elevadas e desafios geográficos e ambientais.

É com esse espírito que nasce a edição especial da Revista Think Energy, dedicada à Rio Pipeline & Logistics 2025.

Este projeto editorial foi concebido com um propósito claro: dar ampla divulgação aos trabalhos técnicos premiados e reconhecidos como destaque na conferência, os quais ilustram a força da inovação e da excelência técnica do setor. Cada artigo selecionado reflete não apenas a excelência do conteúdo apresentado na Rio Pipeline 2025, mas também o compromisso dos autores e avaliadores com o rigor técnico e com a construção de um setor cada vez mais seguro, eficiente e sustentável. Desta forma, buscamos com isto ampliar ainda mais o impacto do evento, permitindo que este conteúdo altamente relevante reverbere para além dos dias de congresso e alcancem profissionais em todo o país e no exterior.

Neste contexto, convido você, leitor, a fazer uma leitura crítica e reflexiva desta edição. Que os artigos aqui reunidos despertem novas ideias, questionamentos, colaborações e soluções. Que esta revista seja o ponto de partida para conversas que continuarão nos grupos técnicos das empresas operadoras e de prestadores de serviços, nos centros de operação, nas faixas de dutos, nas universidades, nos órgãos reguladores e nas futuras edições do nosso congresso.

Aproveito para agradecer calorosamente a todos os autores que submeteram seus trabalhos, aos avaliadores que dedicaram seu tempo e expertise na avaliação técnica dos artigos, e aos leitores que mantêm viva a chama do conhecimento aplicado.

Por fim, reforço o compromisso do IBP e da revista Think Energy com a missão de fortalecer continuamente o setor de dutos e contribuir para a evolução da indústria como um todo. Boa leitura. E que o conhecimento compartilhado aqui nos conduza a novos caminhos de excelência e inovação.

Douglas Thiago da Silva Alves

Engenheiro de Processamento na Petrobras, onde acumula quase 20 anos de experiência nas áreas de Gestão de Riscos Operacionais e Segurança de Processo. Graduado em Engenharia Química (UFMG), possui pós-graduações em Engenharia de Processamento de Óleo e Gás (UERJ), Análise e Gerenciamento de Riscos (UFRJ), e Engenharia de Dutos (Newcastle University-UK), além de mestrado (UFRJ) e doutorado (UFF) com ênfase nas áreas supracitadas. Atualmente, atua como Gerente Setorial de Monitoramento e Inspeção de Riscos Operacionais na Petrobras, é membro da Comissão de Dutos do IBP participando também da coordenação da Subcomissão de Riscos em Dutos, e integra o conselho fiscal da ABRISCO. Douglas também possui diversas publicações em periódicos nacionais e internacionais.

Entrevista

Alexandre Seewald, Chair Técnico da Rio Pipeline & Logistics 2025

Alexandre Seewald é Pipeline Integrity Advisor na Petrobras Transporte, com mais de 18 anos de experiência em dutos. Possui atuação prática em avaliações de integridade, análise de falhas, seleção de métodos de ensaios não destrutivos e técnicas de reparo. Tem forte background em hidráulica de dutos, testes hidrostáticos, classificação de localização e assistência em campo. É mestre em Engenharia Mecânica e, atualmente, está cursando doutorado na área de mecânica da fratura. Atua também como instrutor em treinamentos sobre trincas por corrosão sob tensão (stress corrosion cracking) e integra o comitê técnico da Rio Pipeline Conference, onde coordena o workshop bienal sobre SCC.

> ***Um dos grandes destaques desta edição é a transformação digital, tema que entrou pela primeira vez no temário oficial e atraiu um grande número de papers."***

O prestígio da Rio Pipeline & Logistics.

O grande diferencial da Rio Pipeline & Logistics está na colaboração entre três pilares fundamentais: a indústria, os institutos de pesquisa e as universidades. Essa integração garante a apresentação de trabalhos de altíssimo nível técnico e fortalece a credibilidade do congresso ao longo dos anos.

O papel do IBP.

O IBP tem um papel central na consolidação da Rio Pipeline & Logistics como referência internacional. A instituição atua de forma altamente profissional na organização do evento, cuidando de aspectos como divulgação, marketing e imagem. Além disso, o engajamento dos voluntários – que compõem comitês organizadores, técnicos e avaliadores de papers é considerado essencial para o sucesso contínuo do congresso.

O processo de curadoria e avaliação dos Papers.

O Comitê Técnico da Rio Pipeline & Logistics é formado por profissionais de diversas empresas e áreas. Eles coordenam a escolha dos avaliadores mais adequados para cada trabalho, garantindo rigor técnico e imparcialidade.

Nesta edição, foram mais de 300 trabalhos submetidos, avaliados em três etapas: uma triagem inicial, a avaliação completa e, em alguns casos, uma revisão final. Esse processo criterioso assegura a qualidade dos conteúdos apresentados e reforça a credibilidade dos anais do congressoHoje, estudos mostram que ainda falta cerca de 50% dos recursos tecnológicos necessários para atingir as metas globais de transição. Isso exige inovação, conhecimento e novas formas de pensar — e é isso que a juventude traz. Diferente das gerações mais antigas, que muitas vezes estão presas a modelos já ultrapassados, os jovens têm a capacidade de propor soluções disruptivas.

Perfil das submissões em 2025.

Um dos grandes destaques desta edição é a transformação digital, tema que entrou pela primeira vez no temário oficial e atraiu um grande número de papers. Outra novidade foi a possibilidade de os autores se inscreverem como jovens profissionais (até 35 anos), o que incentivou uma participação recorde desse público. Essa categoria conta, inclusive, com uma premiação exclusiva durante o evento.

A importância dos avaliadores

O trabalho dos avaliadores é fundamental para a qualidade do congresso. Em vez de recorrer a uma seleção automática, cada avaliador foi escolhido cuidadosamente de acordo com sua área de especialidade. Esse cuidado garante a consistência técnica dos artigos e reforça a credibilidade da Rio Pipeline & Logistics.

Tendências emergentes e inovação.

Embora temas tradicionais como: logística, centros de controle, integridade e dutos submarinos continuem fortes, a digitalização surgiu como a grande tendência desta edição. Muitos autores preferiram inscrever seus trabalhos em transformação digital, mesmo quando estavam ligados a áreas clássicas, mostrando o impacto da inovação tecnológica no setor. Além disso, houve espaço para novos temas, como os minerodutos, que atraíram bastante interesse.

Jovens profissionais e valorização da nova geração.

Pela primeira vez, o congresso terá uma categoria específica de papers voltada para jovens profissionais, com direito a premiação exclusiva. Essa iniciativa busca valorizar a nova geração e criar oportunidades de protagonismo para quem está iniciando a carreira.

> ***Em 2025, cerca de 20% dos trabalhos submetidos vieram do exterior, reforçando o caráter internacional do congresso."***

Legado e visão de futuro.

A Rio Pipeline & Logistics já se consolidou como um evento de excelência técnica e um ponto de encontro essencial para a comunidade de dutos, reunindo participantes do Brasil, da América Latina e de diversos países. Em 2025, cerca de 20% dos trabalhos submetidos vieram do exterior, reforçando o caráter internacional do congresso.

Uma inovação importante para esta edição é a tradução simultânea para o espanhol, ampliando ainda mais o alcance na região. E se o IBP continuar investindo em inovação e engajando voluntários, a Rio Pipeline & Logistics tem potencial para se consolidar como o maior congresso de dutos do mundo, ao lado de eventos consagrados como o PPIM (EUA), o IPC (Canadá) e o PTC (Alemanha).

> ***Mais de 300 trabalhos submetidos."***

Mensagem final.

Convido os profissionais de todas as áreas da cadeia dutoviária a participar ativamente da Rio Pipeline & Logistics 2025, não apenas visitando a feira, mas também acompanhando o congresso.

São mais de 300 papers apresentados, distribuídos em cerca de 30 sessões técnicas, workshops, comunicações especiais e plenárias, com palestrantes de referência em cada setor. Tenho certeza de que qualquer profissional encontrará conteúdos de alta qualidade e sairá do evento com muito mais conhecimento e conexões

Envato

Artigos Técnicos

Rio Pipeline & Logistics 2025

Assessing Splits in Pipeline Materials: Challenges and Implications for Fracture Toughness Evaluation

Sergio Luis Gonzalez Assias[1], Juan Elías Perez Ipiña[3], Hector Guillermo Kotik[2]

Abstract

The qualification of pipeline materials is defined by various construction and design codes, which, in part, rely on the experimental determination of fracture toughness through well-established standards such as ASTM, BS ISO, and JWE. During these tests, pop-ins have been observed in the load vs. displacement records as a consequence of delaminations perpendicular to the main crack plane, a phenomenon referred to as splits. Assessing this occurrence in fracture toughness evaluations poses challenges, as existing fracture mechanics standards lack specific procedures and criteria for their consideration. Consequently, materials may, in some cases, face unjustified rejection, leading to significant economic losses for manufacturers. Evidence suggests that splits may not always be critical in fracture toughness assessments. Therefore, this work explores the implications of evaluating splits in pipeline materials, addressing their potential impact on structural integrity, as well as unresolved questions and main issues.

Keywords: Delamination; Fracture toughness; Pipeline; Split.

[1] Universidade Federal do Rio de Janeiro. Brazil. E-mail: lorica@coppe.ufrj.br (https://orcid.org/0000-0002-7400-2119).

[3] Universidade Federal do Rio de Janeiro. Brazil. E-mail: juan.pipina@metalmat.ufrj.br (https://orcid.org/0000-0002-0934-477X).

[2] Universidade Federal do Rio de Janeiro. Brazil. E-mail: hectorkotik@metalmat.ufrj.br (https://orcid.org/0000-0003-4039-9645)

1 Introduction

Steels used in pipeline applications undergo rigorous qualification procedures established by standards and codes. These qualification requirements are designed to ensure the safe operation of pipelines by verifying that the materials exhibit high performance under operating conditions. Moreover, they are usually tested under even more severe conditions than those encountered in actual service.

One of the key aspects of material qualification is the determination of fracture toughness, as this verification is critical to prevent catastrophic fractures caused by crack extension [1]. Emphasis is placed on establishing minimum fracture toughness values at temperatures corresponding to the lowest operating one, as well as detecting the onset of brittle phenomena during testing. Given these requirements, materials must meet a minimum fracture toughness value, and those exhibiting significant brittle behavior should be avoided to ensure structural integrity.

Although well-established standards for determining the fracture toughness of metallic alloys have been published by various institutions worldwide, such as ASTM International [2], BS ISO [3], and JWES [4], these standards define procedures and methodologies for fracture toughness evaluation. However, characterizing fracture toughness in pipeline materials can be particularly challenging due to the occurrence of splits during testing.

Splits correspond to local delaminations that develop parallel to the surfaces and perpendicular to the main crack. It is important to note that delaminations also occur in other mechanical tests, such as tensile tests, Charpy V-notch tests, and Drop Weight Tear Test (DWTT) [5–7].

This phenomenon is triggered by a combination of factors, including high stress triaxiality, anisotropy in the mechanical properties of the material, and a specific range of temperature [6,8,9]. Delaminations have been observed in pipeline steels under various conditions, and this

susceptibility to delamination events in pipeline materials is closely linked to their metallurgical characteristics, which are influenced by thermomechanical and controlled thermomechanical processing techniques typically employed in their fabrication. In the case of ferritic steels, splits are particularly associated with crystallographic texture [10–12]. However, other metallurgical characteristics, such as elongated grain morphology, elongated non-metallic inclusions, centerline segregation, and banded microstructures, are also contributing factors to this phenomenon.

More specifically, splits result from the fracture of weak interphase regions within the material, as previously described. Thus, splits are typically observed in fracture mechanics specimens machined in T-L and L-T orientations [2], as illustrated in Figure 1.

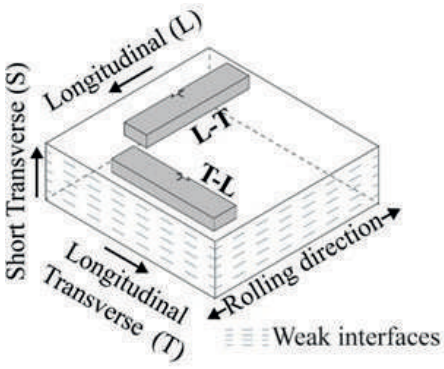

Figure 1 – SE(B) specimens in T-L and L-T orientation following the ASTM classification [13].
Source: Prepared by the authors (2025).

During fracture toughness testing, the occurrence of splits is observed as a pop-in, i.e., a sudden decrease in load (P) accompanied by an increase in displacement or crack mouth opening displacement (CMOD) record [8]. These pop-ins are caused by the brittle extension of the delamination perpendicular to the main crack, followed by its subsequent arrest [8,9].

As a brittle phenomenon, splits exhibit a stochastic nature. Figure 2 illustrates the occurrence of pop-ins in a P vs. CMOD record for a material exhibiting ductile behavior.

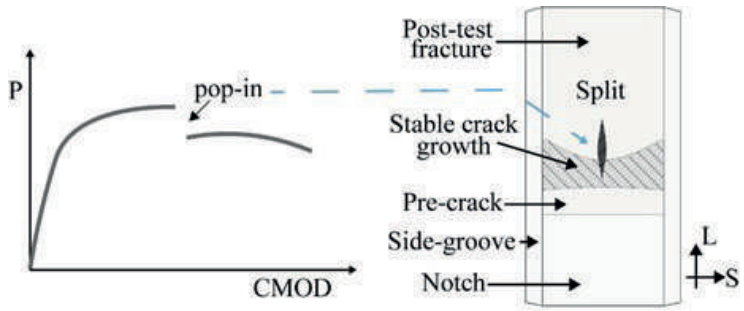

Figure 2 - Illustration of a pop-in caused by a split.
Source: Prepared by the authors (2025). Inspired in [14].

It should be noted that pop-ins can also result from crack extension within the plane of the main crack, a phenomenon commonly observed in local brittle zones (LBZs) of welded joints. These pop-ins are generated by local microstructures with low toughness, causing the crack to propagate brittlely when it reaches these brittle zones [1,8]. The crack is subsequently arrested upon encountering microstructures with higher toughness.

Although pop-ins caused by splits and those resulting from LBZs exhibit similar behavior, their origins are fundamentally different, as explained above.

For pop-ins caused by LBZs, standard methodologies and evaluation criteria are provided to assess their significance, primarily through parameter F, which is calculated as depicted

in Figure 3. This parameter and its associated criteria evaluate pop-ins caused by LBZs by analyzing compliance changes resulting from brittle crack extension within the plane of the main crack [3,4,15].

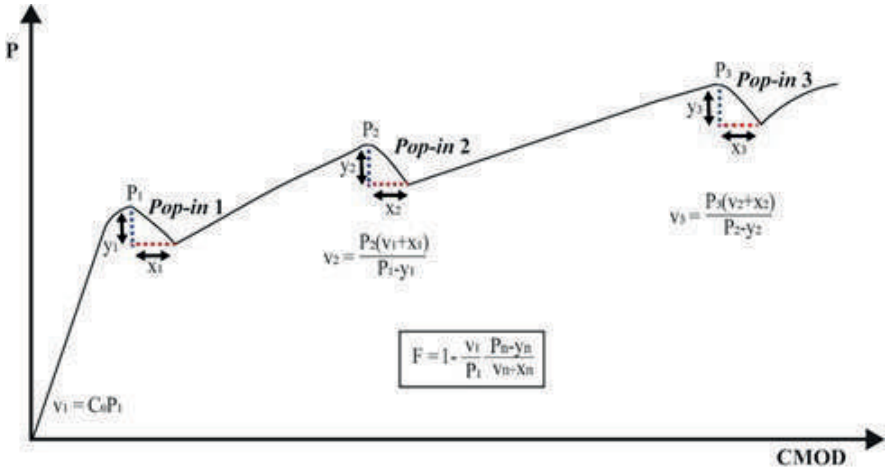

Figure 3 - Exaggerated pop-ins and illustration of the evaluation of F.
Source: Prepared by the authors (2025). Inspired in [2].

In contrast to pop-ins caused by LBZs, current fracture mechanics standards do not provide guidelines, recommendations, or methodologies for evaluating the significance of splits [16]. As a result, materials are often subjected to unjustified rejection due to the absence of standardized assessment criteria. Another commonly observed issue is the misclassification of pop-ins caused by LBZs as pop-ins resulting from splits.

Unjustified rejection of materials can lead to considerable economic losses, further emphasizing the need for standardized evaluation frameworks to ensure accurate material qualification.

Given this context, this study explores the treatment of splits in fracture toughness assessments of pipeline materials. The discussion is focused on the suitability of the assessment of split-induced pop-in through the methodology and criteria to assess LBZ pop-ins. To achieve this, both experimental and numerical approaches were implemented to demonstrate the effect of splits on specimen compliance.

2 Methodology

To analyze the effect of splits on specimen compliance, numerical simulations were conducted using the finite element method (FEM). A linear elastic finite element approach was employed, with side-grooved SE(B) specimen models developed using the commercial software package ABAQUS®. These models corresponded to stationary crack configurations.

The crack tip was modeled as a blunt tip with a radius of 2.5 μm, and the mesh was constructed using tetrahedral elements with four integration points (ABAQUS element C3D10). The specimen dimensions in the finite element model were W = 26.0 mm, B = 13.0 mm, and BN = 10.4 mm. Figure 4 illustrates the meshing and boundary conditions.

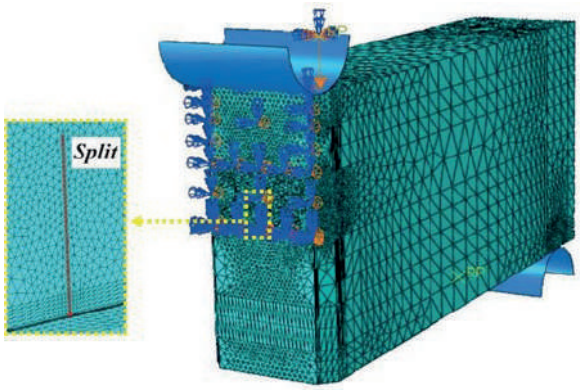

Figure 4 – Meshing and boundary conditions of FEM models.
Source: Prepared by the authors (2025).

In these models, splits were incorporated by removing elements corresponding to their volume. Splits were modeled as circular features, and three diameters (α) were studied: 2 mm, 4 mm, and 6 mm.

The compliance was extracted for each case from FEM results, and the compliance of models with and without splits were compared as follows:

$$\Delta C = \frac{C_{split} - C_{without\ split}}{C_{without\ split}} * 100\ [\%] \qquad (1)$$

In addition to numerical results, experimental data were also analyzed. The variation in compliance during fracture toughness testing was examined in fracture mechanics specimens that exhibited splits. These experimental results correspond to X70 and DH36 steel grades. The variation in specimen compliance between adjacent unloads was computed using Equation (2):

$$\Delta C_j = \frac{C_i - C_{i\text{-}1}}{C_{i\text{-}1}} * 100\ [\%] \qquad (2)$$

Where C_i correspond to the compliance value measured after the split pop-in and C_i–1 is the compliance value before. The specimen compliance was monitored during the fracture toughness tests by periodic and partial unload-reload cycles (unloading compliance technique).

3 Results

Figure 5a) compares compliance between models with and without splits for a/W ratios of 0.30, 0.50, and 0.65. The observed differences did not exceed 0.50%, regardless of the a/W ratio. Notably, no significant effect related to split size was identified.

On the other hand, Figure 5b) presents the experimental data obtained from eight specimens that exhibited splits during fracture toughness testing. The results indicate that the change in compliance before and after the pop-ins associated with splits did not exceed 5%.

In the experimental results, compliance variations of up to 5% were observed between successive unload–reload cycles in specimens without splits. These changes were attributed to the ductile crack extension behavior inherent to the ductile crack extension exhibited by tested materials and were not directly linked to split-related events. As such, the 5% variation was adopted as a reference threshold to distinguish substantial compliance shifts attributable to the presence of splits.

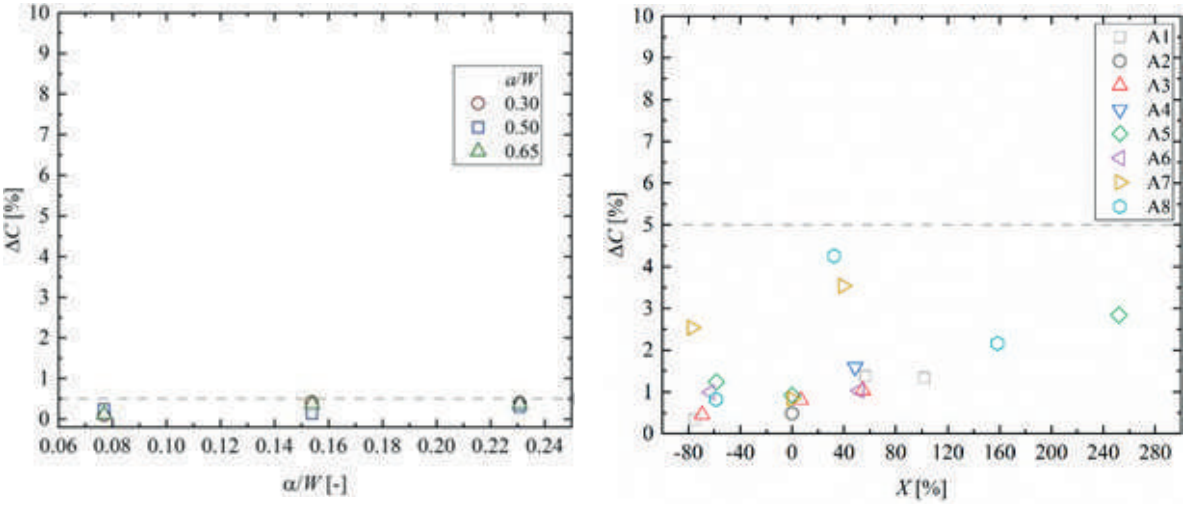

a) b)

Figure 3 - Results of a) specimen compliance change obtained by numerical simulation and b) compliance changes obtained by experimental test.
Source: Prepared by the authors (2025).

X corresponds to the point of occurrence of the splits respect to maximum load (Pmax) in the P vs. CMOD record:

$$x = \frac{CMOD_{split} - CMOD_{\mathrm{Pmax}}}{CMOD_{\mathrm{Pmax}}} * 100\ [\%]$$

In light of the established threshold, the compliance variations depicted in Figure 5b) were considered not substantial, regardless of their occurrence relative to the maximum load or the split size. These events were classified using the X parameter, where negative X values indicate pop-ins occurring before maximum load, X = 0 corresponds to those arising at the maximum load, and positive X values represent pop-ins observed after the maximum load.

4 Discussion

Numerical results (see Figure 5a)) indicate that splits do not cause a considerable change in specimen compliance. This finding can be explained by the fact that delaminations perpendicular to the main crack do not induce crack extension within the main crack plane.

Notably, the simulations allow for the isolation of the effect of splits on specimen compliance, considering only the occurrence of delamination itself. This approach eliminates additional influences such as increased plastic deformation or ductile crack extension, which are commonly observed in experimental results.

Experimental results in Figure 5b) demonstrate changes in specimen compliance, computed from unloads adjacent to pop-ins caused by splits, remaining below 5%. As previously mentioned, these changes were deemed not substantial when compared to compliance variations in cases where split occurrence was absent.

The small compliance changes observed were attributed to ductile crack extension in the main crack plane. Thus, both numerical and experimental findings agree, indicating that splits do not cause an instantaneous change in specimen compliance. Therefore, the causes of pop-ins associated with split events require further investigation.

For a detailed discussion on the effect of splits and their characteristics on specimen compliance, readers are referred to [17].

The fact that splits form completely perpendicular to the main crack highlights a fundamental contradiction in applying standard pop-in treatment for LBZs to split-induced pop-ins. Figure 6 illustrates the geometric foundation of the methodology used to determine parameter F, which is based on the principle of triangle similarity. This approach is intended to indirectly evaluate changes in specimen compliance resulting from brittle extension within the main crack plane. Similarly, the limit value is generally defined to restrict crack extension to approximately 5% of the initial ligament.

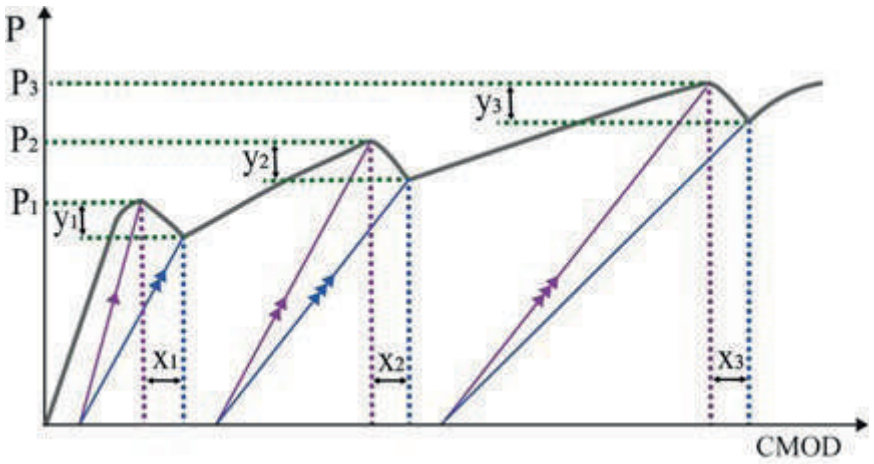

Figure 6 - Determination of parameter F.
Source: Prepared by the authors (2025). Inspired in [2].

However, since splits do not induce any extension of the main crack, as evidenced by the lack of increase in specimen compliance, applying the same evaluation criteria to split-induced pop-ins as those used for LBZ-related pop-ins may lead to misinterpretations of specimen behavior and inaccurate assessments of fracture toughness.

Consequently, split-induced pop-ins should not be treated as LBZ-induced splits. This distinction underscores the need for a revised evaluation approach specifically tailored to splits.

At this stage, it is important to note that a tendency to confuse split events with LBZ has been identified, primarily due to the similarity in their associated pop-ins. One of the key challenges lies in the need for fractographic examination to reliably determine the origin of each pop-in, making routine interpretation difficult during standard testing directly from P vs. CMOD record. However, the most prominent issue in evaluating the fracture toughness of materials exhibiting splits is the absence of standardized criteria or established guidelines to assess the significance and influence of this phenomenon, which complicates the interpretation of test results.

5 Conclusion

From a theoretical perspective, the criteria and methodologies used to evaluate pop-ins caused by LBZs cannot be directly applied to splits. This distinction arises from fundamental differences in their mechanisms: splits correspond to local delaminations that form perpendicular to the main crack and do not induce compliance changes, whereas LBZ-related pop-ins result from a brittle fracture within the crack plane, leading to measurable compliance variations.

To reliably evaluate the fracture toughness of metallic materials exhibiting splits, it is essential to establish specific criteria or recommendations for determining the significance of pop-ins caused by delamination phenomena. For this purpose, existing experimental methodologies and analytical frameworks must be critically validated for fracture specimens that present splits. Furthermore, the mechanical implications of such delaminations on the structural integrity of load-bearing components under specific operational conditions must be thoroughly understood to ensure safe and consistent application in engineering assessments.

6 Acknowledgments

This study was financed in part by the Coordination for the Improvement of Higher Education Personnel (Coordenação de Aperfeiçoamento de Pessoal de Nível Superior – CAPES) - Finance Code 001, Brazil, National Council for Scientific and Technological Development (Conselho Nacional de Desenvolvimento Científico e Tecnológico – CNPq), Brazil, the Carlos Chagas Filho Foundation for Research Support of the State of Rio de Janeiro (Fundação Carlos Chagas Filho de Amparo à Pesquisa do Estado do Rio de Janeiro – FAPERJ), Brazil, and the National Scientific and Technical Research Council (CONICET), Argentina.

Agradecimentos ao Programa de Recursos Humanos da Agência Nacional do Petróleo, Gás Natural e Biocombustíveis – PRH-ANP 7.1 (Resolução ANP nº 50/2015) pelo suporte financeiro para execução deste estudo.

List of Symbols and Abbreviations

$\boldsymbol{C_i}$ compliance measurement after split occurrence. $\boldsymbol{C_{i-1}}$ compliance measurement before split occurrence. $\boldsymbol{C_{split}}$ compliance in FEM models with splits. $\boldsymbol{C_{without\ split}}$ compliance in FEM models without splits. $\Delta\boldsymbol{C_j}$ experimental variation of compliance. a crack length. B specimen thickness. BN effective specimen thickness. BS British Standard. CMOD Crack Mouth Opening

Displacement. DWTT Drop Weight Tear Test. FEM Finite Element Method. ISO International Organization for Standardization. JWES Japan Welding Engineering Society. L Longitudinal direction. LBZ Local Brittle Zone. P Load. S Short Transverse Direction. SE(B) three-point bending geometry specimen. T Traverse direction. v1 elastic displacement at the first pop-in. vn elastic displacement at the nth pop-in. W specimen wide. xn the CMOD increase associated with the nth pop-in. yn the load drop associated with the nth pop-in. $\boldsymbol{F}$ parameter to evaluate pop-ins caused by LBZ. $\boldsymbol{X}$ location of split pop-in relative to maximum load. $\boldsymbol{\alpha}$ diameter of split in the FEM models.

Referências

[1] Anderson, T. L. (2017). Fracture mechanics: fundamentals and applications (4th Ed.). CRC Press.

[2] ASTM International. (2025). E1820-25 Test Method for Measurement of Fracture Toughness. ASTM International. https://doi.org/10.1520/E1820-25

[3] The British Standards Institution. (2021). BS ISO 12135:2021 Metallic materials. Unified method of test for the determination of quasistatic fracture toughness. BSI Standards Limited.

[4] The Japan Welding Engineering Society. (2016). WES 1108:2016 Standard test method for crack-tip opening displacement fracture toughness measurement.

[5] ASM International. Handbook Committee. (2000). ASM Handbook Mechanical testing and evaluation (Vol. 8).

[6] Arnoult, X. C., Růžičková, M., & Kunzová, K. (2016). Short review: Potential impact of delamination cracks on fracture toughness of structural materials. Frattura Ed Integrità Strutturale, 35, 509–522. https://doi.org/10.3221/IGF-ESIS.35.57

[7] Fang, J., Zhang, J., & Wang, L. (2014). Evaluation of cracking behavior and critical CTOA values of pipeline steel from DWTT specimens. Engineering Fracture Mechanics, 124–125, 18–29. https://doi.org/10.1016/j.engfracmech.2014.04.031

[8] Perez Ipiña, J., & Korin, I. (2012). Effects of divider orientation split-out on fracture toughness. Fatigue and Fracture of Engineering Materials and Structures, 36(3), 1–12. https://doi.org/10.1111/j.1460-2695.2012.01717.x

[9] González Assías, S. L., Kotik, H. G., & Perez Ipiña, J. E. (2022). Evolution of the geometrical and morphological characteristics of splits during fracture toughness test. Theoretical and Applied Fracture Mechanics, 117. https://doi.org/10.1016/j.tafmec.2021.103179

[10] Faria Conde, F., Cavalcanti Pinto, H., Masoumi, M., & Arnaldo Avila, J. (2020). Effect of Textures and Microstructures on the Occurrence of Delamination during and after Fracture Toughness Tests of API X80 Steel Plates. In Strength of Materials. IntechOpen. https://doi.org/10.5772/intechopen.88001

[11] Joo, M. S., Suh, D.-W., Bae, J. H., & Bhadeshia, H. K. D. H. (2012). Role of delamination and crystallography on anisotropy of Charpy toughness in API-X80 steel. Materials Science and Engineering A, 546, 314–322. https://doi.org/10.1016/j.msea.2012.03.079

[12] Yang, X. L., Xu, Y. B., Tan, X. D., & Wu, D. (2014). Influences of crystallography and delamination on anisotropy of Charpy impact toughness in API X100 pipeline steel. Materials Science and Engineering: A, 607, 53–62. https://doi.org/10.1016/j.msea.2014.03.121

[13] ASTM International. (2020). E1823-20b Standard Terminology Relating to Fatigue and Fracture Testing (Issue Reapproved). ASTM International. https://doi.org/10.1520/E1823-20B.2

[14] ASTM International. (2023). E1820-23b Standard Test Method for Measurement of Fracture Toughness. https://doi.org/10.1520/E1820-23B

[15] Gonzalez Assias, S. L., Kotik, H. G., & Perez Ipiña, J. E. (2023). Pop-ins by splits in pipeline materials, what do the codes and standards say about their assessment? Rio Pipeline Conference & Exhibition 2023. https://doi.org/10.48072/2447-2069.rpc.2023

[16] Gonzalez Assias, S. L., Kotik, H. G., Perez Ipiña, J. E., & Paredes, M. (2025). Experimental and numerical study of the effect of splits on specimen compliance and Δa results. Engineering Fracture Mechanics, 318. https://doi.org/10.1016/j.engfracmech.2025.110970

Computational Simulation Study for Strategic Replacement of In-Line Chromatographs

Caroline dos Reis[1], Marianna Unes Richa[3], Mauricio Casado[4], Barbara Carlos Bassane[2]

Abstract

SAQGAS – Natural Gas Allocation and Quality System is a software developed by the NTS Operations team and has multiple functionalities based on tracking the gas molecule through the gas pipeline network, under operational conditions. The main functionalities are: definition of the chemical composition of the gas delivered to exit points that do not have chromatograph, identification of chromatographic and flow meter errors by comparing measured and calculated data, calculation of the energy linepack in the pipeline segments for energy balance of the network. In view of the review of ANP Resolution No. 16/2008 - Natural Gas Specification in the year 2024, which governs the obligations that Shippers and TSO have with respect to Natural Gas Quality, an opportunity was found to request the use of computer simulation to indicate the chemical composition at delivery points instead of the current mandatory use of in-line chromatographs, depending on the operational condition. The maintenance cost of chromatographs is high and the results of computer simulation have shown to be extremely adherent to the values measured by chemical analysis equipment in the field. With the aim of optimizing the Operation, reducing maintenance costs and generating a milestone for the Brazilian gas market, this article explains the methodology used in the system, offers benchmark data on the use of computational simulation for this purpose and breaks down the simulation results.

Keywords: Chromatography; Energy; Computational Simulation; Gas; New Market.

[1] NOVA TRANSPORTADORA DO SUDESTE. Brazil. E-mail: caroline.reis@ntsbrasil.com.

[3] NOVA TRANSPORTADORA DO SUDESTE. Brazil. E-mail: marianna.richa@ntsbrasil.com (https://orcid.org/0000-0002-5309-2610).

4 NOVA TRANSPORTADORA DO SUDESTE. Brazil. E-mail: mauricio.casado@ntsbrasil.com (https://orcid.org/0000-0003-2370-5567).

[2] NOVA TRANSPORTADORA DO SUDESTE. Brazil. E-mail: barbara.bassane@ntsbrasil.com (https://orcid.org/0009-0005-6234-4727)

1 Introduction

SAQGÁS, a computational simulation software developed by the NTS Operations team, was initially implemented with the purpose of defining the physical route of the gas molecule. However, with the liberalization proposed by the New Gas Market program and the resulting changes—which led to greater complexity in commercial and operational processes—new applications were envisioned. Among them are the determination of the Gross Calorific Value (GCV) and the chemical composition of the gas delivered at the delivery points, the identification of measurement errors by comparing the results measured by field-installed equipment with those calculated by the software, and the calculation of energy inventory for each segment of the transportation network.

In Brazil, the application of pipeline simulation tools using computational models is widely used, serving as an important tool for decision-making in logistics, operations, and contingency planning, while also providing the speed and accuracy required by Operations departments.

In contrast, the European market, besides the applications mentioned above, already allows the use of simulation software to define the energy delivered to gas distribution networks. One example is Open Grid Europe (OGE), one of the leading gas transmission system operators in Europe, which has validated, with its Regulatory Authority, the use of computational simulation as a substitute for conventional gas quality measurement equipment.

Regarding to regulations on Natural Gas Quality focus in custody transfer systems in Brazil, the draft of the Joint Resolution ANP/Inmetro No. 1 of 2022 points toward the mandatory use of online chromatographs, depending on the maximum design flow rate category of the measurement system.

However, aiming to transform the gas sector by promoting the use of computational simulation models beyond operational routines, seeking international market benchmarks, and considering the current review of ANP Resolution No. 16 of 2008, the NTS Operations team presents the latest results obtained through the use of SAQGÁS in determining the Gross Calorific Value (GCV) of gas and its potential as a study tool to support the suggested flexibility in the current regulation.

2 Methodology

The mathematical methodology underlying SAQGÁS is divided into two main steps: (1) calculation of the intermediate flow rates of the pipeline segments and (2) Determination of the proportion of gas from each origin (entry, or supply, points into the network) for each exit, or delivery, point by tracking the gas flow.

The calculation of the intermediate flow rates of the network is based on the "node" system. Components such as valves, delivery and receipt points, compressors, measurement stations, or any point where there is a branching allowing more than one possible path for the gas to flow, are incorporated into the system as "nodes." After that, segments are created by linking two nodes. Figure 1 shows the flowchart for a specific pipeline section.

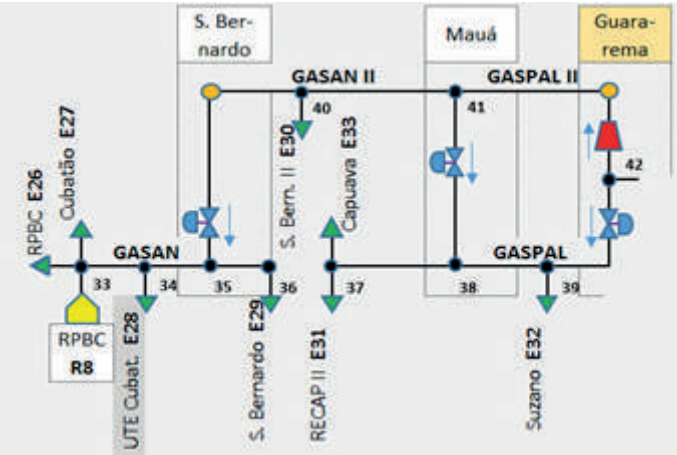

Figure 1 - Flowchart: node and segments
Source: Prepared by the authors (2025)

2.1. Mathematical equations used for calculating the intermediate flow rates of the system:

In order to solve the node and segment equations, the mathematical concept of a system of linear equations is used. The equations are divided into two categories: "node equations" and "segment equations" (Figure 2).

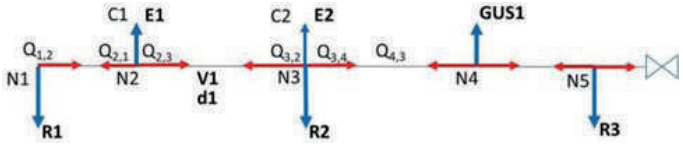

Figure 2 - Schematic for the foundation of the main equations.
Source: Prepared by the authors (2025).

Where:
N: Node; R: Receipt Flow (Volume received during the considered period); E: Delivery Flow (Volume delivered during the considered period); Q: Intermediate Flow to be calculated; V: Volume contained in the segment between two nodes (Segment inventory); d: Imbalance (variation of the inventory in the segment); GUS: Gas for System Use.

Node Equation - The sum of all inputs is equal to the sum of all gas outflows from the node (Equation 1). Since the node neither expands nor collapses, the sum of the total input volume and the total output volume from the node will result in zero, which will always be true.

$$R1 + Q1,2 = 0 \quad (1)$$

Segment Equation - Considering Q1,2 (flow from node 1 to node 2) and the arrow Q2,1 (flow from node 2 to node 1), it is inferred that the sum of Q1,2 and Q2,1 refers to the imbalance (inventory variation between two periods), as shown in Equation 2. It is necessary to consider the compressibility factor of natural gas and its specific physicochemical characteristics.

$$Q1,2 + Q2,1 = 0 \quad (2)$$

The system currently has more than 350 nodes registered, 354 segments which, interconnected, receive 434 gas flows or internal flow rates to be calculated. The NTS network contains configurated on the system has 10 Receipt Points and 47 delivery points.

2.2. Determination of the gas origins for each delivery point in the network through composition tracking of the molecule:

By solving the previously explained system of linear equations, it becomes possible to determine the origin for each delivery point in the network, meaning that the chemical composition delivered to each customer can be simulated.

The value of the chemical composition delivered at the delivery points is represented as a matrix containing vectors with values for each compound in each vector. For the Entry Points R1, R2, and R3 are transformed into the [R1, R2, R3] matrix.

Considering the calculated flow rates indicating the directions of the gas flow, a pipeline section is represented in Figure 3.

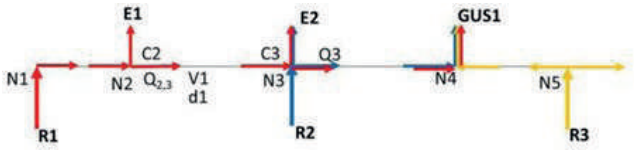

Figure 3 - Flowchart of the mixture inside the pipeline.
Source: Prepared by the authors (2025).

Taking as an example the section between nodes N2 and N3, knowing the value of Q2,3 and the direction of the flow, it is possible to determine the transit time between nodes (Equation 3), that is, the time required for the gas to travel the N2-N3 segment:

$$T = V1/Q2,3 \quad (3)$$

For example, if V1 = 1000 m³ and the flow rate Q2,3 = 200 m³/h, the time for the gas to travel the N2-N3 segment, at the operational working pressure, will be 5 hours. The determination of the chemical composition C = [R1; R2; R3], which flows through each section of the system, at time (T), will occur as Figure 4:

Figure 4 - Gas flow tracking time.
Source: Prepared by the authors (2025).

In other words, the stream C3 will be the same as C2 from 5 hours ago.

In cases of stream mixing, the resulting calculation at each node uses the weighted average of the flow rates of the streams entering the node. In the example for node 4, C4 is calculated as Equation 4:

$$C4 = [10/30] * C3 + [20/30] * CR2 \quad (4)$$

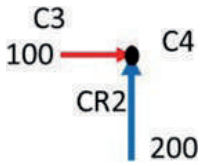

Figure 5 - Stream mixing in a node.
Source: Prepared by the authors (2025).

2.3. Simulation of the Energy Delivered from the Exit Points of the Gas Pipeline Network:

The calorific value (CV) of a substance can be generally defined as the amount of heat produced during the complete combustion of a unit of volume or mass. For natural gas commercialization, this operational variable must be accurately measured and monitored. For this purpose, gas chromatography is used as a chemical analysis method.

In the case of simulation, the metric used is the Gross Calorific Value (GCV), which is the official measurement for billing process. Each chemical compound has a standard GCV, and it is possible to calculate the resulting GCV of a gas mixture.

The calculation consists of using the chemical composition data of each receipt point, which is stored daily as vectors belonging to the matrix [R1, R2, R3]. Knowing the composition delivered at an exit point, this proportion is then used in a weighted manner to calculate the resulting GCV of the mixture.

I) Example of the composition matrix for the stream delivered at the Delivery Point:
[R1, R2, R3] = [0,1; 0,3; 0,6]

II) Resulting Gross Calorific Value (GCV) and chemical composition:
[PCSR1; PCSR2; PCSR3]

Resulting GCV is calculated as Equation 5:
Resulting GCV = [PCSR1 * 0,1] + [PCSR2 * 0,3] + [PCSR3 * 0,6] (5)

The flow time of the gas mixture within the network is essential to ensure the accuracy of the result obtained at the Delivery Point. This means that, if the gas mixture that entered at Receipt Point R1 reaches a Delivery Point five days later, the GCVR1 value used in the weighted average must correspond to the value from five days earlier, considering the transit time of the chemical composition from Receipt Point 2 and its displacement time (Figure 6).

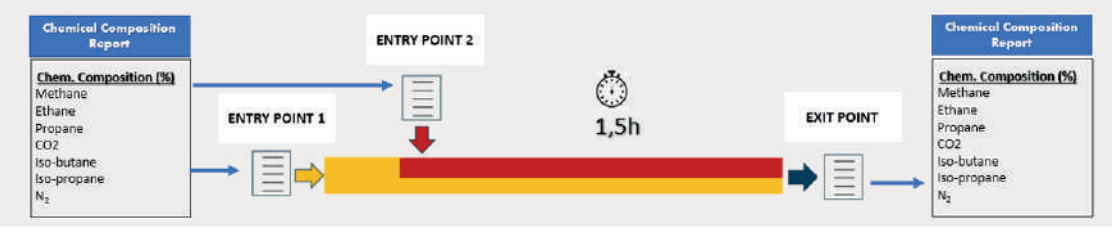

Figure 6 - Schematic of the transition time of chemical composition in a pipeline segment.
Source: Prepared by the authors (2025).

3 Results

The SAQGÁS system has, as one of its results, the calculation of the GCV at delivery points. Thus, in order to validate the results obtained in the system, a comparative analysis was performed between the GCV values resulting from SAQGÁS—calculated based on the values from the receipt points (i.e., entry into the network)—and the GCV values resulting from field measurements using properly calibrated and maintained chromatographs.

For the validation, data from January to November 2023 were used, and four delivery points along the NTS network were selected, two in the state of Rio de Janeiro and two in the state of São Paulo. These are the Delivery Points: Guapimirim, Volta Redonda, Caçapava, and Suzano.

Figures 7 to 14 detail the comparative results between the GCV values obtained from field measurements using chromatographs and those calculated by the SAQGÁS system for the selected delivery points, as well as the percentage differences between the two GCV values. For the analysis, a ±1.5% threshold was considered. This reference is determined in the Transporter's Master Contract for measurement disputes, and it is widely used in the Brazilian industry as the acceptable limit for measurement differences.

For the Guapimirim delivery point, it can be observed from Figure 7 that the GCV calculated by the system (blue line) showed the same behavior over the analyzed period as that simulated by the SAQGÁS system (orange line).

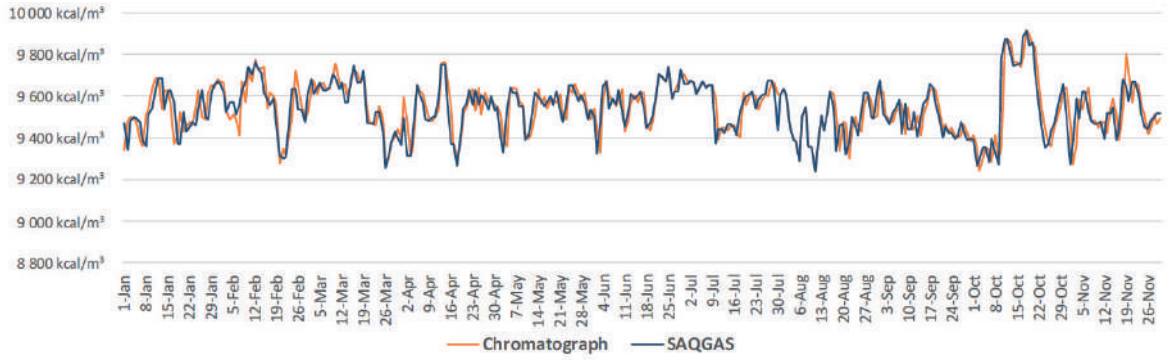

Figure 7 - GCV comparative between computational simulation and chromatograph – Guapimirim.
Source: Prepared by the authors (2025).

Figure 8 shows the absolute differences between the GCV obtained by simulation and by the chromatograph at the Guapimirim delivery point. The red lines represent the defined limits (± 1.5 %), and the gray line represents the difference between the simulator's GCV and the value calculated from the field measurement data from the chromatograph. In fact, the results indicate differences below the established limits for almost the entire period analyzed. With an average GCV of 9543 kcal/m³, an average absolute difference of 0.51 % was observed at this point over the period, with a standard deviation of 70.43 kcal/m³.

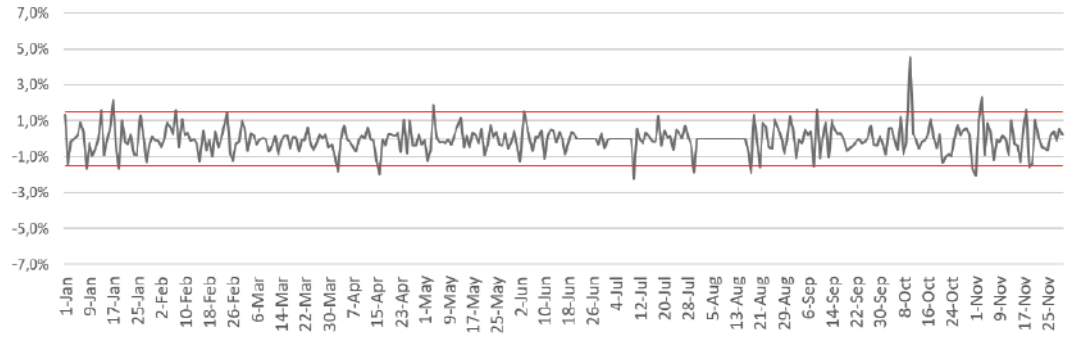

Figure 8 - Simulation versus Chromatography percentage difference – Guapimirim/RJ.
Source: Prepared by the authors (2025).

Another delivery point analyzed in the state of Rio de Janeiro is Volta Redonda. Similarly, the results obtained for the GCV in the SAQGÁS system at this delivery point were compared with the results obtained from field measurements using a chromatograph and can be verified in the orange and blue lines, respectively, in Figure 9.

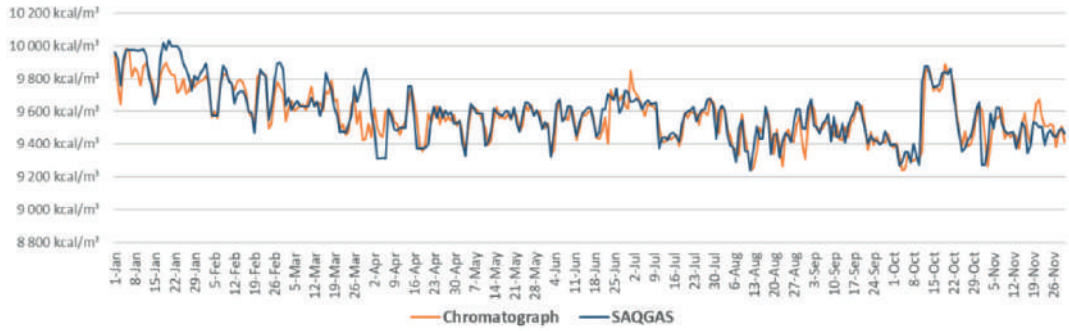

Figure 9 - GCV comparative between computational simulation and chromatograph. Volta Redonda/RJ. Source: Prepared by the authors (2025).

It can be observed that the curves in Figure 9 exhibit similar behavior over time, with a slight deviation at the beginning of the analyzed period. Despite this, when analyzing the percentage differences between the measured and simulated data, the results' consistency is confirmed, with an average absolute difference of 0.65%, which is below the established limits. This result is presented in Figure 10, which shows the difference curve in gray and the established limits in red. For this delivery point, the standard deviation found was 88.3 kcal/m³, and the average calculated GCV was 9574.47 kcal/m³.

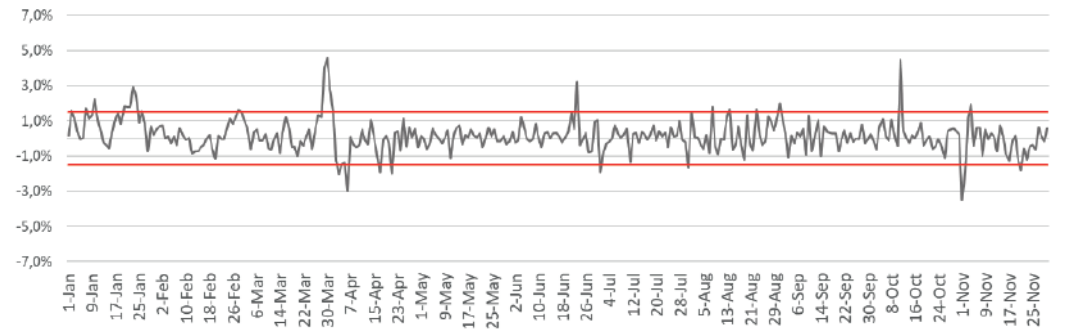

Figure 10 - Simulation versus Chromatography percentage difference – Volta Redonda/RJ.
Source: Prepared by the authors (2025).

The Caçapava delivery point, located in the state of São Paulo, showed, for most of 2023, consistency between the GCV results simulated by SAQGÁS and the values calculated from field measurements, as shown by the blue and orange curves, respectively, in Figure 11. However, between April and June, the period highlighted by the red rectangle, the curves deviated. The data analysis confirmed the observation of a chromatograph failure, which was identified at the time by the NTS measurement and quality team.

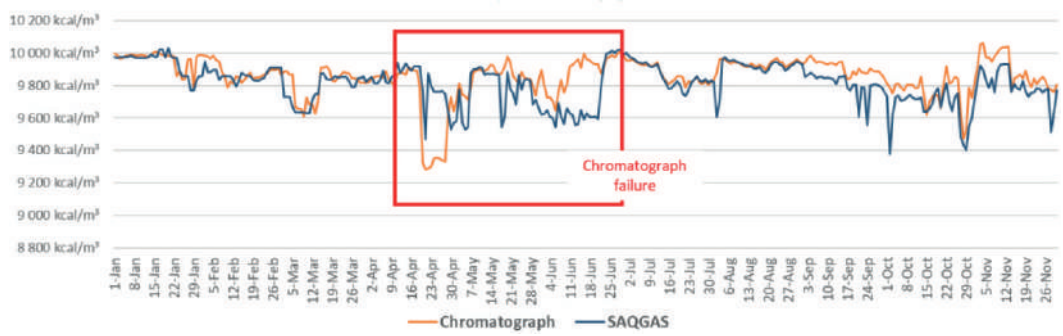

Figure 11 - GCV comparative between computational simulation and chromatograph – Caçapava/SP.
Source: Prepared by the authors (2025).

In the annual view of the differences between the two results, it can be observed in Figure 12 that, most of the time, the result meets the defined criterion, i.e., the difference is within the established limits. The exception occurred between April and June, when there was a field equipment failure, and it was necessary to associate with another nearby chromatograph, that is, to use the chemical composition of another chromatograph with the same current. Despite this, at this delivery point, an average absolute difference of 0.83% was observed, with an average GCV of 9859.06 kcal/m³ and a standard deviation of 1.25 kcal/m³.

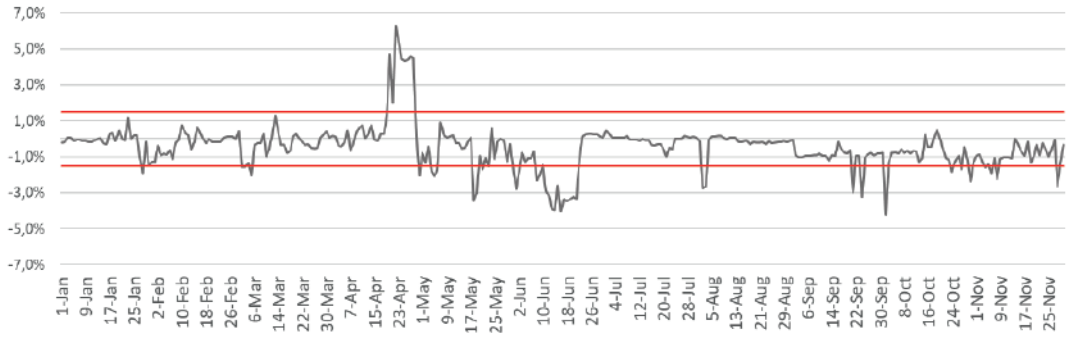

Figure 12 - Simulation versus Chromatography percentage difference – Caçapava/SP.
Source: Prepared by the authors (2025.)

At the Suzano Delivery Point, also located in the state of São Paulo, Figure 13 indicates that the behavior and trend observed between the GCV simulated by SAQGÁS (orange curve) and the GCV calculated based on the chromatograph field measurements (blue curve) are the same, reinforcing the quality of the simulation result.

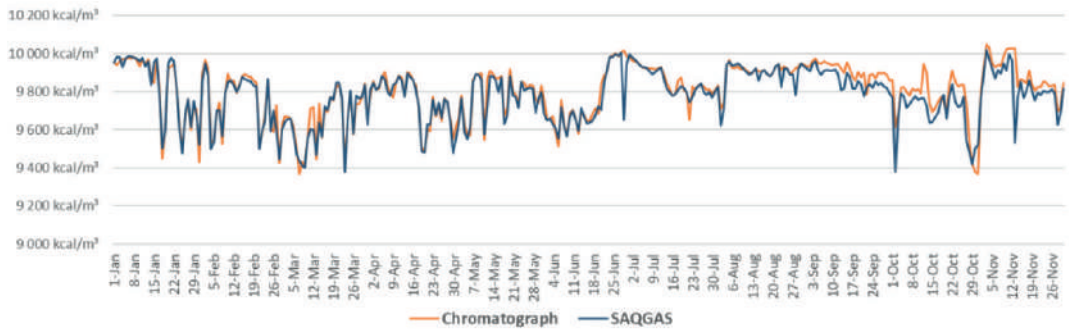

Figure 13 - GCV comparative between computational simulation and chromatograph – Suzano/SP.
Source: Prepared by the authors (2025).

When analyzing the percentage differences between the simulated and calculated results, it can be observed that the result is mostly within the established limits, as shown in Figure 14. At this point, the average difference between the results was the smallest among the delivery points analyzed, at only 0.36%, with an average GCV calculated during the period of 9804.20 kcal/m³ and a standard deviation of 0.33 kcal/m³.

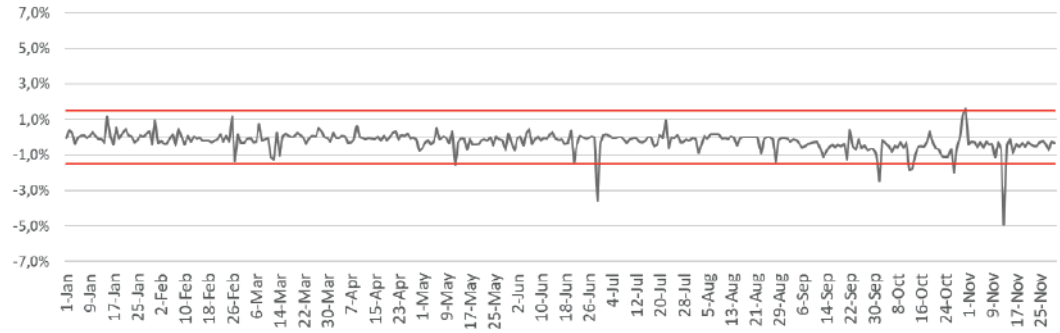

Figure 14 - Simulation versus Chromatography percentage difference – Suzano/SP.
Source: Prepared by the authors (2025).

4 Discussion

Based on the results presented in the previous section, it can be inferred that the outcomes were satisfactory for all analyzed delivery points, as the results generated by the SAQGÁS simulator showed behavior similar to those calculated using field data measured by chromatographs. Moreover, the statistical metrics demonstrated high performance and accuracy for the values derived from the computational simulation, reinforcing the quality of SAQGÁS's output. Overall, the differences between the simulated and calculated values were very small and mostly within the established tolerance limits of ±1.5%.

In the case of the Caçapava Delivery Point, located in São Paulo, the usefulness of computational simulation in identifying failures in field chromatographs became evident. This enables more targeted corrective actions, faster response from technical teams, and improved chemical composition and GCV data for the invoicing process.

In general, the use of GCV simulation methodology via SAQGÁS brings two major benefits to the gas measurement process:

It enables high-precision energy association, i.e., linking the chemical composition of the gas to its GCV for delivery points that are not required to have chromatographs. In these cases, it ensures higher-quality data for invoicing and helps prevent customer complaints and,

It enables a comparison between the chemical composition reported by chromatographs and that calculated by the simulation, thereby identifying chromatograph measurement errors more quickly and accurately.

In addition to the original methodology—where the simulator uses the composition data from receipt points to calculate the GCV at delivery points along the pipeline network—SAQGÁS has also incorporated the association methodology. In this approach, not only are receipt points mapped, but also delivery points equipped with chromatographs. The simulator considers measurements from nearby chromatographs to calculate the chemical composition and GCV at points without chromatographs or where the equipment is malfunctioning. This enhances the accuracy of the simulated values.

5 Conclusion

The accurate determination of the chemical composition and Gross Calorific Value (GCV) of natural gas within the pipeline network—without the need for chromatographs at delivery points—represents a significant advancement in gas quality management. By understanding the transit time of the gas mixture, the characteristics of the sources, entry points, intermediate flow rates, and linepack variations, it is possible to obtain reliable results through computational modeling.

Beyond technical accuracy, this approach enables substantial optimization of operational costs, as it reduces reliance on high-cost equipment and recurring maintenance. If approved by the Regulatory Authority, this methodology will make gas management more efficient, ensuring greater accuracy in energy quantity accounting at delivery points and enhancing the reliability of the transportation system.

Thus, the application of computational simulations for determining the GCV of gas emerges as a strategic solution, combining operational efficiency with analytical precision, bringing direct benefits to both industry players and end consumers.

Referências

REIS, C. B., & MOURA, A. L. C, & KRAUSE, B. P, & NÉRY, T. M. M. & ARAUJO, V. (2019). IBP 1102_19 Gas

Allocation System - Possible applications for a gas routing identification system on a pipeline network.https://www.gov.br/anp/pt-br/assuntos/consultas-e-audiencias-publicas/consulta-audiencia-publica/2024/arquivos/cp-ap-04-2024/atgas_riopipeline2019_1102_ibp_1102_19-oficial-saqgas.pdf

REIS, C. B., & MOURA, A. L. C, & NÉRY, T. M. M. (2020). Sistema de alocação de gás: aplicações inovadoras para o novo mercado de gás de um sistema que identifica a rota do gás em uma rede de dutos. https://biblioteca.ibp.org.br/scripts/bnmapi.exe?router=upload/33920

Nova Transportadora do Sudeste (NTS). (2025, April 29). Contrato Master Serviço de Transporte Firme. https://api.mziq.com/mzfilemanager/v2/d/ea6d235f-ebee-4bf5-82bc-6bc5698718c1/932235d1-cd17-e725-d4cb-5b1be1a7ee75?origin=2

Determining the Key parameters of a Circumferential SCC Susceptibility Model Utilizing Machine Learning

Fernando Merotto[1], Matheus Braz de Souza Viana[3], Larissa Monteiro[2]

Abstract

Stress Corrosion Cracking (SCC) is a challenging threat to manage in pipelines as it may appear in different directions such as Axial (A-SCC) and Circumferential (C-SCC) depending on the main stress direction at the crack location. In addition to direct detection, which will usually require different ILI technologies, direct assessment (SCCDA) may be used to fully manage these threats. Site section for direct assessment may be done through SCC susceptibility assessment however, as the main SCC driving stress from internal pressure will favor axial rather than circumferential SCC, C-SCC susceptibility must consider other conditions, such as excessive soil loads and high residual axial stresses from construction, so that the axial loading can reach the threshold for C-SCC to initiate and propagate. This paper will present how an operator in South America developed a C-SCC specific susceptibility model for one of its pipelines with approximately 3500 verified C-SCC colonies in over than 200 joints utilizing machine learning. A total of 16 parameters considered plausible to influence the presence of the C-SCC were included in the analysis, including geotechnical characteristics of the pipeline route. The model was trained with Randon Forest (RF) and K-nearest neighbors (K-NN) algorithms to obtain a model with theoretical success rate of 70% in identifying joints with C-SCC.

Keywords: Stress Corrosion Cracking; Susceptibility; Circumferential SCC; Integrity Management; Machine Learning

[1] NTS - Nova Transportadora do Sudeste. Brazil. E-mail: fernando.merotto@ntsbrasil.com (https://orcid.org/0009-0002-1787-3548).

[3] NTS - Nova Transportadora do Sudeste. Brazil. E-mail: matheus.viana@ntsbrasil.com (https://orcid.org/0009-0002-7949-579X).

[2] NTS - Nova Transportadora do Sudeste. Brazil. E-mail: larissa.monteiro@ntsbrasil.com (https://orcid.org/0009-0008-1449-7421)

1 Introduction

Stress Corrosion Cracking (SCC) is a challenging threat to manage in pipelines as it may appear in different directions such as Axial (A-SCC) and Circumferential (C-SCC) depending on the main stress direction at the crack location. In addition to direct detection, which will usually require different ILI technologies, direct assessment (SCCDA) may be used to fully manage these threats.

Site selection for direct assessment may be done through SCC susceptibility assessment however, as the main SCC driving stress from internal pressure will favor axial rather than circumferential SCC, C-SCC susceptibility must consider other conditions, such as excessive soil loads and high residual axial stresses from construction, so that the axial loading can reach the threshold for C-SCC to initiate and propagate.

Given these challenges, an operator in South America developed a C-SCC specific susceptibility model for one of its pipelines with approximately 3500 verified C-SCC colonies in over 200 joints utilizing machine learning. A total of 16 parameters considered plausible to influence the presence of the C-SCC were included in the analysis, including geotechnical characteristics of the pipeline route.

2 Circumferential SCC

SCC is a type of cracking assisted by the environment. This phenomenon occurs when there is a combination of susceptible material with sufficient stress and a favorable environment. According to CEPA code SP-0204 [1], SCC typically occurs when the stress present in the pipe wall corresponds to at least 60% of the SMYS of the material. It should be noted that this is the total stress present, considering both the stress induced by the internal pressure of the pipe, when stress is present in places of stress concentration or externally induced, as well as that due to soil movement.

According to ASME B31.8 [2], the axial stress in thin-walled pipes due to internal pressure alone is always lower than the circumferential stress. Therefore, if internal pressure were the only source generating stress in the pipe, circumferential cracks should not occur. As such, if C-SCC is present, there is a possibility that soil movement in the longitudinal or lateral direction of the pipeline could induce axial stresses that would make the pipeline susceptible to axial cracks.

For this operator, what is observed for the verified SCC and can be visualized in Figure 1 with the aid of geometric ILI, is the presence of stress concentration due to small deformations, in this case wrinkles, which probably originated from the cold bending process in the pipeline construction process.

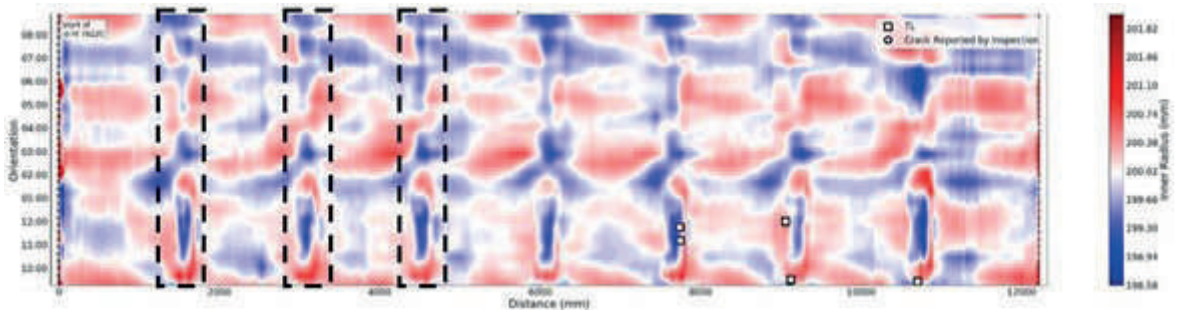

Figure 1 - Geometry of a curved pipe with cracks verified and highlighting the wrinkling pattern.

The white squares in Figure 1 are axial cracks verified in field. The wrinkling pattern is highlighted in the dashed black boxes, and the blue color represents a reduction in the diameter of the pipeline and the red an increase. In the places where there is a transition of colors, in a fixed wrinkling spacing pattern, is where the SCC occurs.

This pattern is found in all the operator's pipelines with SCC to the date. Due to geometry, the direction of the principal stress in each wrinkle due to stress concentration is considered complex, and can accentuate, through stress concentration, both the axial and circumferential stress induced by internal pressure.

3 Geotechnical influence in C-SCC

Lateral forces on pipelines due to geotechnical movements are critical loads for buried pipelines. The stress imposed on pipelines in these types of movements and the interaction of the terrain material with the pipeline can create a stress state that, in susceptible environments, can be the predominant factor for the emergence of C-SCC.

The topography of the terrain is a predominant factor for soil movements that result in geotechnical events that can influence the emergence of circumferential cracks. Therefore, these are two identified factors that correlate and are linked to geotechnics. These movements in the terrain can also generate axial stress in buried pipelines, potentially damaging the coating or, in more extreme cases, leading to pipeline rupture, especially in landslides in mountainous regions.

Landslides both upstream and downstream can induce axial stresses in the pipeline [3]. The magnitude of the axial stress produced by landslides affecting the pipeline depends on various soil properties, such as cohesion and density. The higher the density of the soil, the greater the stress that can be produced [4], and properties of soil-pipeline interaction.

4 Parameters Analyzed

A total of 16 parameters were selected for the first analysis and the susceptibility assessment criteria according to the presence of the parameter in the joint. These criteria were called FIC, Feature Importance Criteria. The curve characteristics were obtained through high-resolution inertial pig data and a brief justification for the consideration of each of the parameters considered is presented.

- → Joint length
- → Wall thickness
- → Coating condition
- → Bend Radius
- → Angle
- → Maximum wrinkle height (if none, then 0)
- → Topographic Classification
- → Tie-in proximity (+- 3 joints)
- → Amount of Milling or Pipe Mill in Joint (> of both)
- → Distance to closest rectifier (m)
- → CP Potential
- → Topography
- → Geotechnical Class
- → Geotechnical Risk
- → Bending Strain
- → Geotechnical Events

4.1. Joint Length

Three criteria were created for the ILI reported joint length, which indicate, in this evaluated pipeline, the pipe manufacturer and the possible pipe bending conditions. The pipeline has three manufacturers, with the characteristics described in Table 1.

Manufacturer	Typical joint length (m)	Nominal wall thickness (mm)
1	12	6.35, 9.52, 11.91
2	6	7.92
3	6	6.35

Table 1 - Pipe manufacturers for the studied pipeline and their characteristics.

It can be observed that two manufacturers only have 6m pipes. Typically, in the construction of this pipeline, the 3m of pipe closest to the circumferential weld are not curved, to avoid the emergence of bending stresses in the weld region and to allow the alignment of the pipes for the circumferential welding without ovalization due to the bending. Thus, it is possible to assume that pipes of 6 meters or less are not cold field bent. A tolerance of +-1 meters was included for the typical joint lengths of 12m and 6m. Pipes shorter than 5 meters were considered tie-ins pipes.

4.2. Proximity to tie-in pipe.

During the cold bending process in the field in the construction of pipelines, the alignment of the curved pipe with the terrain profile is considered complex and, sometimes, the alignment of the pipe with the designed bending radius may not occur. In these cases, it is common to use a short pipe (less than 5 m) to be able to weld the bent pipes to the rest of the pipeline. These short pipes are called tie-ins.

The presence of a tie-in near a bent pipe may indicate the presence of bending stresses introduced to align the pipes for welding. These stresses are potentially the stresses required for the emergence and growth of C-SCC.

4.3. Wall thickness

As one of the main factors for the emergence of SCC in pipelines is the presence of high stress, thinner-walled pipes, such as the 6.35 mm wall thickness case, can be considered more susceptible than thicker pipes, in which the stresses would be lower [2]. This, however, does not exclude the possibility of SCC existing in thicker pipes.

4.4. Coating Condition

The presence of a corrosive environment is one of the main factors for the existence of SCC. The disbondment of the coating of this pipeline could, therefore, be an influencing factor for the presence or absence of SCC.

The coating condition result of the EMAT ILI was then considered as a parameter. It should be noted, however, that these condition results are presented for the entire pipe, and not necessarily tree for the specific location where a SCC colony was verified in the field.

4.5. Bend Radius

Since SCC is verified in cold field bends, the characteristics of the bends are a fundamental parameter of susceptibility to C-SCC. To evaluate all susceptible joints in this pipeline, the bend information was obtained by processing data from a high-resolution inertial ILI, which provided information every 0,1m, to determine the bend characteristics. To date, most bends where SCC was verified in-field in this pipeline have radius between 40D up to approximately 130D.

4.6. Bend angle

Bends with larger angles are considered tighter and, to fit these bends, the pipeline would be exposed to greater bending stresses. Therefore, in tighter bends, greater susceptibility to C-SCC would be expected. Similarly to bend radius, the bend angle information was obtained by processing data from a high-resolution inertial ILI.

4.7. Wrinkles

Since wrinkles are locations of small geometric deformations and stress concentrations, where SCC is expected to occur, the latest ILI report, where wrinkles were reported, was considered for the susceptibility assessment.

It is worth noting, however, that the wrinkles visible in the high-resolution geometric ILI plots (Figure 1), and where cracks are verified in the field, are often smaller than the geometric ILI specification, and therefore may not have been reported. From this perspective, it is expected that the reported wrinkles are the worst of these anomalies present in terms of depth and, therefore, where the greatest stresses could be concentrated.

4.8. Topographic Classification

The topographic classification of pipelines is a concept related to the curvature of pipelines, extracted from the Bend Assessment, from ILI data. It will inform the direction (sag, over, left and right) of the bend considering the direction of the ILI run.

4.9. Distance to the nearest CP rectifier

As the presence of an electrochemical environment is necessary for SCC to exist, measurements of the cathodic protection potential (CP) were considered.

CP OFF potentials lower than -1250 mV indicate the presence of cathodic overprotection, which can lead to the creation of atomic hydrogen and consequently embrittlement of the pipeline material. In these locations, the emergence and growth of the crack requires a lower stress since there is a reduction in the toughness of the material with this embrittlement.

On the other hand, locations with a higher OFF potential (less negative) than -850 mV indicate under-cathodic protection, which can lead to the emergence of external corrosion in places where the external coating fails and can lead to the emergence of NN-pH SCC.

Therefore, by assessing the distance to the rectifier, the possible historical condition of the pipeline's cathodic protection since conditioning is assessed, and whether there is a concentration of C-SCC in the locations closest or farthest from the rectifier. A similar analysis was conducted in 2024 [5].

Cathodic protection potential was also a parameter, and the historical OFF measurements were considered.

4.10. Topography

The topographic aspect is directly linked to the types of geotechnical occurrences that may arise in each region. For example, in regions with flat terrain, occurrences related to flooding and hydrogeological issues are more likely, while steep terrains with very uneven reliefs are consequently more susceptible to landslides. In the case of correlation with regions where C-SCC is present, there tends to be a correlation with uneven reliefs, which allow lateral loads on the pipeline.

4.11. Geotechnical Class

The geotechnical class represents the type of soil present in a given location, for example, whether it is a rock, or a residual soil (a product of rock weathering) or a soft soil, such as organic clay. Each type of geological-geotechnical material has its own physical properties and is susceptible to different geotechnical risks. Rock is susceptible to falls and rolling, depending on other factors such as its fracture pattern. Residual soil may be more susceptible to erosion and landslides, and organic clay to settlement and subsistence processes.

Therefore, understanding the type of material helps the understanding of the types of mechanisms to which it is susceptible, and consequently, helps you manage geotechnical risks, when combined with other data.

4.12. Geotechnical Risk

The operator has developed a methodology to characterize the areas of greatest geotechnical interest along the rights-of-way. The methodology considers several data sources, such as information from national geological survey susceptibility maps, topography information, geotechnical occurrences. With all this data, a static risk analysis is presented, called Geotechnical Risk Map.

4.13. Bending Strain

By evaluating the pipeline deformation, outside the expected profile as reported by ILI inspections, it is possible to estimate a bending strain that the pipeline can undergo according to the stress-strain curves of steels. The presence of these bending strain areas may be related to the presence of C-SCC. Figure 2 shows an example.

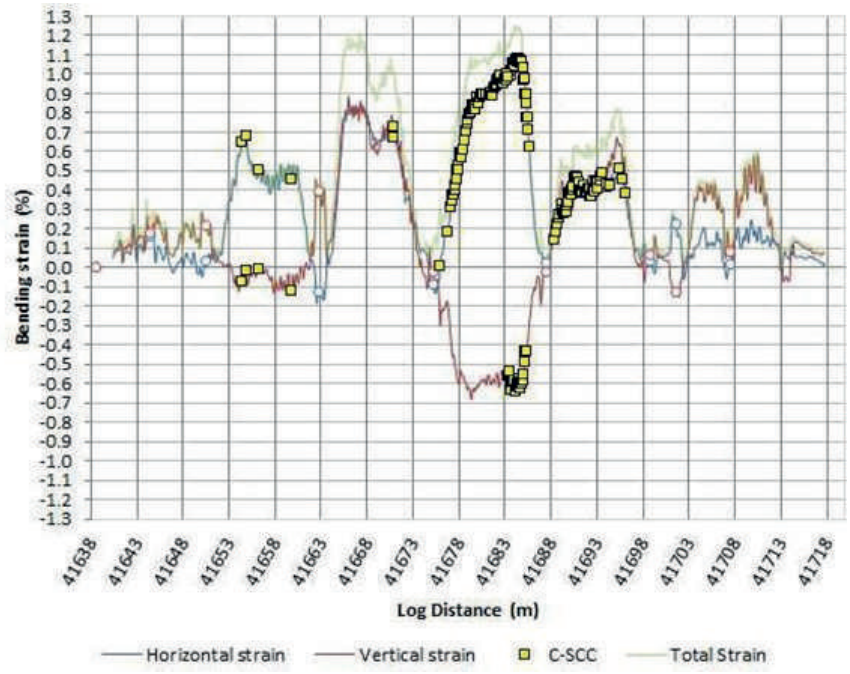

Figure 2 - Results of total, horizontal and vertical bending strain for an investigated site. The squares represent the SCC colonies verified at this site.

4.14. Geotechnical Event

Geotechnical events are geohazards of different types identified in field inspections along the operator right-of-way, i.e., locations with some indication of activity related to erosion, landslides, creeping, damaged structures, among others, which were cataloged according to their type and risk level.

5 Methodology

5.1. Parameters Selection

After defining the potentially influential parameters in the susceptibility assessment for the presence of C-SCC in pipelines, it is possible to assess which of these data is more correlated with the appearance of these cracks.

For this variable selection, the Python algorithm called Feature Importance from the Random Forest model was used, which consists of ranking the attributes considered most relevant to least relevant for defining a class, based on a known training set, in this case, the excavation set, some of which identified C-SCC and others did not, which produces the output to be identified in the test set. The result is shown in Figure 3.

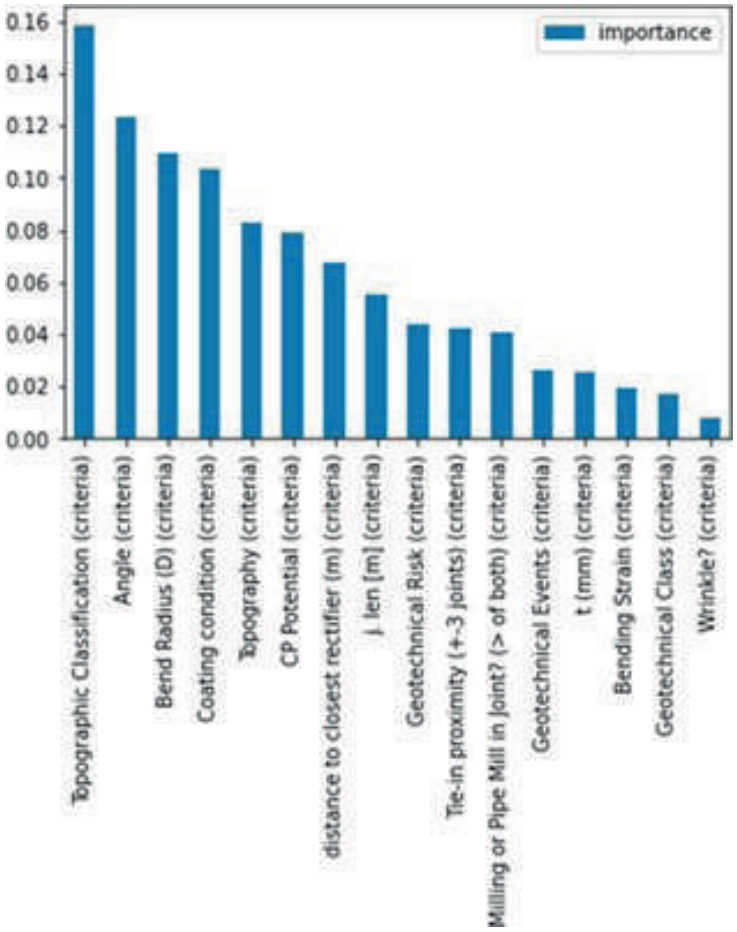

Figure 3 - Ranking of variables based on their importance for C-SCC identification, using the Feature Importance model.

Based on this result, each variable above the defined cutoff line (0.05) was individually analyzed by experts to identify real correlations and possible noise from the selection model. Each of these variables above the cut-off were then individually analyzed regarding their accuracy predicting C-SCC.

For this statistical analysis of the variables validated by the Feature Importance algorithm, the training dataset data were graphically distributed according to the classes of each variable, with the columns colored based on the output values, indicating the verification or not of C-SCC for each excavation in the dataset.

The output 0 indicates excavations without detected C-SCC and is colored blue, while the output 1 indicates excavations with identified C-SCC and is colored orange. The gray area represents the overlap of the columns of the two outputs in the same category of that variable, as shown in Figure 4 for the joint length variable, where joints with a length less than 5m were given the criteria value 0 (tie-ins), joint between 5m and 7m (manufacturers 2 and 3) were given the criteria value 1, and joints greater than 7m were given the criteria value of 2.

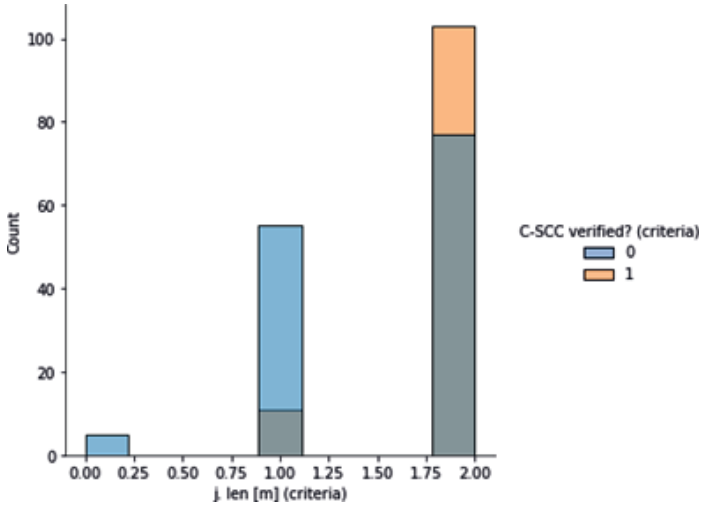

Figure 4 - Statistical Analysis of the variable j. len (m).

The coating condition, for example, showed a low correlation to the presence of C-SCC in a specific condition, shown in Figure 5, where the coating condition criteria 1 is very poor, 0 is Poor, 3 is Fair, 4 is Good and 5 is Excellent, as reported by the EMAT inspection. At any of these criteria, C-SCC could be almost equally verified or not, showing low prediction ability towards C-SCC. As discussed, this is likely due to EMAT coating condition being a result of the whole joint condition, and as long as a single location has localized coating disbondment, SCC may occur.

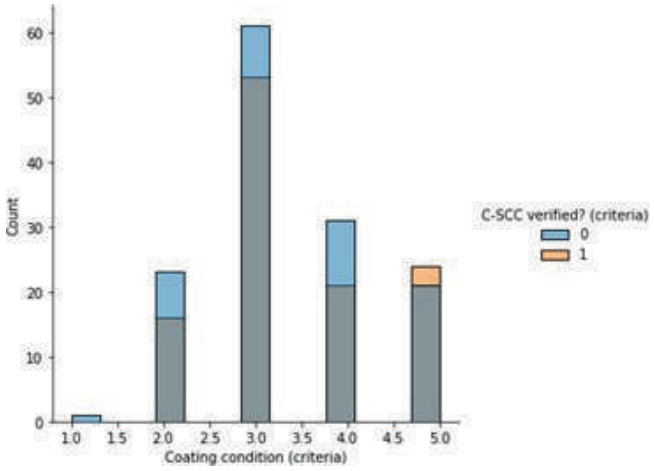

Figure 5 - Statistical analysis of the Coating Condition variable.

Based on the statistical analysis of all variables above the specified cutoff level, a baseline (minimum) combination of parameter was established, with the variables with the best correlations, as listed below.

- → Topographic Classification;
- → Bend Radius;
- → Angle;
- → Joint Length.

It is noted that, although joint length is not the 4th most relevant parameter, it served as an strong indicator if the joint was cold field bent or not, with a strong correlation towards C-SCC not verified if joint was criteria 0 or 1 (less than 7m) and was thus included in the baseline.

5.2. Machine Learning Models

Two different machine learning models were used to analyze the C-SCC dataset and try to identify whether a joint is susceptible to C-SCC. The selected models are: Random Forest and K-means.

The Random Forest algorithm is a supervised ensemble method. Ensemble methods consist of combining different models to obtain a single result, making the model more comprehensive and robust, but with a higher computational cost consequently. In the case of Random Forest, the model will consist of a random set of decision trees, which in turn, is a decision-making model based on rules that form a structure similar to a flowchart, associated by nodes, where a new condition is verified, causing the flow to follow in one direction, and so on, until the result.

For classification models, Random Forest is, therefore, a collection of structured trees {h(X; θk), k = 1, · · ·}, where { θk } are random vectors, independently and identically distributed, and each tree indicates a vote for the most popular class for the input X [6].

The K-nearest neighbors (K-NN) algorithm is also a supervised method, used for both regression and classification problems. This method basically consists of comparing the characteristics of the item to be classified with those of the training database. That is, the method is based on the Euclidean distance, for example, between the test data and the closest data from a training set [7].

In this algorithm, the variable k represents the number of neighbors that will be used; the choice of this value varies according to the database, and optimization algorithms can be used to assist in this determination.

Based on the value of k, the Euclidean distance from the test data to the closest neighbors in the training database is calculated. The class that predominates among these neighbors will be the class determined for the new test data."

6 Results

Accuracy, which is the ratio between correctly classified samples (C-SCC verified) by total samples (verified sites), was the metric used to evaluate the models and allowed, in a simpler way, to understand the percentage of samples that were correctly classified, regardless of their parameters.

To perform the analyses based on the machine learning models, the data that would be used were defined based on the universe of the FICs. After evaluating the results, 4 variables were defined to be treated as fixed (baseline) and would therefore be used in all further models' analyses, as they were considered essential based on the literature and experience of the points excavated by NTS, for the emergence of C-SCC, and based on the Feature Importance assessment presented previously. They were joint length, bend radius, bend angle and topographic classification.

From this data set, several analysis were conducted, using both the Random Forest model and the K-NN, with only the fixed variables first and then with the fixed variables, plus the parameters of CP potential, distance to closest rectifier and topography, which were above the FICs cutoff, to verify if they, individually or combined, had an influence on the accuracy of the output data. These combinations of this information to understand the best data set for establishing the susceptibility model to circumferential cracks in pipes.

6.1. RF Model

The Random Forest model that presented the best maximum accuracy, reaching 75%, was the model with only the 4 baseline variables. The RF average accuracy of the model, which used training and testing datasets, in a proportion of 70% (training) and 30% (testing) and several possibilities of parameters inherent to the Random Forest model, showed little difference when

combining the other variables mentioned, where their inclusion whether reduced the accuracy, or made no improvement to it, showing they had no relevance to the model.

6.2. K-NN Model

The K-NN model was run with different values for the variable "k", and the best performance was achieved with k = 5, reaching the maximum accuracy of 75% as well, considering the same scenarios of the Random Forest model. Again, the baseline case had a 75% accuracy and the combination with other variables mentioned either reduced the accuracy or made no improvement to it, showing no relevance to the model.

6.3. Susceptibility Ranking

From the results of the analysis models for susceptibility, it was concluded that the most accurate combination of parameters for susceptibility to C-SCC, among those analyzed, were:

- → Joint length (m)
- → Bend Radius (D)
- → Bend Angle (º)
- → Topographic Classification

The choice of only these 4 parameters, the most relevant according to analysis, is a function of the results presented in the accuracy of the models for which both methodologies presented their best accuracy result, of 75%, with just these 4 parameters.

When introducing the other parameters considered most relevant to the occurrence of C-SCC verified in the field, according to the FIC analysis, this accuracy, considered as a base, varied less than 1%. This small variation indicates that these parameters do not influence the accuracy of the model, that is, they are not relevant to the susceptibility to SCC according to the machine learning analysis. Therefore, they were not considered for the susceptibility ranking.

7 Discussion

7.1. Low correlation with geotechnical data

In the evaluation of the 16 parameters, information associated with geotechnical data was considered to identify the possible correlation in the literature between C-SCC and geotechnical events such as ground movement.

The result obtained did not identify a significant correlation with any of the geotechnical data considered. However, it confirmed a strong correlation with the geometry of the pipe, supporting the theory that the axial stresses that cause C-SCC are probably due to the concentration of stress in the small wrinkles caused by the cold bending of the pipe.

It should also be noted that there are few cases of geotechnical events in the studied pipeline with excavated joints. In other words, although the susceptibility to C-SCC associated with the geometry of the pipes has been confirmed, it cannot be confirmed that the locations with geotechnical events do not have C-SCC. But these are considered the root causes for the overall C-SCC occurrence in this pipeline.

7.2. Terrain topography data

Terrain topography data is constantly correlated with regions of susceptibility to C-SCC in the literature [8]. In this study, however, this correlation was not clearly evident, however, the data used in the database is based on the Digital Terrain Model called SRTM [9], which is an open product with a resolution of 30 meters per pixel, that is, each pixel of 900m² has the same topography value.

Low-resolution data, such as this one, can negatively influence a possible correlation of this variable with pipes susceptible to C-SCC, as indicated in the literature. There are digital terrain models on the market with a resolution of up to 50cm. Performing a new verification of the correlation of topography with C-SCC with a product with a resolution of up to 10 meters may present different results from those detected for this variable in the present work.

7.3. Final susceptibility ranking

The result of the analysis of the 16 parameters that could, according to theory, influence susceptibility to C-SCC resulted in only 4 parameters being selected to evaluate this susceptibility. All 4 are directly related to the presence of field bends and, therefore, it is not possible to generate a ranking of the joints exclusively with these 4 parameters and their weights. The operator then utilized an overall SCC (any direction) susceptibility model, which was much more sophisticated to support prioritization [10].

The final step for the operator, as in any new developed model, is to go in-field and investigate the concluded most susceptible joints according to the new model to verify how it is performing, feed the data back into it and analyze its performance.

Referências

Canadian Energy Pipeline Association (2015). CEPA SP-0204: CEPA Recommended Practices for Managing Near-neutral pH Stress Corrosion Cracking. Canadian Energy Pipeline Association (CEPA)

American Society of Mechanical Engineers (2022). ASME B31.8: Gas transmission and distribution piping systems. American Society of Mechanical Engineers (ASME)

Pettinger, A.M., Sykora, D.W. (2011). Landslide risk assessment for pipeline systems in 84 mountainous regions. J. Pipeline Eng., 161–171.

Trautmann, C.H., O'Rourke, T.D. (1985) Lateral Force-Displacement response of buried pipe. J. Geotech. Eng., 1077–1092.

Guillen, P.; Merotto, F.; Monteiro, L.; Gamboa, E. Key elements to consider when managing circumferential SCC in pipelines. International Pipeline Conference, IPC2024-134014. September 2024. Alberta, Canada.

Breiman, L. (2001). Random Forests, Machine Learning. Kluwer Academic Publishers, 45. Boston, p. 5-32.

Peterson, L. E. (2009). K-nearest neighbor. Scholarpedia, v. 4, n. 2, p. 1883.

Bates, P. D., Neal, J. C., Sampson, C. C., Smith, A. M., Alonso, L., & Giustarini, L. (2018). Global flood hazard mapping using satellite remote sensing and hydrologic modeling. Natural Hazards and Earth System Sciences, 18(5), 1093–1101

NASA. (2000). Shuttle Radar Topography Mission (SRTM) – 1 Arc-Second Global. Washington, DC: NASA Jet Propulsion Laboratory.

Monteiro, L.; Loback, R.; Géa, P.; Silva, C. Improving SCC susceptibility models with data analytics and AI in gas transmission pipeline. Rio Pipeline Conference, RPC ISSN 2447-2069. August 2023. Rio de Janeiro, Brazil.

Dynamic Process Safety Barrier Management System Based on Risk Hierarchy

Jose Sandoval Dias dos Santos Junior[1], Gildasio Ferreira dos Santos[2], Luana Marques[4], Icaro de Vasconcelos Brito[3]

Abstract

Process safety is critical across industries, especially in complex sectors like Oil and Gas, where managing safety barriers is both essential and challenging. This paper presents a dynamic process safety barrier management system for midstream assets, integrating the Bowtie (BT) method with corporate and automation data to monitor barrier integrity in real time. Unlike static models, this system adapts to operational changes, offering a semi-quantitative safety assessment. It follows ANSI Z10, ISO 45001, and ISO 45002 standards, mapping hazards on a 5x5 risk matrix and adjusting risk scores based on barrier effectiveness. Developed using the Python-based Django framework, the system features an interactive front-end platform where the tank's bowtie (BT) diagram was built. The platform also guides through layer of protection/mitigation analysis (LOPA/LOMA) based on a predefined set of threats, consequences, and barriers. The system back-end, on the other hand, collects real-time data from various facility areas, adjusting risk scores when controls fail. By consolidating BTs across assets, the system provides a comprehensive risk overview, improving decision-making. Results show enhanced safety by identifying weaknesses, supporting resource allocation, and strengthening safety culture, leading to incident reduction and continuous improvement

Keywords: Process Safety; Risk Analysis; Midstream; Bowtie; Dynamic Management.

[1] Petrobras Transporte SA. Brazil. E-mail: jose.sandoval@transpetro.com.br (https://orcid.org/0009-0008-5471-3053).

[2] Petrobras Transporte SA. Brazil. E-mail: gildasio.santos@transpetro.com.br.

[4] TRANSPETRO. Brazil. E-mail: l.marques@transpetro.com.br.

[3] Petrobras Transporte SA. Brazil. E-mail: icaro.brito@transpetro.com.br (https://orcid.org/0000-0002-2729-8703)

1 Introduction

Process safety management (PSM) is a fundamental aspect of industrial operations, particularly in high-risk sectors like Oil and Gas [1] [2]. As industrial facilities grow in complexity, the necessity for robust and adaptable safety systems increases. Traditional safety management approaches often rely on static models that fail to account for real-time operational changes, which can lead to delayed responses to emerging risks and compromise safety and operational integrity [3]. To address these challenges, this paper presents a Dynamic Process Safety Barrier Management System (DPSMS) that integrates real-time data with risk hierarchy principles to improve safety barrier management.

The system applies the Bowtie (BT) method while incorporating automation and corporate data to continuously monitor the integrity and effectiveness of preventive and mitigative controls. A practical application of the Bowtie methodology in the PSMS involves analyzing a midstream oil and gas facility, where critical assets like storage tanks and pipelines are assessed for potential hazards.

A real-world example highlighting the importance of such assessments is the catastrophic accident at the Caribbean Petroleum (CAPECO) terminal facility near San Juan, Puerto Rico. On October 23, 2009, an overfilled gasoline storage tank led to a massive explosion and fire, causing significant environmental damage and revealing deficiencies in safety management systems. According to the U.S. Chemical Safety Board (USCSB), the incident resulted from inadequate management of gasoline storage tank overfill hazards, emphasizing the critical need for continuous monitoring and effective safety barriers [4]. The CAPECO accident underscores the importance of implementing advanced risk management frameworks, such as the Dynamic Process Safety Management System (DPSMS) presented in this paper.

The DPSMS framework, by integrating real-time data and Bowtie analysis, aims to prevent similar occurrences by dynamically assessing risk factors and ensuring that preventive and mitigative measures remain effective. The Bowtie diagram is used to map out the causes and consequences

of incidents, linking them to specific preventive and mitigative barriers. In this paper, a simulated scenario is analyzed using a Bowtie analysis for a midstream oil and gas facility, considering a major hazard: the large release of fuel from a naphtha tank.

The methodology and System Architecture section will demonstrate how various threats, including overpressure, structural damage, and operational failures, can contribute to such incidents. To mitigate these risks, preventive barriers—such as level alarms and automated shutdown systems—are employed to reduce the likelihood of occurrence, while mitigative measures, including emergency response protocols and secondary containment, help minimize potential consequences.

The results demonstrate that the DPSMS significantly enhances process safety by dynamically updating risk assessments and enabling faster response times to barrier failures. Developed using the Python-based Django framework [5], the system provides a visual and automated framework that helps operators identify non-compliant barriers, optimize risk mitigation strategies, and improve resource allocation. Additionally, compliance with international safety standards (ISO 45001, ISO 45002, ANSI Z10) ensures alignment with best practices in hazard identification and risk control.

By implementing real-time monitoring, adaptive risk evaluation, and structured risk reduction methodologies, DPSMS contributes to a safer, more resilient process safety management framework, ultimately reducing incidents and reinforcing safety culture in the midstream sector.

2 Methodology

This section describes the elements required for implementation of the PSMS, from the asset risk analysis to the development of the computational framework.

2.1. Layers of Control and Risk Hierarchy

An essential feature of the DPSMS is its risk reduction capability, which is evaluated using a structured risk assessment framework. The risk table assigns risk levels based on the likelihood and severity of hazards, utilizing a 5x5 matrix with scores ranging from 1 to 25 [5], as shown in Figure 1. These scores are then adjusted based on the effectiveness of preventive and mitigative barriers, ensuring that residual risk (RR) is dynamically updated to reflect current operational conditions [5]. To further enhance the effectiveness of the risk assessment, the DPSMS designed a risk hierarchy approach based on the risk reduction factor table from ISO 45002 [5]. The Table 1 details the expected effectiveness of the different control measures in reducing risks.

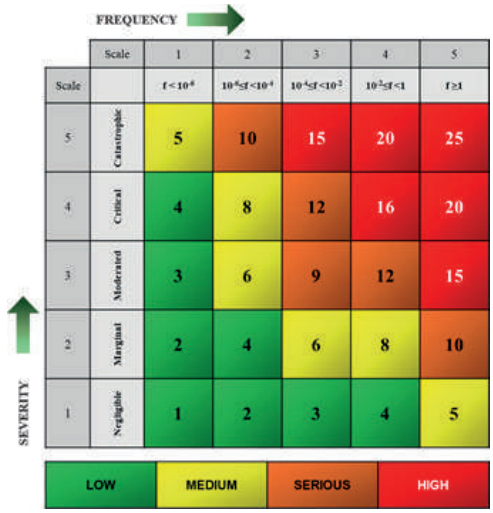

Figure 1 – 5x5 Risk matrix and its corresponding risk level.
Source: Prepared by the authors (2024).

Control Type	Risk Reduction Factor (RRF)	Description
Elimination	0.1	Complete removal of the hazard.
Substitution	0.2	Replace hazard with a safer option.
Engineering Controls	0.6	Physical changes to processes.
Alarms	0.8	Warnings and operational response
Administrative Controls	0.9	Procedures and training measures.
Personal Protective Equipment (PPE)	0.95	Last line of defense for workers.

Table 1 - Risk Reduction Factor.

Additionally, the DPSMS integrates methodologies from **Layer of Protection Analysis (LOPA), Layer of Mitigation Analysis (LOMA), and Layer of Control Analysis (LOCA)** to enhance risk mitigation. These methodologies are described in ISO 31010 [6] as essential techniques for risk assessment and management in high-risk environments. Their application ensures compliance with internationally recognized best practices and enhances the robustness of process safety frameworks. These three methodologies serve different but complementary purposes in managing process safety risks:

- **Layer of Protection Analysis (LOPA):** A semi-quantitative risk assessment tool that evaluates the adequacy of independent protection layers (IPLs). LOPA helps determine whether additional safeguards are required beyond existing control measures. It is particularly effective in decision-making for cost-effective risk reduction while ensuring compliance with safety standards [7].
- **Layer of Mitigation Analysis (LOMA):** Focuses on the effectiveness of mitigative controls after an initiating event has occurred. Unlike LOPA, which emphasizes prevention, LOMA evaluates how well the system can minimize damage and control the consequences of an incident. This analysis is critical for ensuring emergency response readiness and minimizing operational disruptions [7].
- **Layer of Control Analysis (LOCA):** A comprehensive assessment of control layers, including preventive, mitigative, and emergency response measures. LOCA provides a holistic view of risk control effectiveness by assessing the integrity of safety barriers and their compliance with safety regulations. It enables organizations to prioritize investments in safety improvements and optimize risk management strategies [7].

By incorporating these approaches, the DPSMS framework ensures a well-rounded and proactive risk management strategy, reducing vulnerabilities and enhancing safety resilience. LOPA provides a structured approach to assessing independent protection layers [7], LOMA focuses on the effectiveness of mitigative controls post-incident initiation, and LOCA evaluates preventive, mitigative, and emergency response measures to optimize control effectiveness. The integration of these methodologies within the DPSMS framework ensures a comprehensive approach to risk management, allowing dynamicity and effectiveness on risk level assessment.

Traditionally, risk calculations were performed using a simple model:

$$\text{Risk Level (RL)} = \text{Severity X Likelihood} \quad (1)$$

However, this approach does not account for the effectiveness of safety controls. In contrast, the DPSMS applies a more advanced risk assessment methodology:

$$\text{Residual Risk (RR)} = \text{Severity X Likelihood X} \prod \text{RRF} \quad (2)$$

where RRFs (Risk Reduction Factors) represent the efficiency of various control measures.

A key advantage of the DPSMS is its real-time adaptability, allowing for continuous adaptation to operational changes and emerging risks. Unlike static safety models, the DPSMS updates risk assessments in real time, integrating live data streams from automation and corporate systems.

2.2. Dynamic model

The main purpose of this work is to provide a computational framework to dynamically calculate and display the initial risk level, the impact of the barriers RRF and the final residual risk (RR) for each asset. Hence, once an asset has its scenario (bowtie) and the list of controls ready, the user can upload these data for the system to create the dynamic model.

By using the Django framework, the system back-end periodically runs an algorithm that collects real-time corporate and automation data related to the controls assigned to their respective bowtie. Each bowtie's preventive or mitigative barrier starts with its maximum reduction factor, i.e., all controls compliant. However, as soon as the algorithm detects non-conformities, as a critical alarm, the corresponding multiplication factor is impaired, reducing the barrier efficiency and increasing the risk level of the related hazard/consequence.

2.3. User interface

Since the DPSMS is packaged in a Django framework, it also contemplates the front-end, i.e., the interface where the user can interact with the system. The Figure 2 illustrates the system architecture.

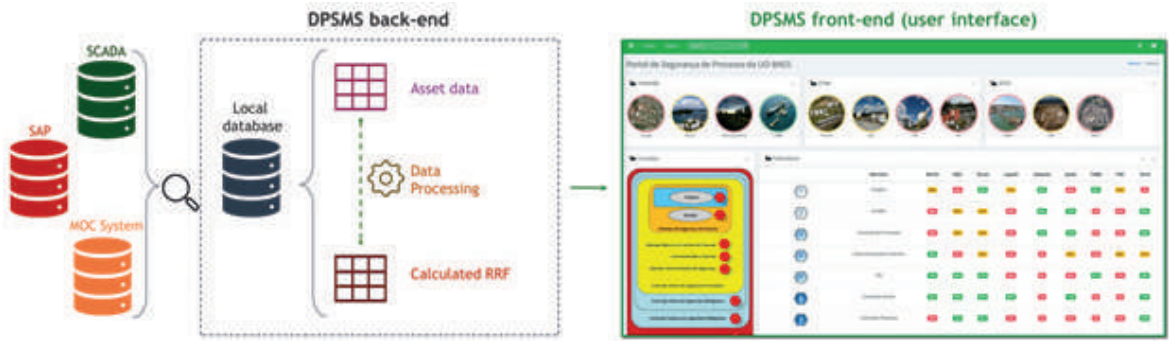

Figure 2 - PSMS system architecture.
Source: Prepared by the authors (2024)

The front-end was conceived in a way that allows users to build BT diagrams for the required scenarios and assets. It also guides users through LOCA analysis based on a predefined set of hazards, consequences, and barriers mapped by the process safety (PS) team. Hence, the stages described in Section 2.1 does not need to be done in a traditional spreadsheet. Instead, the team is given a web-based interface to help them make the risk analysis and send the input data required for the dynamic model.

2.4. Simulated Scenario: Dynamic Risk Assessment and Barrier Management

In a midstream facility, the main critical assets are storage tanks and pipelines. Therefore, each equipment of this set was chosen to undertake an initial risk assessment. First, the PS team identified the corresponding material unwanted event (MUE) and its hazards. Then, a traditional bowtie analysis was carried out, considering the available preventive and mitigative controls. In

Figure 3 is shown an example of BT analysis for a naphtha tank, whose MUE is "large release of fuel", with five potential hazards and three types of consequences.

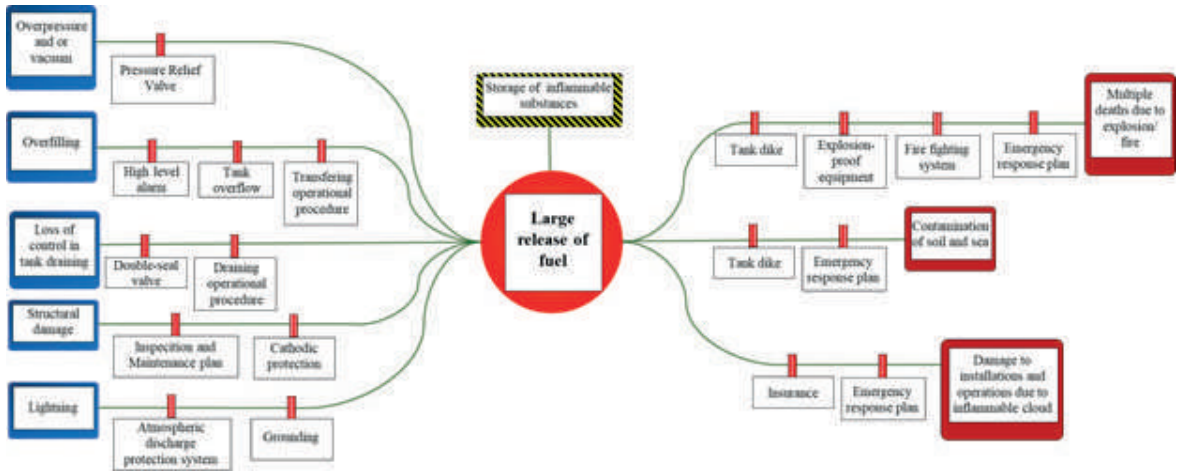

Figure 3 - Example of bowtie analysis for a naphtha tank.
Source: Prepared by the authors (2024)

Next, the PS team started a more quantitative approach. Considering the absence of control, each hazard was judged based on likelihood and severity. The likelihood was quantified in frequency of events/year using [8] and the terminal historical data, as shown in Table 2. Moreover, by using the 5x5 risk matrix (Figure 1), different frequency ranges and severity levels were mapped in the 1-5 scale, resulting in the 1-25 risk level score (RL) assigned to each possible combination.

Taking as an example the hazard "overfilling" in the BT of Figure 3, without measures of control. As in Table 2, its estimated frequency is 9.52E-02 event/year (scale 4 on the frequency axis), and its severity is classified as catastrophic (scale 5 on the severity axis). Therefore, this hazard is mapped to the (5, 4) coordinate in the matrix, resulting, using Equation 1, in a risk of 20 (RL = 20), which is considered high risk level.

Hazard	Frequency (events/year)	Severity
Overpressure/Vacuum	4.76E-02	Catastrophic
Overfilling	9.52E-02	Catastrophic
Loss of control in tank draining	2.38E-02	Catastrophic
Structural damage	1.00E-03	Catastrophic
Lightning	2.38E-02	Catastrophic

Table 2 - Risk Assessment Table for large release of fuel in a naphtha tank.

Finally, using the LOCA and the barrier hierarchy principles outlined in Section 2.1, the PS team calculated the contribution of the several measures of control to reduce the risk level. For the case of the "overfilling" hazard, the naphtha tank has as barriers an alarm control (RRF = 0.8), a tank overflow system (RRF = 0.6) and a transfer operational procedure (RRF = 0.9). When all the elements are compliant, the risk is reduced by

$$RRF = 0.8 \text{ X } 0.6 \text{ X } 0.9 \quad \rightarrow \quad RRF = 0.432 \qquad (3)$$

which, from Equation 2 and RL = 20, leads to a residual risk (RR) of

$$RR = 20 \text{ X } 0.432 \quad \rightarrow \quad RR = 8.64 \qquad (4)$$

In this case, the risk level is reduced from **high** to **medium** with the existing layers of control.

The compliance of the barriers depends on several corporate and automation data. In the simulated naphtha tank scenario, the alarm control may lose its risk-reducing factor if a HIHI alarm level occurred within the last week or if the level switch maintenance is overdue. The business rules for assessing barrier compliance vary depending on the terminal and asset, and they must be clearly defined to support the computational model.

In the simulated naphtha tank scenario, the alarm barrier is supposed to reduce 20% (RFF = 0.8) the risk level of the "overfilling" hazard. In the considered naphtha tank, the PS team listed for this barrier three rules of compliance:

- → No occurrence of critical level alarm within the last week
- → No overdue maintenance of the level transmitter
- → Level transmitter (LT) currently available

If the Level Transmitter (LT) is unavailable, the entire barrier becomes ineffective, reducing its effectiveness from 20% to 0% (RRF = 1.0). However, if the LT is available, the effectiveness of the barrier depends on the compliance of the remaining control elements. In this simulation, each of the remaining factors—critical alarm status and overdue maintenance—contributes equally, with a 10% reduction factor each. Table 3 presents a truth table that outlines the eight possible combinations of the alarm barrier control elements along with their corresponding Reduction Risk Factors (RRFs). In this simulated case, the number of control elements was intentionally limited for exemplification purposes.

LT available	Overdue maintenance	Critical alarm	Reduction factor	RRF
0	0	0	0%	1.0
0	0	1	0%	1.0
0	1	0	0%	1.0
0	1	1	0%	1.0
1	0	0	0%	1.0
1	0	1	10%	0.9
1	1	0	10%	0.9
1	1	1	20%	0.8

Table 3 - Truth table (1: compliant, 0: non-compliant) for the alarm barrier rules.

Considering the initial RL = 20, if the alarm barrier RFF increases to 0.9, and the remaining barriers are compliant, the RR in Equation 3 becomes

$$RR = 20 \text{ X } 0.9 \text{ X } 0.6 \text{ X } 0.9 \quad \rightarrow \quad RR = 9.72 \qquad (5)$$

In this case, the prior **medium** risk (8.64) would change to the **serious** risk level.

Moreover, for every asset and its risk analysis added to the platform, a dynamic bowtie is generated, displaying the hazards, consequences, risk level scores and the elements of control with RRFs, as shown in Figure 4.

The dynamic bowtie style in Figure 4 is inspired on the striped bow-tie model with layers of control analysis, devised by [8]. In the naphtha tank case, the diagram represents the bowtie example in Figure 3. The hazard boxes were generated after the inputs from Table 2, and the layers of control were added in the system based on the existing controls for the naphtha tank. It can be seen that the box hazard #2, "overfilling", has the original RR = 20. which is reduced by the three barriers Engineering (RFF = 0.6), Alarms (RFF = 0.8) and Administrative (RFF = 0.9). Since all three layers are fully compliant, the risk level is effectively reduced from 20 to 8.64, classifying it as a medium-risk level.

Conversely, for hazard #3, "Loss of control in tank draining", its initial level risk of 20 could be reduced by the Engineering and Administrative layers, i.e.,

$$RR_{\#3} = RL_{\#3} \text{ X } RRF_{Eng} \text{ X } RRF_{Adm} \quad \rightarrow \quad RR_{\#3} = 20 \times 0.6 \times 0.9 = 10.8 \tag{6}$$

However, the respective RR#3 is displayed as 11.20 (Figure 4). This discrepancy suggests that one of the elements within the Administrative layer is not fully compliant. When the user clicks on the barrier in the system interface, a pop-up window appears, detailing the control elements and identifying which specific factor is hindering the expected risk reduction, as illustrated in Figure 5.

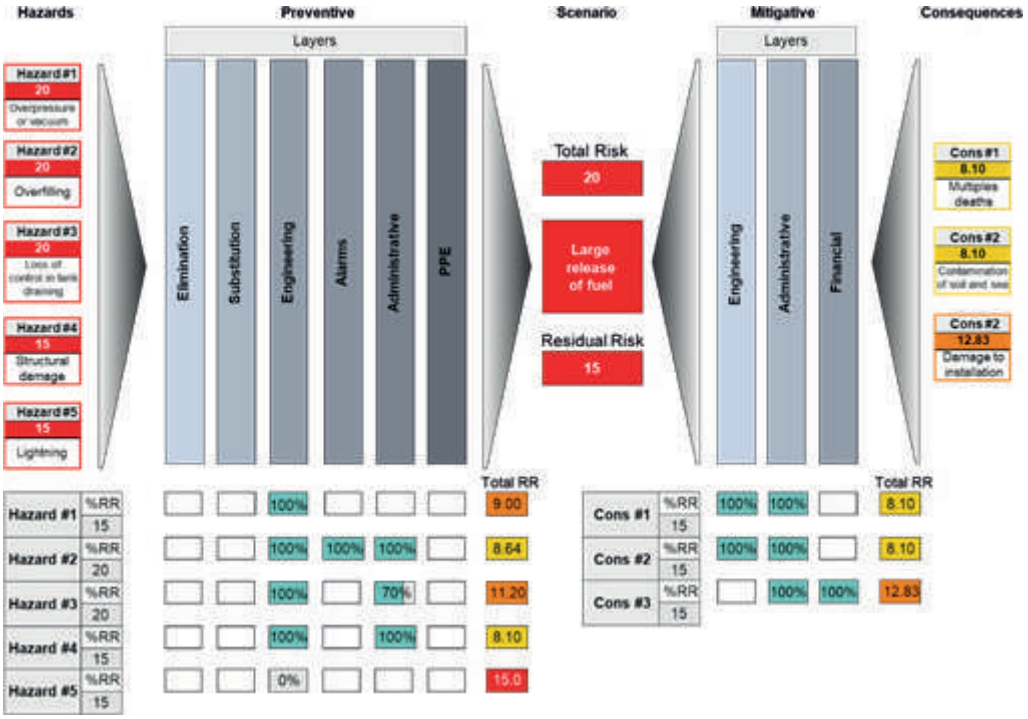

Figure 4 - Example of dynamic bowtie.
Source: Prepared by the authors (2024)

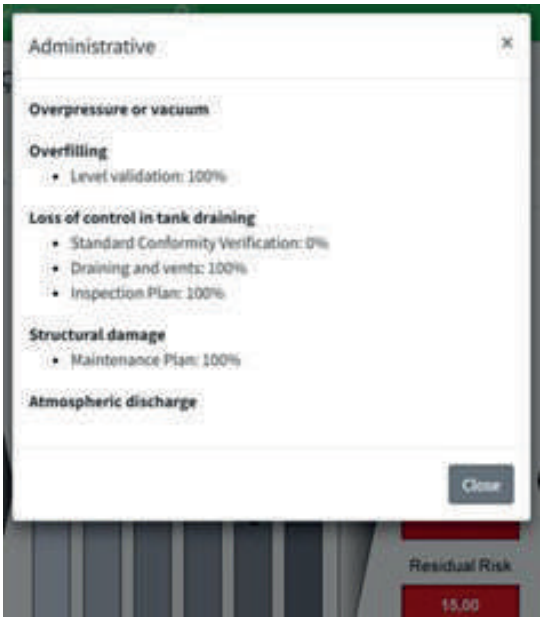

Figure 5 – Example of control elements and barrier rules. Source: Prepared by the authors (2024).

From Figure 5, one of the elements of control related to hazard #3, namely, "Standard Conformity Verification", is the one not compliant. This means, for example, that the draining operation procedure was not validated in the required date. As the Administrative layer has three elements, each of them is responsible for 1/3 of the 10% (RFF = 0.9) reduction. Hence, without the "Standard Conformity Verification", the current effectiveness of this layer will be 2/3 (around 70%) for the hazard #3, and the Equation 6 becomes:

$$RR_{\#3} = 20 \times 0.6 \times 0.9 = 11.20 \quad (7)$$

3 Conclusion

The implementation of the Dynamic Process Safety Barrier Management System (DPSMS) demonstrates a significant advancement in risk assessment and process safety management. By integrating real-time data with the Bowtie methodology, this system allows for continuous monitoring of safety barriers, ensuring that preventive and mitigative controls remain effective in mitigating operational risks. Unlike traditional static models, which rely on periodic assessments, the DPSMS dynamically updates risk scores based on real-time compliance data, providing operators with immediate insights into emerging risks and necessary interventions.

One of the key strengths of the DPSMS is its structured approach to risk visualization and mitigation. The system's ability to automatically adjust risk levels based on control layer effectiveness fosters a proactive approach to safety management. By incorporating risk hierarchy principles and international safety standards, the system enhances regulatory compliance while improving operational safety.

The simulated case highlights the practical application of the DPSMS in a naphtha tank, demonstrating how hazards like overfilling and loss of control in tank draining can be effectively managed. Through real-time monitoring, the system not only identifies deviations from compliance but also quantifies their impact on overall risk reduction. The ability to visualize safety barriers and their current status through an interactive interface further enhances its usability, making it a valuable tool for process safety teams.

A comparison between traditional static risk assessment methods and the DPSMS underscores the advantages of a dynamic model, as summarized in Table 4.

Aspect	Traditional Model	DPSMS (Dynamic Model)
Risk Calculation	Static (Severity × Likelihood)	Dynamic (Severity × Likelihood × $\prod$ RRF)
Barrier Effectiveness	Not considered in real-time	Continuously updated
Response Time	Delayed response	Instant adaptation
Compliance Check	Periodic (e.g., audits)	Real-time automation
Data Integration	Manual (spreadsheets)	Automated (corporate & automation data)

Table 4 - Comparison between Traditional Risk Assessment and DPSMS.

Referências

[1] G. Popov, B. K. Lyon e B. . D. Hollcrof, Risk Assessment: A Practical Guide to Assessing Operational Risks., John Wiley & Sons, 2016.

[2] A. P. I. (API), API 780: Security Risk Assessment Methodology for the Petroleum and Petrochemical Industries., First Edition ed., Washington, DC, 2013.

[3] C. f. C. P. S. (CCPS), Proactive and Reactive Indicator Selection Guide, 2022.

[4] U. C. S. A. H. I. B. "Final Investigation Report - Caribbean Petroleum Tank Terminal. Explosion and Multiple Tank Fires," 2010.

[5] I. O. f. S. (ISO), ISO 45002 - Occupational health and safety management systems, Geneva, Switzerland: ISO.

[6] I. O. f. S. (ISO), ISO 31000: Risk Management — Guidelines, Geneva, Switzerland: ISO, 2018.

[7] . B. . K. Lyon e G. Popov, Managing risk through layers of control, Professional Safety, 2020.

[8] P. -. P. B. S.A., CRITERIA FOR DESIGN, OPERATION AND MAINTENANCE OF SAFETY INSTRUMENTED SYSTEMS IN INDUSTRIAL UNITS, Rev. D ed., 2015.

[9] I. O. f. S. (ISO), ISO 45001: Occupational Health and Safety Management Systems — Requirements with Guidance for Use, Geneva, Switzerland:: ISO, 2018.

[10] I. E. C. (IEC), IEC 31010: Risk Management — Risk Assessment Techniques, IEC, 2019.

[11] D. S. Foundation, "Django Project," [Online]. Available: https://www.djangoproject.com/.

Online Monitoring System for Electrical Signature in Oil and Gas Sector Assets

Victor Zoratti Ferreira[1], Eduardo Poleze[2]

Abstract

This work presents the development of an online system for the acquisition and automatic analysis of electrical signatures in induction motors operating within the oil and gas sector. Electrical signature analysis represents a non-invasive diagnostic technique for identifying faults in induction electric motors. During operational conditions, current and voltage signals from the stator are externally collected utilizing a data acquisition system (DAQ) and current transducers affixed to the motor panels. These signals, initially recorded in the time domain, embody both the characteristic signatures of the equipment and pertinent information regarding potential defects. Subsequent processing of these signals is performed using the Fast Fourier Transform, converting them into the frequency domain. This transformation enables the generation of a distinct "electrical signature" for each motor, thereby allowing for the differentiation of typical characteristics, noise, and potential faults. Such electrical signatures delineate the overall operational state of the equipment, thus enabling the inference of both electrical and mechanical anomalies. Furthermore, a web-based platform has been developed employing the Python programming language, which permits specialists to access the online history of electrical signature collections and analyze the equipment conditions through telemetry graphs, waveforms, and spectra.

Keywords: Data acquisition system; condition monitoring; electrical signature

[1] PETROBRAS TRANSPORTE S/A. Brazil. E-mail: zoratti@transpetro.com.br (https://orcid.org/0009-0008-4359-4984).

[2] PETROBRAS TRANSPORTE S/A. Brazil. E-mail: eduardo.poleze@transpetro.com.br

1 Introduction

Rotating machines play a fundamental role in industry, being widely used in mechanical and electromechanical systems. With the advancement of industrialization and automation, the complexity of these machines has increased, which elevates the risk of component failures. Induction motors stand out as the most employed due to their robustness, high productivity, and low cost. It is essential that these machines operate safely and continuously to avoid unexpected shutdowns, making fault detection a priority in industrial maintenance.

For the oil and gas sector, equipment availability guarantees an even greater degree of importance, since unplanned downtimes for corrective maintenance can lead to high costs and logistical impacts that may affect the entire production chain. Furthermore, many machines are installed in areas with difficult access, making remote condition monitoring of these equipments, using non-invasive techniques, an increasing necessity in the sector.

To ensure equipment reliability, predictive maintenance is adopted according to NBR 5462 standard, with Electrical Signature Analysis (ESA) being an important part of the set of techniques used.

In Transpetro's context, the workflow related to electrical signature predictive maintenance involves a manual process, which begins with scheduling the data acquisition service. In the next step, the technician responsible for the activity performs the work with a collection case in the field. Finally, the acquisition files are sent to the analyst, who issues a report on the equipment condition. Considering the development and expansion of IoT technologies for the industrial environment, several improvement opportunities were identified for this process within the company:

- Periodicity: data acquisition is performed annually, which is insufficient for monitoring the evolution of failures;
- Safety: the manual collection process requires opening energized panels or accessing cable vaults, thereby exposing technicians to potential hazards;
- Operational costs: data acquisition needs to be scheduled, competing with other maintenance activities. Additionally, technicians often need to travel to remote facilities to perform the activity. Furthermore, the data acquisition case needs to be shared among various installations, which involves transportation costs between them;
- Database: manually collected data is stored in a proprietary encrypted format, making it impossible to access without using the manufacturer's specific software.

This work presents the development of an online system for the acquisition and analysis of electrical signatures in induction motors in the oil and gas sector, focusing on solving the limitations existing in the current process.

2 Methodology

This work addresses three techniques pertinent to electrical signature analysis: Motor Current Signature Analysis (MCSA), Concordia Current Vector (CVV), and Extended Park Vector Approach (EPVA).

Motor Current Signature Analysis (MCSA) is a non-invasive technique that diagnoses faults in induction motors through electrical current data (Thomson & Fenger, 2001). The signals are initially acquired in the time domain and then converted to the frequency domain using Fast Fourier Transform (FFT). The resulting frequency spectrum enables the identification of characteristic motor parameters, as well as anomalies and defects. This methodology is particularly valuable in environments where physical access to motors presents safety hazards.

MCSA can identify different failure modes such as broken rotor bars or fractures in the rotor ring; dynamic or static air-gap eccentricity; stator winding faults; and abnormal connections of stator windings (Verucchi et al., 2008). Current signals are acquired by current transformers (CT), and the data obtained is normalized relative to the fundamental frequency. The broken bar fault mode, for instance, manifests as characteristic sidebands in the spectrum, located at a distance equivalent to twice the slip frequency of the electric motor in relation to the fundamental frequency, as shown in Figure 1. The assessment of the motor condition is made by comparing the amplitude of the fundamental frequency peak with the amplitude of the sideband peaks. This difference is quantified in decibels, with smaller values indicating more severe fault conditions.

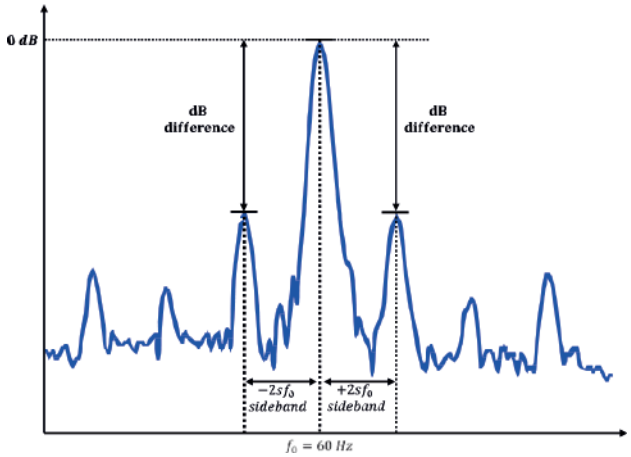

Figure 1 – Illustration of sidebands around the fundamental frequency, characteristic of the broken bar fault mode.
Source: Prepared by the authors (2025).

The approach through Concordia Current Vector (CCV) or Park Vector analysis is another electrical signature analysis technique. The three phases of the induction motor, I_R, I_S and I_T, are transformed to Concordia currents, I_α and I_β, following the Equations 1 and 2:

$$I_\alpha = \sqrt{\frac{2}{3}} I_R - \sqrt{\frac{1}{6}} I_S - \sqrt{\frac{1}{6}} I_T \quad (1)$$

$$I_\beta = \sqrt{\frac{1}{2}} I_S - \sqrt{\frac{1}{2}} I_T \quad (2)$$

$$|I_{park}| = \sqrt{I_\alpha^2 + I_\beta^2} \quad (3)$$

The Concordia currents are then represented in a Concordia Current Vector (CCV) plane, also called Park Vector, as shown in Figure 2. Under ideal conditions, without the presence of electrical imbalance or induction motor faults, the Park Vector traces a circle centered at the origin of the coordinate plane. However, under abnormal conditions, the circular pattern is disrupted, resulting in deviations in the Park Vector. The magnitude of these deviations correlates directly with the severity of the fault condition (Das et al., 2008).

The Extended Park Vector Approach (EPVA) is a spectral analysis technique that uses the Park Vector modulus, $|I_{park}|$, represented in Equation 3. The current signals are collected and transformed through the Park transformation, allowing the calculation of the vector modulus and, subsequently, its spectrum (Cruz & Cardoso, 2001), as represented by the block diagram in Figure 3.

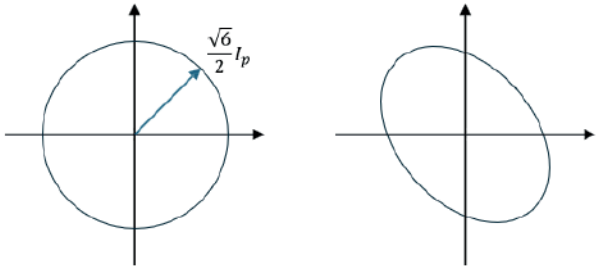

Figure 2 – Park Vector pattern for conditions without and with fault. Source: Prepared by the authors (2025).

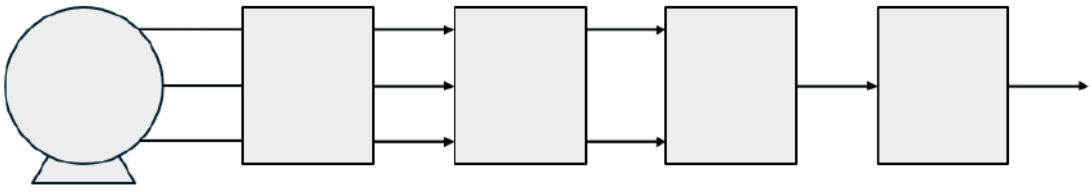

Figure 3 – Block diagram of the EPVA technique. Source: Prepared by the authors (2025).

This technique is especially useful for evaluating electrical imbalance in motors that do not have torque control, resulting in a demodulated spectrum that considers variations in the three current phases. Under ideal operating conditions, without the presence of faults, the EPVA will be free of

any frequency component, with only the DC value of the Park Vector magnitude. The emergence of failure modes in the induction motor results in the appearance and evolution of components at certain frequencies in the EPVA.

MCSA, by preserving the fundamental frequency, makes it difficult to identify frequencies close to the fundamental frequency (sidebands), in cases of incipient failures in the induction motor, especially due to noise. EPVA, however, eliminates the fundamental frequency of the power supply, and thus allows the identification of fault frequencies in the spectrum more clearly.

In the work presented in this article, the data acquisition hardware consists of a compact chassis (one slot) with Ethernet connection and a multichannel analog input module. The system offers 16 differential input channels with synchronous sampling, measurement range of ±10 V, 24-bit resolution, and maximum sampling rate of 10 kHz. This hardware configuration was specified to optimize installation costs through a compact and modular solution while still ensuring the necessary requirements for electrical signature analysis. For capturing electrical current signals, split-core current transducers (CT) are used, which have a quick and practical installation, without the need to interrupt the motor power circuit.

The data acquisition (DAQ) system is positioned near the panels of the monitored electric motors. The current transducers can be coupled either directly to the motor power cable or to the secondary of the measurement CT in the electrical panel. Each DAQ system can monitor five motors with complete three-phase measurements or up to eight motors with two-phase measurements, with the third phase being estimated from the application of Kirchhoff's current law at the isolated wye point (Y) of the motor. Finally, the acquisition system chassis is connected to a switch port of Transpetro Corporate Internal Network (RIC)

Figure 4 – Data acquisition (DAQ) system components: NI-9202 module, cDAQ-9181 chassis and current transducer (CT).
Source: National Instruments / PS Soluções (2025).

Figure 5 – Data acquisition (DAQ) system installed in the electrical panel.
Source: Prepared by the authors (2025).

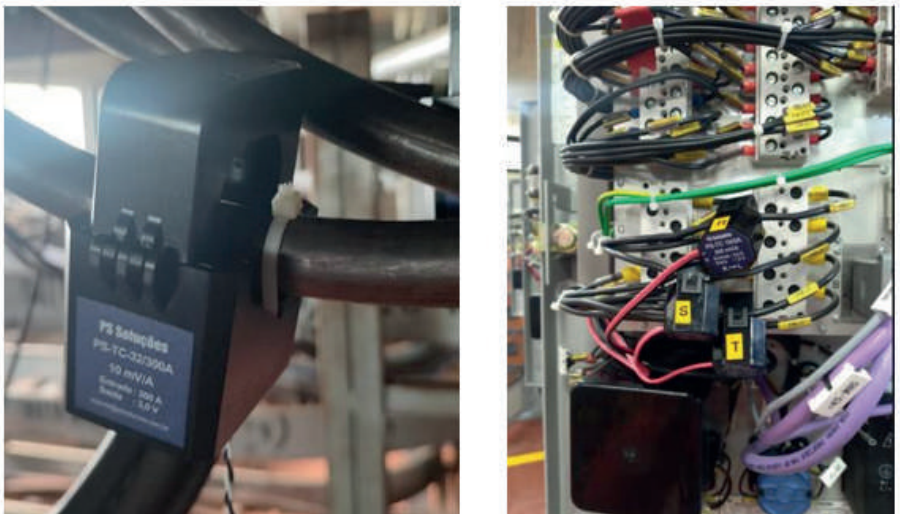

Figure 6 – Current transducers on the power cable and in the induction motor panel.
Source: Prepared by the authors (2025).

A server connected to the RIC is used to trigger acquisitions, process, and store the collected data obtained from the monitored induction motors. On this server, drivers, for communication with the acquisition hardware, and Python libraries are installed. A script has been developed to establish connections with various chassis distributed across Transpetro's terminals, enabling periodic collection of electrical current signals. Data collection occurs every five minutes, with a sampling frequency of 2500 Hz and a total acquisition time of 50 seconds. From the acquired data, several telemetry global parameters are extracted and stored, including the root mean square (RMS) values of phase currents, estimated rotational speed, fundamental frequency of the electrical network, phase angles, level of broken bars, EPVA level, and current imbalance. Additionally, for every 24 hours of accumulated operation, the complete oscillography signals are also stored.

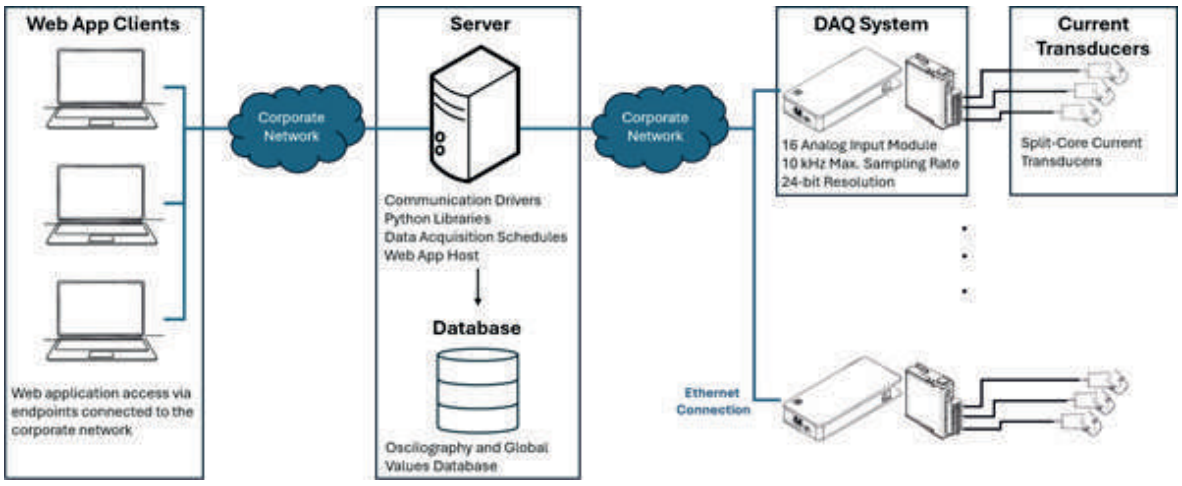

Figure 7 – Schematic of the online electrical signature collection system.
Source: prepared by the authors (2025).

Subsequently, these data are made available for analysis through a modern and intuitive web application developed using the Streamlit library in Python. This application allows users to select a specific induction motor and analyze the historical data of global telemetry parameters and electrical signature collections associated with that particular equipment.

Finally, an algorithm was developed to estimate the rotational speed of the induction motor based on the electrical signature signals. This algorithm relies on the principle that the EPVA eliminates the fundamental frequency of the waveform and allows the identification of other frequencies in the spectrum more clearly. Initially, the fundamental frequency of the electrical network is detected as the frequency corresponding to the peak of highest amplitude in the MCSA. Subsequently, the DC component is removed from the EPVA spectrum, and the frequency with the highest amplitude peak is selected for frequencies below 4 Hz. According to the theory of electrical behavior of the induction motor, explained previously, this frequency extracted from the EPVA corresponds to twice the motor slip frequency. With the fundamental frequency and the slip frequency, the slip value is obtained, which consequently allows for the estimation of the rotational speed of the induction motor through Equation 4, where n is the motor speed in RPM, f_o is the fundamental frequency in Hz, s is the motor slip and P is the motor number of poles.

$$n = {120.f_o.(1-s)}/{P} \qquad (4)$$

3 Results

The initial screen of the developed web application features a sidebar on the left side of the screen. This sidebar includes three selection boxes that allow users to select the region, site, and equipment to be analyzed. Upon selecting a specific induction motor, the main technical information is loaded in the "Ficha de Dados" tab (Figure 8). Information such as nominal rotational speed, nominal current, number of bars, and number of slots are made available to assist the specialist in conducting a more accurate diagnosis of the analyzed induction motor. In the "Valores Globais" tab (Figure 9), users can view the historical data of all telemetry values monitored at five-minute intervals.

Finally, in the "Análise Espectral" tab (Figure 10 and Figure 11), users can access and perform the electrical signature analysis of the induction motor in three distinct ways. The first method involves examining the oscillography of the electrical current signal collected for each phase. The second method utilizes the MCSA for each phase of the electric motor.

In the MCSA option, users can interactively adjust visualization settings and add frequency markers to the graph. The third method consists of the Park Vector and the EPVA, obtained from the simultaneous measurement of the motor's phases.

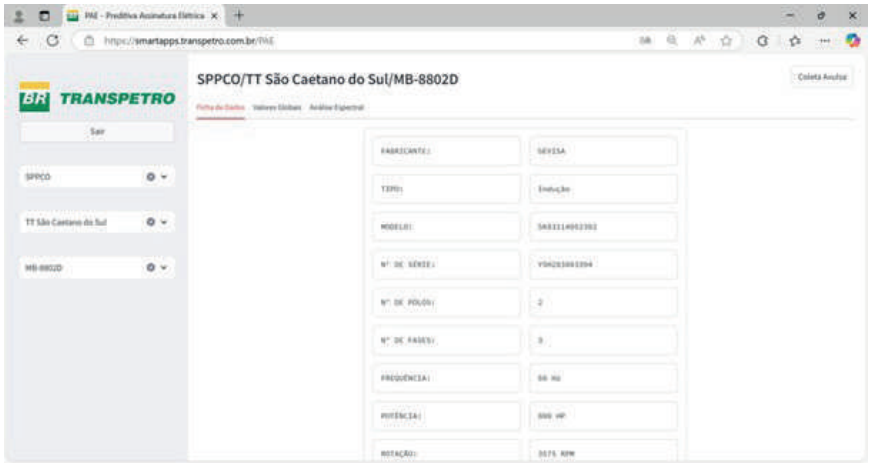

Figure 8 – "Ficha de Dados" (Datasheet) tab.
Source: Prepared by the authors (2025).

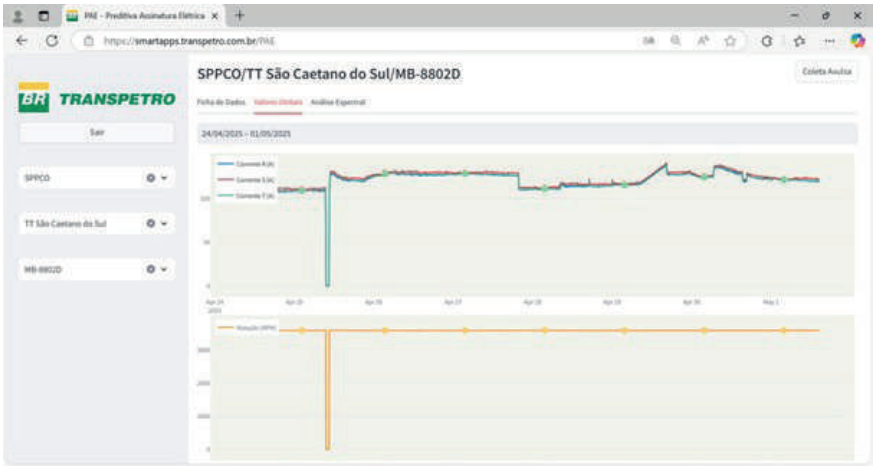

Figure 9 – "Valores Globais" (Global Values) tab.
Source: Prepared by the authors (2025).

Figure 10 – MCSA graph in "Análise Espectral" (Spectral Analysis) tab.
Source: Prepared by the authors (2025).

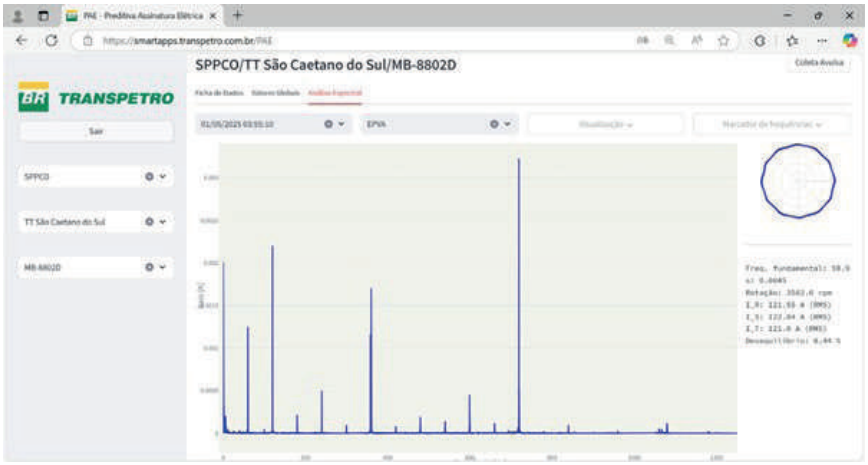

Figure 11 – EPVA and Park Vector graphs in the "Análise Espectral" (Spectral Analysis) tab. Source: Prepared by the authors (2025).

In addition to these tabs for data visualization, a functionality has been implemented in the web application to perform a manual collection of the electrical signature of the induction motor as illustrated in Figure 12. Through this feature, users can configure the sampling rate and collection duration, and initiate an instantaneous acquisition of the motor's electrical signature directly from the application. Subsequently, the electrical current signals are saved in the database and become automatically available for visualization and analysis within the web application.

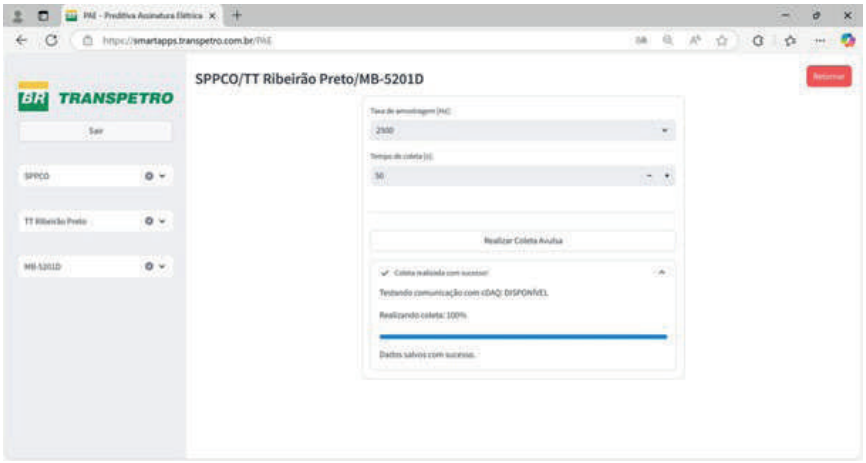

Figure 12 – Screen for configuration and execution of manual collection.
Source: Prepared by the authors (2025).

Furthermore, the developed web application is responsive and automatically adapts to various screen sizes and devices, ensuring a consistent and optimized user experience. Consequently, the application can also be accessed from corporate mobile devices that are connected to Transpetro Corporate Internal Network (RIC).

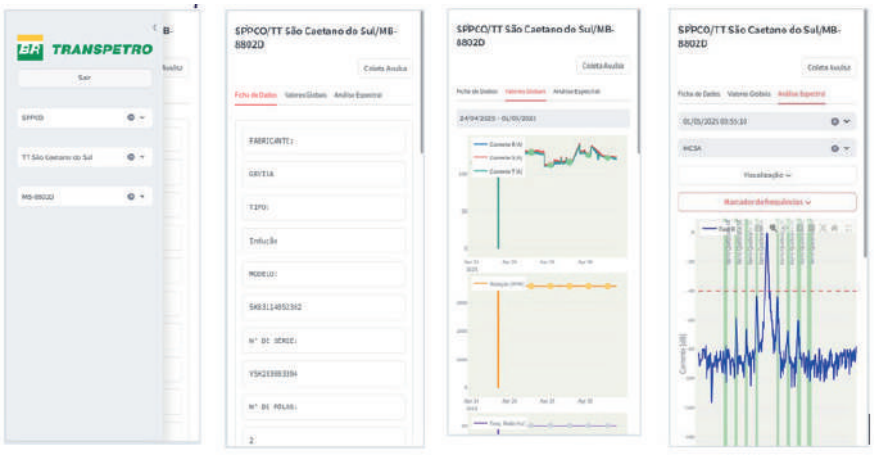

Figure 13 – Web application screens on smartphones.
Source: Prepared by the authors (2025).

To illustrate the proposed methodology for estimating rotation speed, a case study involving the MB-8802B motor is presented. This study compares the speed value derived from electrical signature analysis with direct measurement using a stroboscope.

Upon analyzing the EPVA spectrum collected on May 25, 2023, at 10:20:18 (Figure 14), it is possible to clearly identify a predominant peak below 4 Hz, located at the frequency of

0.4 Hz, which corresponds to twice the slip frequency. The MCSA applied to this signal reveals that the fundamental frequency is 60 Hz. By applying Equation 4, the estimated rotational speed obtained is 3588 RPM, as also illustrated in Figure 14.

For comparative purposes, during the same collection moment, a manual measurement of the MB-8802B motor's speed was conducted using the SKF stroboscope model TKRS 10. The stroboscopic measurement indicated a speed of 3588.3 RPM, as illustrated in Figure 15. The results demonstrate that the employed method was effective for estimating rotational speed.

Figure 14 – Speed estimation of the MB-8802B induction motor.
Source: Prepared by the authors (2025).

Figure 15 – Speed of the MB-8802B induction motor measured with a stroboscope.
Source: Prepared by the authors (2025).

4 Discussion

The online monitoring system presented in this work costs around 20% to 30% of the value of a similar system from market companies. In addition to the cost advantage, being developed internally at Transpetro, it can be easily expanded, customized, and integrated with other systems used in the company, as needed.

The Manual Acquisition functionality, from the maintenance team's point of view, proves to be extremely useful. It is common for situations where the induction motor begins to present some type of anomaly and the maintenance team needs to perform a specific collection (with a certain sampling rate and duration) to better investigate and diagnose the situation in which the equipment is found.

During the development stage, a comparative study was also conducted of the values obtained from the online system with the values of an analyzer considered a benchmark in the market. A comparison was made with the Preditor from PS SOLUÇÕES, and the results are very similar, which validates the developed online solution.

It is worth noting that the methodology of estimating the rotation of the induction motor through the demodulated electrical current signature signal is not always assertive (Bonet-Jara et al., 2021). The presence of other harmonics close to the fundamental, or the possibility that the amplitude of the broken bar level is below the noise level, compromises the assertiveness of the model. Bonet-Jara et al. (2021) shows that the MCEMAX market analyzer from PdMA had an error in the rotation estimate for 65.82% of the motors analyzed in the article.

5 Conclusion

The development of this online monitoring system presents several benefits for predictive maintenance processes within the company. Continuous monitoring provides consistency in data collection, as global parameters are acquired every five minutes and oscillographies are stored at least once per machine operation, which overcomes the limitations of the current maintenance plan focused on electrical signature collection, whose periodicity is annual.

From an operational perspective, remote monitoring contributes to the safety of maintenance activities, eliminating the need for technicians to perform on-site collections in potentially dangerous environments such as electrical panels and cable holds, in addition to avoiding travel to distant facilities.

Furthermore, building a solid and continuous database of oscillographies opens possibilities for the future development of more advanced analysis techniques, including the application of artificial intelligence models for anomaly detection.

Despite the positive results, there are some opportunities for improvement in the system, mainly related to the rotation estimator. Although the technique currently employed has satisfactory performance in determining failure frequencies related to MCSA during manual graphical analysis, automatic analysis based on global values, such as the amplitude of broken bar levels, ends up being susceptible to errors in the rotation estimate. This automatic verification of results, associated with email notifications, is a functionality that is in the process of implementation, and its effectiveness is linked to the need to seek more accurate models for rotation estimation.

Regarding future work, the installation of voltage transducers is in the implementation phase at some facilities, which will enable power quality monitoring and the application of other predictive analysis techniques, such as electrical power signature. Currently, the developed system monitors 35 motors in 7 Transpetro facilities. The expectation is to expand coverage to serve 10 facilities, with at least 50 motors monitored by the end of 2025.

Referências

Thomson, W. T., & Fenger, M. (2001). Current signature analysis to detect induction motor faults. IEEE Industry Applications Magazine, 7(4), 26–34. https://doi.org/10.1109/2943.930988

Verucchi, C. J., Acosta, G. G., & Benger, F. A. (2008). A review on fault diagnosis of induction machines. Latin American Applied Research, 38(2), 113-121.

Das, S., Purkait, P., & Chakravorti, S. (2008). Space-vector characterization of induction motor operating conditions. In Fifteenth National Power Systems Conference (NPSC). IIT Bombay.

Cruz, S. M. A., & Cardoso, A. J. M. (2001). Stator winding fault diagnosis in three-phase synchronous and asynchronous motors, by the extended Park's vector approach. IEEE Transactions on Industry Applications, 37(5), 1227–1233. https://doi.org/10.1109/28.952496

Bonet-Jara, J., Quijano-Lopez, A., Morinigo-Sotelo, D., & Pons-Llinares, J. (2021). Sensorless speed estimation for the diagnosis of induction motors via MCSA. Review and commercial devices analysis. Sensors, 21(15), 5037. https://doi.org/10.3390/s21155037

Perfomance of Corrosion Inhibitors In Saline CO_2-Containing Environments: Evaluation by Mass Loss and Potenciodynamic Polarization

Brenda Caroline da Silva Cardozo[1], Tatiana Das Chagas Almeida[3], Oscar Rosa Mattos[2]

Abstract

Corrosion by CO_2 is one of the main forms of deterioration in carbon steel installations in the oil and gas industry. This type of corrosion is influenced by several variables, such as pH, temperature, pressure and salt concentration. OBJECTIVE: To investigate the behavior of inhibitors in the corrosion of carbon steel, varying the pH, keeping constant the CO_2 pressure, temperature and salt concentration. To carry out this study, mass loss tests to characterize the anticorrosive performance of the inhibitors and polarization curves were performed to characterize the inhibition mechanisms of each compound. METHODOLOGY: Carbon steel samples in triplicate were immersed in solutions containing the same salt concentration, pressure and temperature, only varying the pH. Linear polarization measurements were performed using a classic three-electrode system, namely: the platinum counter electrode, the carbon steel working electrode and a reference electrode. The potential range used was + or - 500 mV in relation to the OCP at a speed of 0.125 mV/s. RESULTS: The influence of pH can be evaluated by comparing the corrosion rate behavior of the solutions called blanks with those containing the inhibitors. The linear polarization curves will still be performed. CONCLUSION: By comparing the values obtained, it is possible to determine the anticorrosive efficiency of the inhibitors for carbon steel in environments with high saline and CO_2 concentrations.

Keywords: CO_2 corrosion; mass loss; CO_2 inhibitor; linear polarization

[1] UFRJ. Brazil. E-mail: brendacscardozo@metalmat.ufrj.br (https://orcid.org/0009-0001-4787-6507).

[3] UFRJ. Brazil. E-mail: talmeida@metalmat.ufrj.br (https://orcid.org/0000-0002-7677-8375).

[2] UFRJ. Brazil. E-mail: omattos@metalmat.ufrj.br (https://orcid.org/0000-0003-1551-0997)

1 Introduction

CO_2 corrosion is one of the main forms of destruction in carbon steel installations in the oil and gas industry. This type of corrosion is influenced by several variables, such as pH, temperature, pressure and salt concentration. The progressive metal loss caused by corrosion directly undermines the structural integrity of pipelines, increasing the likelihood of leaks, ruptures, and operational failure. In extreme cases, this can lead to environmental contamination, economic losses, and serious safety hazards.

To mitigate corrosion issues, several corrosion inhibitors have been developed, with increasing emphasis on inhibitors obtained from renewable sources. Biomass is a renewable and low-cost raw material with great potential for obtaining organic compounds through sustainable routes (CORTÉS et al., 2013; ANTUNES et al., 2021).

Thus, this work aims to evaluate the performance of furfural, vanillin and cysteamine as corrosion inhibitors in saline media containing CO_2, through mass loss and potentiodynamic polarization tests. The objective is to identify the potential of these compounds as sustainable and effective alternatives for anticorrosive protection of 1020 carbon steel.

2 Methodology

The evaluation of the performance of the molecules tested as inhibitors was performed through mass loss tests and electrochemical tests.

2.1. Test media solutions

The solutions of each medium were prepared according to the simulations performed in the Oli systems® software and are described in Table 1.

Medium	pH	Temperature (°C)	NaCl (ppm)	NaOH (ppm)	Inhibitor (ppm)	Ethanol co-solvent (mL)
Blank	6,0	25	80000	905	-	-
Inhibitor TF			80000	905	50	50
Inhibitor TV			80000	905	25	50
Blank	8,0		80000	23000	-	-
Inhibitor TF			80000	23000	50	50
Inhibitor TV			80000	23000	25	50

Table 1 - Composition of the solutions used in the potentiodynamic polarization and mass loss tests of carbon steel 1020 at pH 6 and 8.
Source: Prepared by the authors (2025).

2.2. Anti-corrosive performance characterization tests

2.2.1. Potentiodynamic Polarization Tests

To perform the potentiodynamic polarization test, a 3-electrode electrochemical cell was used: the 1020 carbon steel working electrode with the surface prepared using silicon carbide papers (grit sizes 600), a saturated calomel reference electrode (SCE) and a platinum grid as counter electrode. Electrochemical analyses were performed using an Autolab PGSTAT30 potentiostat. Potentiodynamic polarization tests were performed from -500 mV to +500 mV in relation to the stable OCP with a scan rate of 0.167 mV/s. The tests were performed in duplicate.

2.2.2. Mass Loss Tests

The immersion of the specimens was carried out in a 1000 mL glass for 24 hours of duration, at room temperature using the solutions contained in Table 1 under continuous CO2 bubbling. After the immersion, the mass loss was performed according to ASTM G1 standard.

3 Results

The mass loss results are shown in Figure 3. In this figure, both media with addition of TF and also TV inhibitor presented lower mass loss compared to the "blank" media (contained in Table 1).

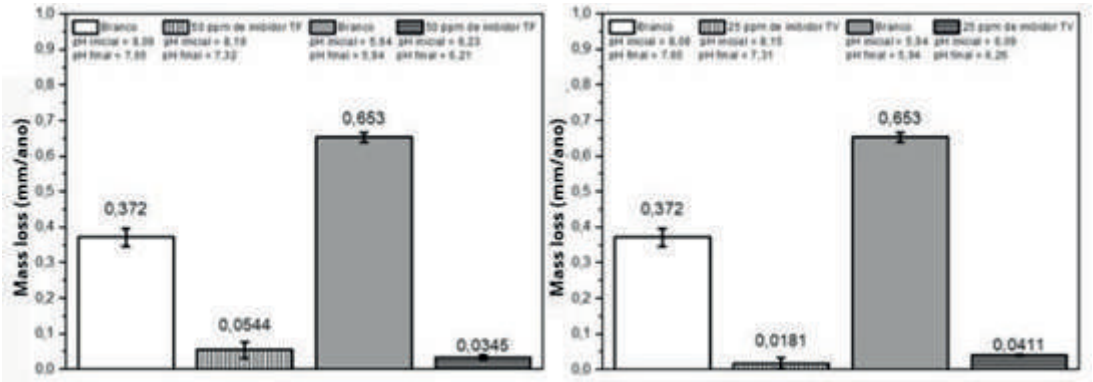

Figure 3 - Mass loss of the average of triplicates after 24 hours of immersion of 1020 carbon steel in different media (a) with and without TF inhibitor and (b) with and without TV inhibitor.
Source: Prepared by the authors (2025).

Medium	pH	Temperature (°C)	NaCl (ppm)	NaOH (ppm)	Inhibitor (ppm)
Blank	5,94	5,94	0,653	0,0141	Reference to pH 6
Inhibitor TF	6,23	6,21	0,0345	0,00645	94,72%
Inhibitor TV	6,09	6,26	0,0411	0,00154	93,71 %
Blank	8,09	7,65	0,372	0,0253	Reference to pH 8
Inhibitor TF	8,19	7,32	0,0544	0,0230	85,37%
Inhibitor TV	8,15	7,31	0,0181	0,0167	95,13 %

Table 2 - Corrosion inhibitor performance after 24 hours of immersion of 1020 carbon steel in different media, with and without inhibitors.
Source: Prepared by the authors (2025).

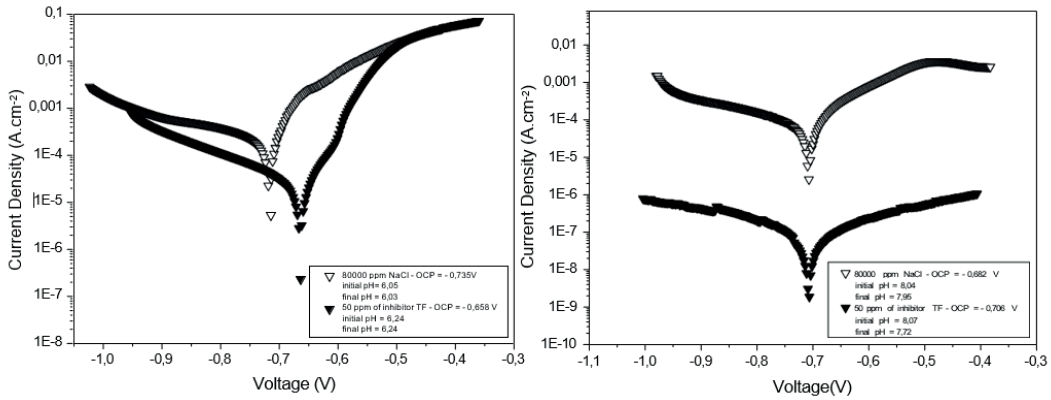

Figure 4 - Potentiodynamic polarization with and without addition of TF inhibitor (a) pH 6 and (b) pH.
Source: Prepared by the authors (2025).

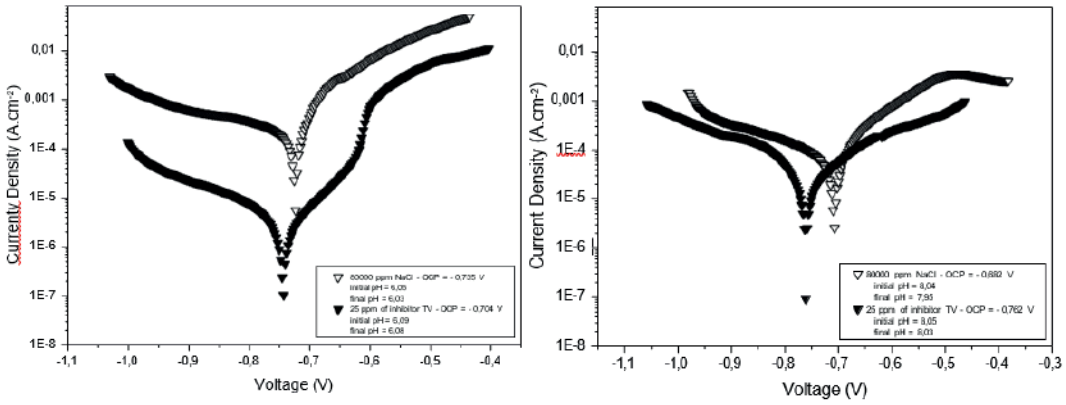

Figure 5 - Potentiodynamic polarization with and without addition of TV inhibitor (a) pH 6 and (b) pH 8.
Source: Prepared by the authors (2025).

4 Discussion

Table 2 shows that the TF inhibitor demonstrated good efficiency at pH 6, 94.72 %. At pH 8, the efficiency was 85.37 %. For TV inhibitor, the efficiency at pH 6, was 93.71% and at pH 8 reached the best performance, 95.13%.

The polarization curves performed in both media, blank and with the addition of TF inhibitor are presented in Figure 4. At both pH 6 and pH 8, a decrease in anodic and cathodic current density was observed with no significant displacement of Ecorr, with the addition of TF at pH 8. For TV inhibitor a similar behavior can be seen at Figure 5, in which TV inhibitor played a role in the anodic and cathodic branches.

5 Conclusion

TF inhibitor demonstrated good efficiency in a medium containing a high concentration of sodium chloride and the presence of CO2, at pH 6, reaching 94.72%, close to the target of 95%. At pH 8, although lower than the target, a significant reduction in the corrosion rate was observed, with an efficiency of 85.37%. The study indicated that the effectiveness of the TF inhibitor decreases with increasing pH. The TV inhibitor presented promising results, with an efficiency of 93.71% at pH 6 and 95.13% at pH 8, showing a slight improvement at the most basic pH.

6 Acknowledgments

I would like to thank Dr. Jéssica Nogueira, Dr. Michelle Jakeline and Mechanical Engineer Felipe Renan. And I would also like to thank the National Petroleum Agency (ANP) and São Paulo State Research Support Foundation (FAPESP) for the prh7 scholarship.

Referências

Antunes, M. M., Silva, A. F., Bernardino, C. D., Fernandes, A., Ribeiro, F., & Valente, A. A. (2021). Catalytic transfer hydrogenation and acid reactions of furfural and 5-(hydroxymethyl)furfural over Hf-TUD-1 type catalysts. Molecules, 26(23), 7203. https://doi.org/10.3390/molecules26237203

ASTM International. (2017). ASTM G1-03(2017): Standard practice for preparing, cleaning, and evaluating corrosion test specimens. ASTM International. https://doi.org/10.1520/G0001-03R17

Banuprakash, G., [et al.], (2021). Failure analysis and prevention of corrosion in mild steel: A review. Journal of Failure Analysis and Prevention, 21, 89–96. https://doi.org/10.1007/s11668-020-01036-z

Borges, J. N. (n.d.). Preparação de amostras para análise microestrutural [Apostila]. Universidade Federal de Santa Catarina. https://pavanati.com.br/doc/Apostila%20Ana%20Maliska%20-%20Preparacao%20Microestrutural.pdf

Cortés, W., Piñeros-Castro, Y., & Campos Rosario, A. M. (2013). Conversion of D-xylose into furfural with aluminum and hafnium pillared clays as catalyst. Dyna, 80(180), 105–112.

Da Cunha, J. N., [et al.], (2019). Study of furfural derivatives as a possible green corrosion inhibitor for mild steel in CO_2-saturated formation water. Corrosion Science, 155, 36–47.

D'Arrigo, P., Rossato, L. A. M., Strini, A., & Serra, S. (2024). From waste to value: Recent insights into producing vanillin from lignin. Molecules, 29(2), 442. https://doi.org/10.3390/molecules29020442

Jacob, K. S., & Parameswaran, G. (2010). Corrosion inhibition of mild steel in hydrochloric acid solution by Schiff base furoin thiosemicarbazone. Corrosion Science, 52, 224–228. https://doi.org/10.1016/j.corsci.2009.09.007

Kamarul Baharin, N. A. N., Sheikh Ahmad Izaddin Sheikh Mohd Ghazali, S. A. I., Sirat, S. S., Tajuddin, A. M., Pungot, N. H., Normaya, E., Kamarudin, S. R. M., & Dzulkifli, N. N. (2024). In-depth investigation of corrosion inhibition mechanism: Computational, electrochemical, and theoretical studies of vanillin meldrum's acid on mild steel surface in 1 M HCl.

Negm, N. A., [et al.], (2012). Gravimetric and electrochemical evaluation of environmentally friendly nonionic corrosion inhibitors for carbon steel in 1M HCl. Corrosion Science, 65, 94–101.

Song, P., Guo, X.-Y., Pan, Y.-C., Shen, S., Sun, Y., Wen, Y., & Yang, H.-F. (2013). Insight in cysteamine adsorption behaviors on the copper surface by electrochemistry and Raman spectroscopy. Electrochimica Acta, 89, 503–509. https://doi.org/10.1016/j.electacta.2012.11.096

Wu, B.-Q., Wang, Y.-J., Chang, C.-C., Juang, T.-Y., Huang, Y.-H., & Hsu, Y.-C. (2024). Clinical efficacy of cysteamine application for melasma: A meta-analysis. Journal of Clinical Medicine, 13, 7483. https://doi.org/10.3390/jcm13237483

Zhao, C., Xu, Y., Li, D., Zhao, X., Xu, Y., Zhang, L., & Wu, Y. (2019). Cysteamine modified polyaspartic acid as a new class of green corrosion inhibitor for mild steel in sulfuric acid medium: Synthesis, electrochemical, surface study and theoretical calculation. Progress in Organic Coatings, 129, 159–170. https://doi.org/10.1016/j.porgcoat.2018.12.028

Stress corrosion cracking of flexible steel pipe wires in CO_2 environments

Jackson Wo[1], Fabricio Pinheiro dos Santos[2], John Rothwell[3], Kasra Sotoudeh[4], Michael Dodge[5]

Abstract

Stress corrosion cracking (SCC) in CO_2 environments poses a significant challenge to flexible steel pipe armour wires but remains poorly understood due to difficulties in laboratory replication, hindering mitigation strategies. This study outlines an experimental methodology to initiate SCC under controlled conditions. Un-corroded flexible steel wire samples underwent 4-point bend loading tests in an autoclave containing CO_2 and 3.5% NaCl solution. By varying parameters such as immersion depth, temperature, and duration, conducive conditions for SCC were identified. Advanced characterisation identified several surface-initiated cracks propagating into the parent metal with multiple branching paths. Significant oxide scales within the cracks suggested a potential link between oxidation/pitting and crack initiation. The implications and applicability of the methodology for elucidating SCC mechanisms are discussed, with potential applications in developing novel prediction techniques to prevent catastrophic failures and ensuring long-term durability of flexible steel pipes in CO_2-rich environments across various industries.

Keywords: Stress corrosion cracking; CO_2; Steel

[1] TWI Ltd. United Kingdom. E-mail: jackson.wo@twi.co.uk (https://orcid.org/0000-0002-7635-947X).

[2] Petrobras. Brazil. E-mail: fabricio.santos@petrobras.com.br (https://orcid.org/0009-0008-3080-4639).

[3] TWI Ltd. United Kingdom. E-mail: john.rothwell@twi.co.uk.

4 TWI Ltd. United Kingdom. E-mail: kasra.sotoudeh@twi.co.uk.

5 TWI Ltd. United Kingdom. E-mail: michael.dodge@twi.co.uk

1 Introduction

Steel armour wires are an integral component of flexible pipes. Located in the annulus of the pipe between the inner and outer polymer sheathes, these wires provide the tensile strength required to transfer load from seabed to surface (American Petroleum Institute;, 2008). Deep-water fields rich in CO_2 can lead to elevated CO_2 partial pressures in the annulus and potentially CO_2 stress corrosion cracking (SCC-CO_2).

The chemical reactions and mechanisms that underpin CO_2 corrosion have been relatively well documented (Pimentel, et al., 2025; Nesic, 2007; Fonseca, et al., 2024) where an increase in CO_2 pressure can result in the formation of a pseudo-passivating iron carbonate ($FeCO_3$) scale on the surface of the metal. While it is expected that the $FeCO_3$ scale may reduce corrosion rates, SCC-CO_2 cracking has been nonetheless reported in flexible pipes after two years of operation (Agência Nacional do Petróleo, 2017; da Silva, 2022) and is widely recognised as a failure mechanism of concern to the industry, (Macleod, 2023).

In recent years, several experimental studies have focused on understanding the conditions and underlying mechanisms that lead to SCC-CO_2 of armour wires. Santos et al. (Santos, Poloponsky, Modiano, Ribeiro, & Motta, 2020) subjected two carbon steel grades to four-point bending tests (4PB) and slow strain rate testing (SSRT). The study revealed that 4PB specimens tested at 10.6 bar CO_2, 40°C, and 90 days resulted in SCC-CO_2 failures. Specimens that were tested for longer periods did not result in any observed failures. De Motte et al. (De Motte, et al., 2022) studied the effects of CO_2 fugacity, temperature and applied stress on SCC in several carbon steel armour wires that were partially submerged in water. They observed that the formation of $FeCO_3$ was enhanced with increasing CO_2 fugacity and temperature. Moreover, it was observed that cracks tended to occur more frequently in the specimen areas that were located in the vapour space (i.e. above the water line in the test vessel). Similarly to Santos et al. (Santos, Poloponsky, Modiano, Ribeiro, & Motta, 2020), it was found that 40°C was conducive to SCC failure. In addition, the authors also observed

that 15 bar of CO_2 and an applied stress equal to 100% of the yield strength resulted in SCC. Pimentel et al. (Pimentel, et al., 2025) recently studied SCC-CO_2 phenomena in tensile armour wires using several laboratory methods at 10.6 barg CO_2 and 40°C in synthetic seawater. In particular, the study employed SSRT, 4PB, constant load tests, as well as a novel "alternating load" test. The various methods showed mixed success in replicating SCC-CO_2, but the alternating load test was relatively successful in inducing SCC-CO_2. This was associated with the periodic disruption of the protective FeCO3 scale, providing a localised corrosion pathway at the sample surface. Decreasing the CO_2 pressure and temperature generally led to reduced SCC-CO_2 behaviour.

It is clear that SCC-CO_2 poses a significant challenge to the integrity of subsea flexible pipes. Although some studies have reported success in replicating SCC-CO_2, it remains relatively difficult to predict and reproduce in laboratory settings, hindering mitigation strategies and reliable qualification within reasonable timeframes. For example, previous tests carried out by the authors of this study at 20 bar CO_2 at temperatures of 40 to 60°C for 60 days did not result in cracking. As such, the purpose of this paper is to further investigate the requisite experimental conditions, with the heats of material available to the authors, that could potentially lead to SCC-CO_2 cracking and compare results obtained with other investigators.

2 Methodology

In this study, samples were prepared from commercial flexible armour wires that were designated as "A", "B", and "C" (Table 1), with strength grades defined by UTS values of >1400 MPa, >1200 MPa, and > 1350 MPa, respectively. The wires were pre-formed to a curvature such that a cold strain representative of that in a helically wound wire was present. The C specimens also featured welds at the mid-length position, in order to evaluate a range of microstructures that may be susceptible to cracking.

Sample	Composition (wt.%)											
	Fe	C	Cr	Cu	Mn	Ni	Si	P	S	N	O	Al
A	Bal.	0.68	-	-	0.78	-	0.25	0.02	0.01	-	-	0.002
B	Bal.	0.72	-	-	0.86	-	0.23	0.01	0.01	-	-	0.053
C	Bal.	0.69	0.03	0.02	0.63	0.01	0.18	0.01	0.01	0.004	0.002	-

Table 1 – Composition of the steel wires used in this study (wt.%).
Source: Prepared by the authors (2025).

To replicate SCC, each sample was subjected to a 4-point bend configuration such that the intrados was placed in tension, loaded to a strain equivalent to 0.2% proof stress. The samples were placed in custom autoclaves filled with 3.5 wt.% NaCl solution deaerated with N2 (< 5 ppb O2) such that the samples were half-submerged (Figure 1). This allowed for a comparison between the submerged and non-submerged (vapour space) conditions. This process was repeated for equivalent samples that were completely submerged as well as completely in the vapour space. However, characterisation of these samples were not included in the scope of this study for brevity. The test pressure was set to 15 barg in each autoclave. Autoclave tests were carried out at: (i) 40°C for 180 days, (ii) temperature cycling from 30°C to 60°C for 100 days (temperature was changed from 30°C to 60°C and vice versa on a weekly basis), and (iii) 60°C for 128 days (Table 2). The solution volume to sample surface area ratio was 1 mL/cm2. In situ monitoring of the pH and dissolved iron content were conducted.

Wire	A	B	C	A	B	C	A	B	C
Testing Temperature (°C)	40	40	40	30-60	30-60	30-60	60	60	60
Sample Name	A40	B40	C40	A3060	B3060	C3060	A60	B60	C60

Table 2 – Sample names and testing temperatures.
Source: Prepared by the authors (2025).

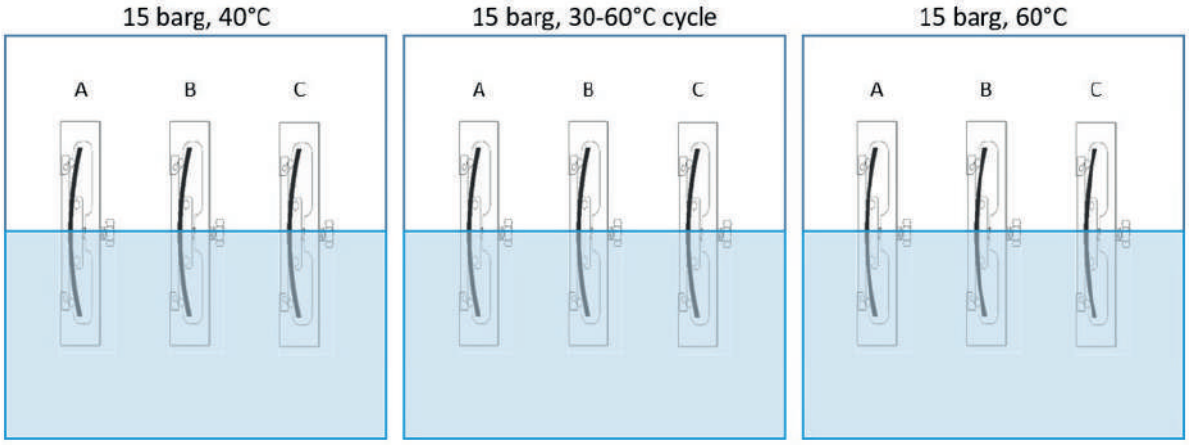

Figure 1 – Three samples were loaded in 4-point bend configurations and half-submerged in 3.5 wt.% NaCl solution in each deaerated CO2-containing autoclave. Tests were carried out at 40°C for 180 days, 30-60°C for 100 days, and 60°C for 128 days. The pressure was 15 barg in all tests.
Source: Prepared by the authors (2025).

After SCC-CO_2 testing, samples were subjected to magnetic particle inspection (MPI) to identify indications of cracks. Benchtop MPI with a coil (current flow) at light levels of 0.5 lux and 2000 µW/cm2 with fluorescent magnetic ink was used. The sample surfaces were also visually examined at several magnifications. Metallographic cross-sections were subsequently prepared from the samples and hot-mounted in conductive resin, followed by grinding and polishing to a suitable finish for scanning electron microscopy (SEM).

Microstructural examination of the polished cross-sections was performed with a Zeiss Σigma Field-Emission Gun SEM (FEGSEM) equipped with an Oxford Instruments electron dispersive X-ray (EDX) detector. Both secondary electron (SE) and backscattered electron (BSE) imaging modes were used. The accelerating voltage was 20 kV and the working distance was approximately 8.5 mm. In addition, electron backscatter diffraction (EBSD) analysis was carried out with an attached Oxford Instruments EBSD detector with an accelerating voltage of 30 kV. The sample orientation was such that the rolling direction was parallel to the length of the wires. EBSD data was collected at step sizes ranging from 0.06 to 0.15 µm and outputted as an orientation image map with inverse pole figure (IPF) colouring. HKL Channel 5 software was used to carry out a light clean-up routine to reduce noise and interpolate any misindexed data points was used on all samples. All SEM data were collected and processed in Oxford Instruments AZtec software.

Powder X-ray diffraction (XRD) data were acquired for samples (where surface corrosion scale products could be physically removed after SCC-CO2 testing) for phase identification using a Bruker D8 ADVANCE fixed sample X-ray diffractometer fitted with a LynxEye XE position-sensitive detector. The diffraction data was collected over a 2θ range of 10-70° with a step size of 0.01°, 250 ms/step dwell time, and wavelength of 1.54060 Å. TOPAS software (Coelho, 2018) was used to compile the data and PDF files were obtained from the Inorganic Crystal Structure Database (ICSD) through the Physical Sciences Data-Science Service (PSDS) (FIZ Karlsruhe GmbH, 1985).

3 Results

3.1. Post-test Images

Photographs of the samples (both sides) after SCC-CO2 testing are shown in Figure 2. Samples had generally similar appearances. However, B40 showed signs of severe corrosion such that large pits corroded through the thickness of the sample. Samples C40, C3060, and B60 showed significant formation of non-adherent corrosion scales that were relatively easy to remove.

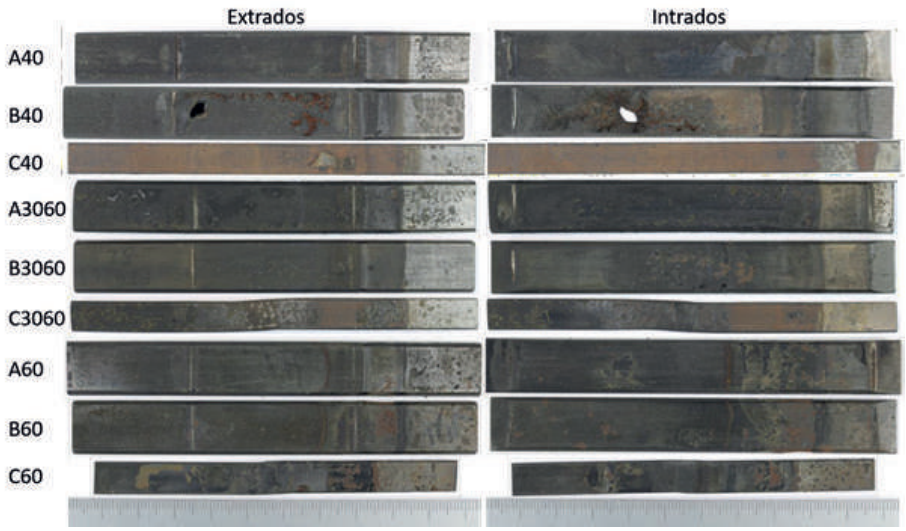

Figure 2 – Photographs of samples after SCC-CO_2 testing. Note the severe corrosion observed in sample B40. Source: Prepared by the authors (2025).

Light microscopy images of the microstructures of the samples are shown in Figure 3. In general, similar microstructures were observed in all samples, i.e. very fine pearlitic microstructure with elongated grains in the rolling direction except in the location of the weld in sample C3060, which had a more equiaxed structure.

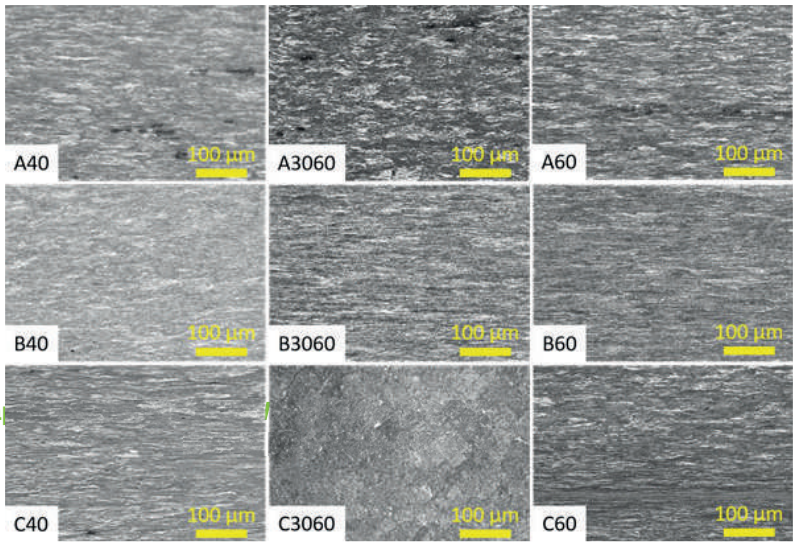

Figure 3 – Light microscopy images of sample microstructures. Elongated grains (left to right) are generally visible. Samples were etched with ~2% Nital. Source: Prepared by the authors (2025).

3.2. MPI

Indications of interest were detected in samples A3060, B60, and C60 (Figure 4). No indications were detected in the other samples.

In sample A3060, several indications with lengths ranging from 1 mm to 5 mm were detected (intrados). In sample B60, two indications with approximate lengths of 4 mm and 5 mm were detected at the intrados. In sample C60, one indication with an approximate length of 7 mm was detected on the extrados. All indications were located perpendicular to the length of the samples. Metallographic cross-sections through these indications were prepared for SEM analysis. It was subsequently determined that only the indications in B60 were cracks.

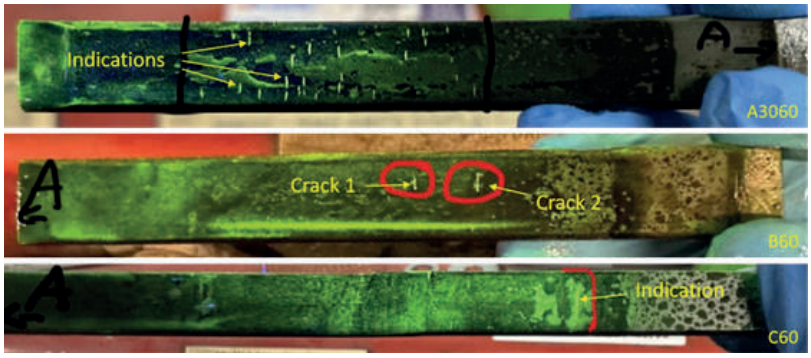

Figure 4 – Magnetic particle inspection (MPI) results for samples A3060, B60, and C60. Indications are visible on the surface of the samples as denoted by the yellow arrows. Cracks were identified in B60. The letter A denotes the datum. No indications were detected on other samples. Source: Prepared by the authors (2025).

3.3. XRD

XRD diffraction patterns for corrosion products removed from samples C40, C3060, and B60 are shown in Figure 5. Prominent diffraction peaks corresponding to FeCO3 (siderite), FeO(OH) (Akaganeite-Q), and Fe3C (Cohenite/Cementite) were identified in all samples. Pattern fitting was performed with the following powder diffraction files (PDF): 01-083-1764 (Siderite), 03-065-2411 (Cohenite/Cementite), and 00-034-1266 Fe3+O(OH) (Akaganeite-Q, syn). Minor peaks (~29° and 30.8°) could not be conclusively identified – these may be attributed to Fe3O4 (magnetite) but further investigation is needed for confirmation.

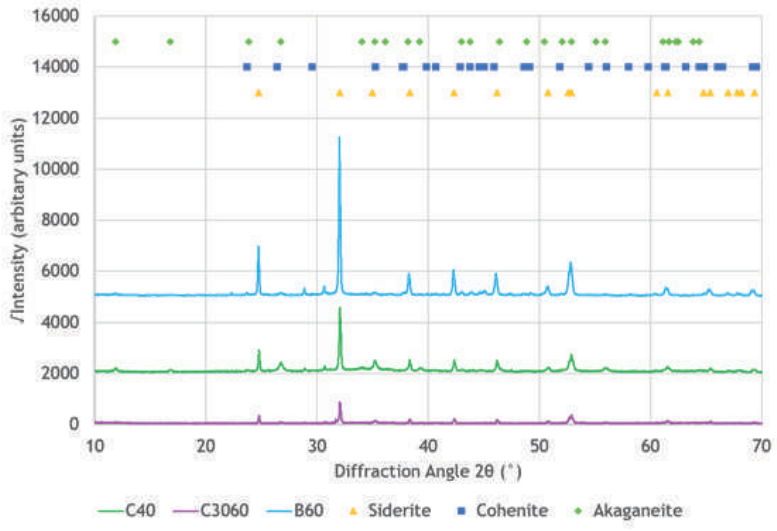

Figure 5 – X-ray diffractograms for surface corrosion scale powders (shown with increasing offset) removed from samples C40 (green), C3060 (magenta), and B60 (blue). Symbols at the top of the plot denote peak locations associated with siderite, cohenite, and akaganeite. Source: Prepared by the authors (2025).

3.4. SEM

Two cracks were detected in sample B60 by MPI. SEM-BSD micrographs of crack 1 in B60 and the corresponding EDX spectrum is shown in Figure 6. The crack appears to have initiated at the surface at a shallow pit and propagated approximately 200 μm into the substrate. The inner region of the crack is characterised by a 'core' of corrosion product homogeneous in character, whereas the adjacent outer 'shell' region has the 'ghost' structure of the steel still visible. This form of product is consistent with a penetrative form of CO2 corrosion where a cementite network acts as the cathodic pathway and the corrosion product remains within it. Cell boundaries are visible in the 'ghost' structure, and it appears that the crack 'core' has progressed with relative insensitivity to these cell boundaries, indicating a transgranular nature. The EDX spectrum shows elevated levels of Fe, Mn, and O, with relatively minor concentrations of C, S, and Cl.

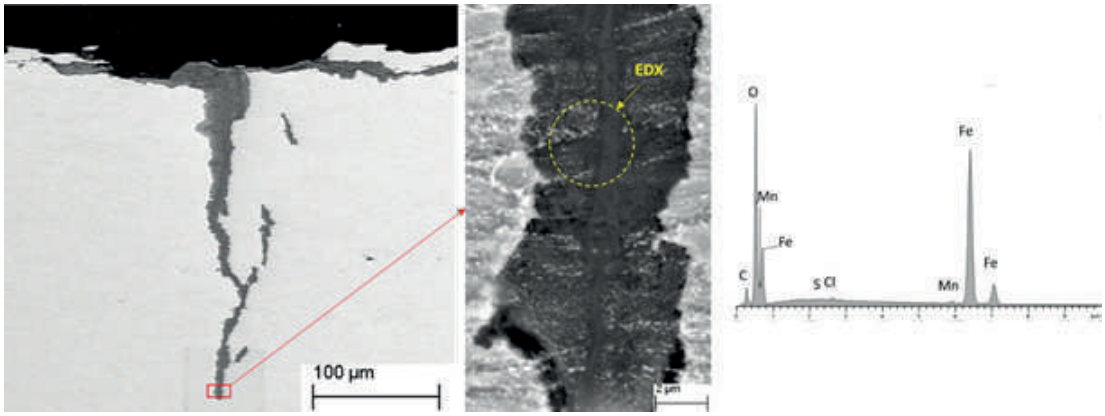

Figure 6 – SEM-BSD cross-sectional images of crack 1 in sample B60 (left, middle). The middle figure is a high-magnification image of the area ensconced within the red rectangle in the left image. The EDX spectrum (right) corresponds to the spot size of the beam (2.5 μm, dotted yellow circle) in middle image. Source: Prepared by the authors (2025).

The EBSD IPF map for the tip of crack 1 in B60 is shown in Figure 7. It shows mostly fine grains are visible adjacent to the crack tip, but relatively large grains were observed in front of the crack tip. It is unclear if these grains were coincidentally located or had a stopping effect on crack propagation.

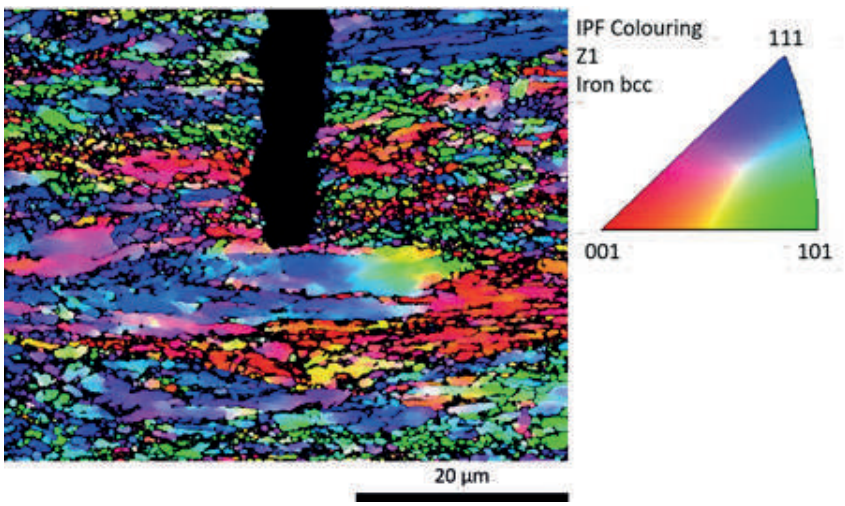

Figure 7 – EBSD orientation image map with inverse pole figure (IPF colouring) of the tip of crack 1 in sample B60. Fine grains are visible adjacent to the crack and relatively large grains are present in front of the crack. Source: Prepared by the authors (2025).

SEM-BSD cross-sectional micrographs of crack 2 in B60 and corresponding EDX spectrum are shown in Figure 8. Similar to crack 1, crack 2 may have originated from a shallow surface pit and propagated about 450 μm into the substrate with similar inner and outer crack regions. A degree of side branching was observed. Both the core and shell were rich in Fe, Mn, and O while the shell region had minor concentrations of Mo.

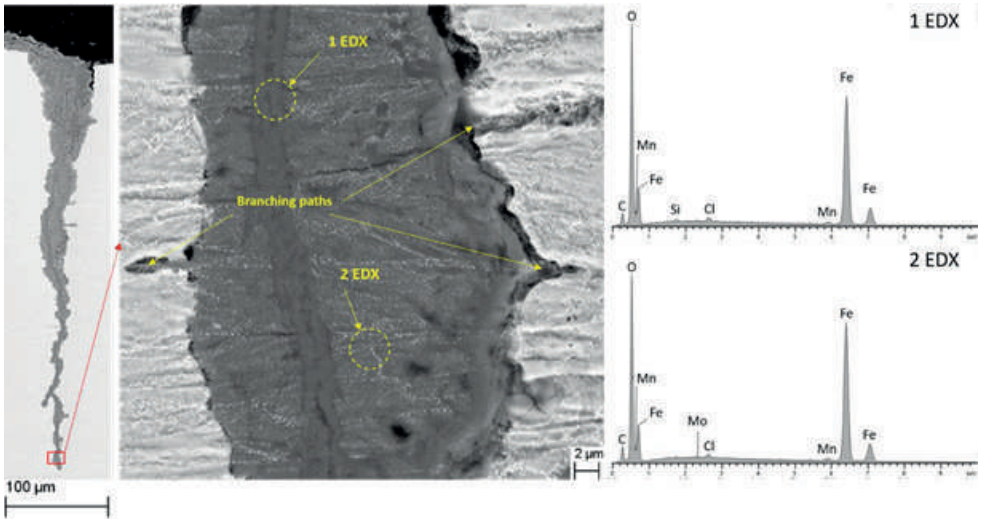

Figure 8 – SEM-BSD cross-sectional images of crack 2 in sample B60 (left, middle). The middle figure is a high-magnification image of the area ensconced within the red rectangle in the left image. The EDX spectra (right) correspond to the dotted yellow circles (spot size of the beam, 2.5 μm) in the middle image. Source: Prepared by the authors (2025).

The EBSD IPF map for crack 2 in B60 is shown in Figure 9. Significant distributions of fine grains are visible adjacent to the crack – no preferential grain orientation for crack propagation is apparent. A concentration of grains oriented along the [111] direction is visible approximately 35-40 μm above the crack tip.

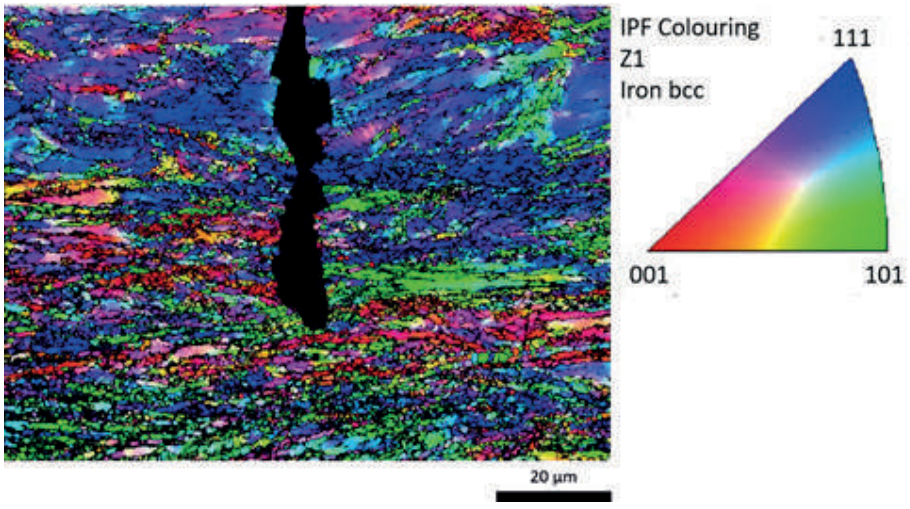

Figure 9 - EBSD orientation image map with inverse pole figure (IPF colouring) of the tip of crack 2 in sample B60. Fine grains are visible adjacent to the crack. A region of grains oriented along the [111] direction is visible approximately 35-40 μm above the crack tip. Source: Prepared by the authors (2025).

Although no MPI indications were found, a cross-section through pitting that was identified visually on the intrados surface of B3060 revealed cracking. The SEM-BSD image and corresponding EDX spectrum are shown in Figure 10. The crack is located at the base of a significant pit. A "bulbous" morphology of the crack with wide and narrow sections is also observed, indicating a degree of arrest. Similar to the cracks in B60, a core and shell corrosion structure was observed within the crack. The EDX spectra identified Fe, Mn, and O and trace amounts of Si, P, C, and Cl. Trace amounts of Al were detected in the corrosion scale of the pit in addition to Fe, Mn, and O.

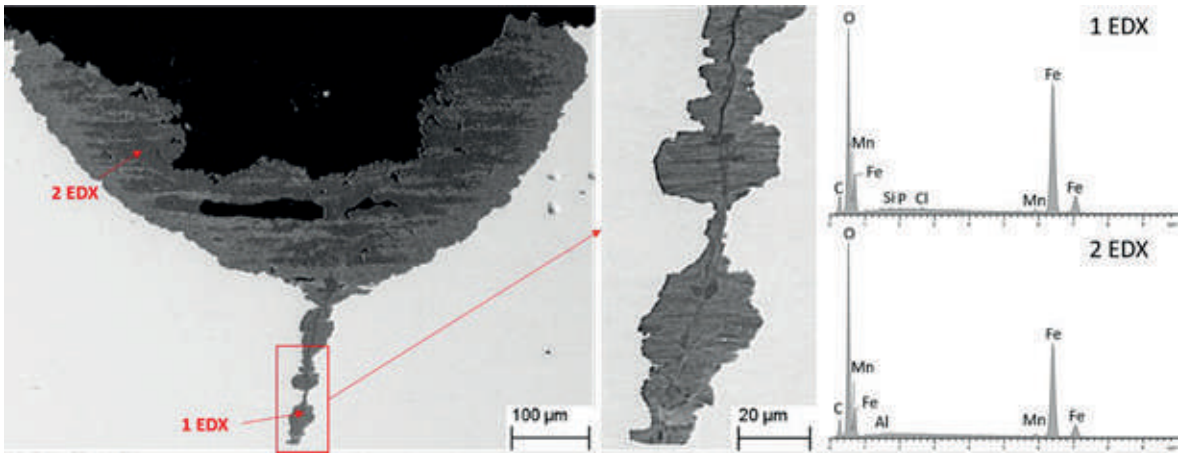

Figure 10 - SEM-BSD cross-sectional images of the crack and pit in sample B3060 (left, middle). The middle figure is a high-magnification image of the area ensconced within the red rectangle in the left image. The EDX spectra (right) correspond to the red arrows (beam spot size: 2.5 µm) in the left image. Source: Prepared by the authors (2025).

The EBSD IPF map for the crack in B3060 is shown in Figure 11. A significant number of elongated grains are visible adjacent to the crack. A concentration of grains oriented along the [001] direction (red) are consistent with the narrow channel between the wider sections of the crack.

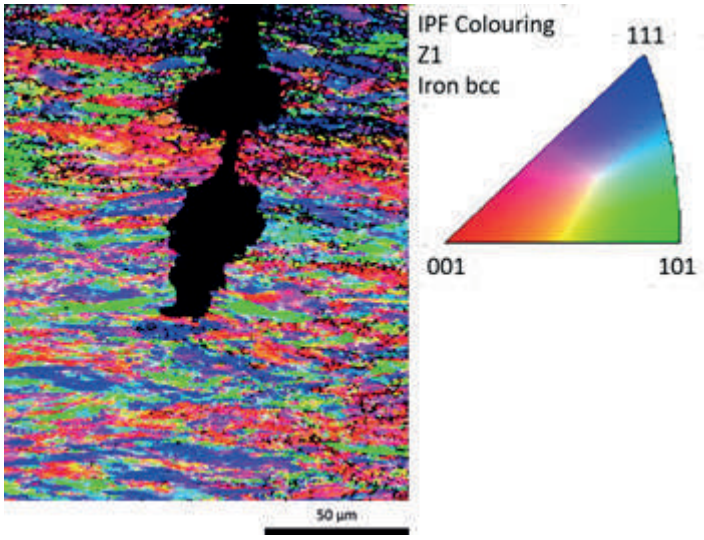

Figure 11 - EBSD orientation image map with inverse pole figure (IPF colouring) of the crack tip in sample B3060. Significant concentrations of elongated grains are visible adjacent to the crack. Several grains oriented along the [001] direction are located around the narrow channel of the crack between wider crack sections.
Source: Prepared by the authors (2025).

4 Discussion

It is notable that only two out of nine test specimens were found to contain SCC-CO2 cracks, which were relatively isolated instances and located in the submerged portion of the specimens.

Furthermore, no instances of cracking were identified at the lower temperature of 40°C. The findings are in contrast to nominally similar studies (Hanonge, Ferraz, & Ferre, 2022; Santos, Poloponsky, Modiano, Ribeiro, & Motta, 2020; De Motte, et al., 2022) in which extensive cracking was identified in the vapour phase portion of specimens tested at 40°C, 15 bar, and similar loads. These results suggest that there may be additional factors other than the applied stress, CO_2 concentration, and temperature that have significant effects on SCC-CO_2 initiation in these materials.

In the present study, tests at 40°C induced aggressive pitting corrosion behaviour in sample B40 sufficient to penetrate the full thickness of the sample, but without any observable cracking. For the same material B, cycling the temperature appeared to offer a transition between pitting and cracking whilst testing at 60°C resulted in cracking being present with only shallow pits.

In the case of B3060, the formation of a large pit where thick oxide/corrosion scales formed on the surface was observed. The initiation of a crack at the base of this pit potentially suggests that a local area in the substrate was subjected to locally aggressive conditions that subsequently led to crack initiation. The bulbous shape of the crack, as evidenced by the SEM-BSD and EBSD images, suggests a degree of intermittent arrest and the potential existence of preferential paths of lateral selective corrosion along the internal crack surfaces, where corrosion of the parent metal is promoted. Therefore, differences in the microstructure (e.g. number of grain boundaries, strain) may have a resistance effect to crack propagation and corrosion, leading to the bulbous crack morphology.

Materials A and C appeared unaffected by SCC-CO_2 or pitting, despite having higher strengths. The lack of demonstrated susceptibility is remarkable given the aggressive test conditions and broadly similar metallurgical characteristics. Further characterisation of these materials might aid the understanding of any further metallurgical factors that may have positively enhanced their resistance to SCC-CO_2.

The detected phases in the XRD diffractograms aligned well with the intensities and peak locations of the diffraction patterns and were generally consistent with compounds expected to form on iron surfaces exposed to CO2 in deaerated solution, with siderite appearing as the dominant product. It is hypothesised that minor peaks at approximately 29° and 30.8° may correspond to magnetite (Fe_3O_4), as reported by Wang et al. (Wang, Ye, Li, & Liu, 2022).

In general, the relatively high temperatures and insensitivity to specimen strength suggests that an anodic SCC mechanism is in effect rather than hydrogen-driven mechanisms. Cracking appeared largely insensitive to grain boundaries and significant corrosion products were present at the crack tips, suggesting that a protective film rupture mechanism was active, in agreement with other studies. In addition, it is acknowledged that SEM imaging only provides information for a 2-D cross-section while cracks may exhibit 3-D networks. Advanced techniques such as atom probe tomography (Meisnar, Moody, & Lozano-Perez, 2015) and/or focused ion beam SEM (FIB-SEM) may be beneficial for further work in understanding 3-D SCC-CO2 crack growth in these materials.

5 Conclusion

Flexible steel armour wires were tested in 4-point bend configurations in a 3.5 wt.% NaCl and CO2 environment at various temperatures (40°C, 30 to 60°C cycling, 60°C), 15 barg, and loaded to near yield stress. Despite the relatively aggressive conditions, only three instances of cracking were observed. Cracking was limited to submerged regions of material B and test temperatures above 40°C, which differed significantly from other studies that used nominally similar materials and testing conditions (Hanonge, Ferraz, & Ferre, 2022), suggesting that factors other than stress, CO_2 concentration, and temperature may influence SCC-CO_2 cracking. Microstructural features, such as coarse grains at the crack tips, suggested that metallurgical factors could play a critical role in defining the susceptibility of steel wires to SCC-CO_2 cracking.

6 Acknowledgments

The authors acknowledge the joint financial and technical support of Petróleo Brasileiro S.A. (Petrobras) and TWI Ltd. In addition, the authors wish to thank colleagues at TWI Ltd for experimental assistance (Diane Shaw, Ramin Taheri, Sally Day, and Triston Dourado) and administrative support (Amitha Vivian, Diena Bolton, and Hollie Breed). Special gratitude is extended to Prof. Shiladitya Paul for technical review of the manuscript.

Referências

Agência Nacional do Petróleo. (2017). Safety alert 001-ANP/SSM: CO_2 stress corrosion cracking (SCC-CO2). ANP. https://www.gov.br/anp/pt-br/assuntos/exploracao-e-producao-de-oleo-e-gas/seguranca-operacional/incidentes/arquivos-alertas-de-seguranca/alerta-01/safety-alert_001_ssm_scc-co2_en.pdf

American Petroleum Institute. (2008). Recommended Practice for Flexible Pipe 17B Fourth Edition. Washington, D.C. API Publishing Services. https://www.api.org/~/media/files/publications/whats%20new/17b%20e5%20pa.pdf

Coelho, A. (2018). TOPAS and TOPAS-Academic: an optimization program integrating computer algebra and crystallographic objects written in C++. Journal of Applied Crystallography, 51, 210-218. https://doi.org/10.1107/S1600576718000183

da Silva, P. (2022). Investigation into the Stress Corrosion Cracking of Tensile Wires of Flexible Pipes in Different Simulated Annulus Environments Containing CO2 (Doctoral dissertation). COPPE UFRJ, Rio de Janeiro, Brazil. https://www.researchgate.net/publication/367990889_Investigation_into_the_stress_corrosio n_cracking_of_tensile_wires_of_flexible_pipes_in_different_simulated_annulus_environments_containing_CO2

De Motte, R., Joshi, G., Chehuan, T., Legent, R., Kittel, J., & Désamais, N. (2022). CO_2-SCC in Flexible Pipe Carbon Steel Armor Wires. Corrosion, 78(6), 547-562. https://doi.org/10.5006/4025

FIZ Karlsruhe GmbH. (1985). Inorganic Crystal Structure Database (ICSD). https://www.psds.ac.uk/ Fonseca, D., Tagliari, M., Guaglianoni, W., Tamborim, S., & Borges, M. (2024). Carbon Dioxide Corrosion Mechanisms: Historical Development and Key Parameters of CO_2-$H_2$0 Systems. International Journal of Corrosion, 2024. https://doi.org/10.1155/2024/5537767

Hanonge, D., Ferraz, J., & Ferre, R. (2022). CO_2-Stress corrosion cracking risk mitigation for flexible pipe design. Subsea Pipeline Technology. London.

Mack, R. (2001). Stress Corrosion Cracking of High Strength Steels in Aqueous Solutions Containing CO_2 - Effects of Yield Strength, Dissolved Oxygen, and Temperature. Corrosion, 1-19. https://onepetro.org/NACECORR/proceedings-abstract/CORR01/All-CORR01/112647

Macleod, I. (2023). Flexible Pipe Integrity Management Guidance & Good Practice. Wood JIP report 807511-00-IM-GLN-001.

Meisnar, M., Moody, M., & Lozano-Perez, S. (2015). Atom probe tomography of stress corrosion crack tips in SUS316 stainless steels. Corrosion Science, 98(September), 661-671. https://doi.org/10.1016/j.corsci.2015.06.008

Nesic, S. (2007). Key issues related to modelling of internal corrosion of oil and gas pipelines - A review. Corrosion Science, 49, 4308-4338. https://doi.org/10.1016/j.corsci.2007.06.006

Pimentel, T., da Silva, C., Santos, F., Baptista, I., de Souza, J., & Panossian, Z. (2025). Evaluation of test methodologies for assessing SCC-CO2 in tensile armor of flexible pipes. International Journal of Pressure Vessels and Piping, 216. https://doi.org/10.1016/j.ijpvp.2025.105515

Santos, F., Poloponsky, I., Modiano, S., Ribeiro, C., & Motta, E. (2020). Evaluation of the SCC-CO2 Susceptibility of Flexible Pipe Tensile Armor Wires. Rio Oil Gas Expo Conference. Rio de Janeiro. http://dx.doi.org/10.48072/2525-7579.rog.2020.177

Vynar, V., Vasyliv, K., Ratska, N., Ivashkiv, V., Chuchman, M., & Datsko, B. (2021). Influence of Temperature and Carbon-Dioxide Pressure on the Corrosion and Stress-Corrosion Fracture of Pipe Steels in Model Stratal Water. Materials Science, 56, 739-747. https://doi.org/10.1007/s11003-021-00490-w

Wang, J., Ye, X., Li, L., & Liu, P. (2022). Distribution Law of Corrosion Products in a Marine Chloride Environment. Materials, 15(4339). https://doi.org/10.3390/ma15124339

Zhang, L., Li, X., Du, C., & Cheng, Y. (2009). Corrosion and Stress Corrosion Cracking Behavior of X70 Pipeline Steel in a CO2-Containing Solution. Journal of Materials Engineering and Performance, 18, 319-323. https://doi.org/10.1007/s11665-008-9282-9

Structural Optimization of a 20-Inch Pipe Clamp Using Arc-Based Additive Manufacturing

Daniel Galeazzi[1], José Carlos de Carvalho Pereira[3], Laercio Meneses Silva Junior[4], Mateus Barancelli Schwedersky[5], Régis Henrique Gonçalves e Silva[6], Cláudio Marques Schaeffer[2]

Abstract

In the oil and gas sector, from extraction to petroleum-derived product distribution, pipelines are extensively employed. For maintaining these systems, an alternative involves bolted and welded clamps, which combine the speed of a temporary repair (after bolting) with the integrity of a permanent repair (after welding). This work presents the development and structural optimization of a 20-inch pipe clamp produced through arc-based additive manufacturing. The optimization aimed to reduce the shell thickness while ensuring the critical test pressure of 15.1 MPa (2190 psi) was sustained. The clamp features sealing rings at the interface with the pipeline, specifically in the damaged region. These o-rings are mounted in grooves machined into the clamp shell. However, due to shell thickness optimization, this machining critically reduces the minimum thickness required to withstand the internal pressure specified by the API 5L standard. Numerical simulations identified critical regions that could potentially lead to device failure. To mitigate this, a reinforcement technique using localized additive manufacturing was developed and applied, enabling controlled thickness increases in critical areas. Test results showed the reinforcement enabled the clamp to withstand pressures of 15.7 MPa, even with reduced shell thickness (12 kg weight reduction). These results confirm the effectiveness of localized reinforcement combined with structural optimization.

Keywords: WAAM; Structural Optimization; Pipe Clamp; Numerical Simulation; Oil and Gas Industry.

[1] UFSC. Brazil. E-mail: daniel.galeazzi@live.com (https://orcid.org/0000-0001-8527-469X).

[3] UFSC. Brazil. E-mail: j.c.carvalho.p@ufsc.br.

4 UFSC. Brazil. E-mail: laerciomeneses@gmail.com (https://orcid.org/0000-0002-2780-0839).

5 UFSC. Brazil. E-mail: m.barancelli@ufsc.br (https://orcid.org/0000-0002-4537-3228).

6 UFSC. Brazil. E-mail: regis.silva@ufsc.br (https://orcid.org/0000-0003-0660-6495).

[2] UFSC. Brazil. E-mail: claudio.schaeffer@posgrad.ufsc.br (https://orcid.org/0000-0003-2639-4338)

1 Introduction

Wire and Arc Additive Manufacturing (WAAM) is an emerging fabrication process that has been gaining significant attention in Brazil and worldwide due to its ability to produce complex parts with intricate and customized geometries, combining materials and mechanical properties (Galeazzi, 2024).

This process focuses on the full manufacturing or composition of component parts through the controlled deposition of material along a predefined path, where fusion is achieved via the action of an electric arc. In the GMAW (Gas Metal Arc Welding) process, the electric arc is established between the substrate and a consumable wire electrode. This wire is continuously fed by the welding torch and melted by the arc, depositing material in a controlled manner as it moves along the travel path.

In contrast, in the GTAW (Gas Tungsten Arc Welding) and PAW (Plasma Arc Welding) processes, the arc is formed between a non-consumable electrode, typically made of tungsten, and the substrate. In these processes, the filler material is added into the arc region, where it is melted and deposited as required to form the desired part (Frazier, 2014).

The choice of deposition process for additive manufacturing depends on the complexity of the part and the material being used. Autogenous processes with external wire feeding, despite offering the advantage of independent control between current and material feed, tend to present greater challenges in additive manufacturing due to variability in feeding direction during multidirectional paths, since the feeder is fixed adjacent to the arc. This is not the case in GMAW, where the feeding is coaxial with the arc, making it the most widely used process in wire and arc additive manufacturing today.

One of the main challenges in additive manufacturing is the CAD-to-part relationship, i.e., the integration between computer-aided design (CAD) and the fabrication of the physical component (part). In additive manufacturing, this relationship involves several critical steps. Highlights include process planning and parameterization—welding parameters and operational guidelines that must be programmed into the path, which should ensure that the final part meets the established dimensional and mechanical requirements (Ding et al., 2015a, 2016; Wang et al., 2021). Given this scenario, it is imperative to map and understand the physical phenomena related to metal transfer in the chosen deposition process and its impact on the geometric profile of the deposited beads.

In this context, high-tech welding processes are widely employed in additive manufacturing due to their greater control over metal transfer and welding variables, with the CMT (Cold Metal Transfer) variant of the GMAW process standing out. According to the literature, the CMT system provides geometric control of the deposit, high stability, and allows for high deposition rates—features that are particularly advantageous for manufacturing parts via additive manufacturing (Ali et al., 2019; Furukawa, 2006; Mvola, Kah & Layus, 2018; Posch, Chladil & Chladil, 2017; Yang et al., 2019).

However, even when applying highly reliable equipment and processes, parameterizing an additive manufacturing operation goes beyond the welding process itself, extending to heat input control, interpass or interlayer temperature, path planning and control, among other variables. Neglecting these aspects can render additive manufacturing operations unfeasible (Bai et al., 2018; Ding et al., 2014, 2015a, b, c; Mehnen et al., 2011).

In addition to the fabrication of structural parts and customized components, WAAM also proves to be a viable alternative for applications in sectors such as oil and gas, especially for the production of repair components such as half-shells and clamps, allowing for greater flexibility in manufacturing these structures. Furthermore, this technology can be applied in the fabrication and restoration of critical components, such as valves, flanges, and special fittings, extending the service life of equipment and reducing the need for costly replacements.

In the oil and gas sector, the use of pipelines for transportation is currently one of the most efficient and safest methods. Due to this high level of reliability, such structures are manufactured under strict quality requirements, both mechanical and metallurgical. However, even when using high-grade materials, these structures are subject to defects that may affect their integrity over time. The defect that most compromises the integrity of pipelines is wall thickness loss due to corrosion. In addition, vandalism—such as fuel theft—is another concern. Modifications, such as the insertion of components or expansion of lines, are also common. Given these situations, in-service welding repair techniques are frequently applied, allowing interventions without interrupting fluid flow.

These techniques typically involve welding elements known as half-shells or clamps, which consist of assembling a split housing device with compartments to accommodate leaks and seals, making for a quick—and in some cases permanent—repair.

One of the challenges of these techniques lies in the fabrication of these components, which must meet specific mechanical requirements, often demanding customized parts. In the case of the type B double half-shell technique, it is common to use a section of the pipeline itself, which is adjusted to fit properly within the required specifications. On the other hand, clamps, which are typically contingency solutions but can become permanent in some cases, require the use of high-strength steel alloys, and their manufacturing may involve complex techniques such as casting or forging. Besides the cylindrical structure, accessories such as various types of fittings may be needed.

Moreover, because it is a low-volume commercial product, the costs are high, and logistics are limited. However, companies such as PLIDCO, WESTATLANTIC, among others, offer this solution as an alternative for pipeline repair.

In this regard, as part of a national development initiative, Petrobras, in collaboration with LABSOLDA and GRANTE from the Federal University of Santa Catarina (UFSC), developed a R&D project entitled: "Alternative repair processes: in-service welding of bolted clamps and cap (cover) – SIGITEC: 2017/00379-0." Within the scope of this clamp project, the focus was on reducing the shell thickness. However, computer simulations indicated the need for additional thickness in critical regions to ensure mechanical integrity. Therefore, this study aims to demonstrate the reinforcement process via additive manufacturing on an industrial clamp used in temporary and permanent repairs of pipelines in the oil and gas sector, presenting the steps of process parameterization, path programming, and hydrostatic testing.

2 Methodology

Clamps for the repair or isolation of leak points consist not only of the shells that form the main structure, but also include a sealing system using O-rings and a cap, as shown in Figure 1. Initially, for the design of the clamp model proposed in this study, a 20" diameter and a dual-sealing system for the cap were defined.

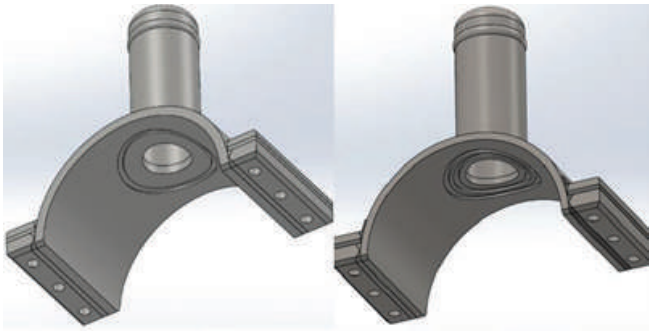

Figure 1 – Clamp with two channels for housing the dual O-ring sealing system.

Subsequently, the shell optimization step was carried out in a virtual environment using numerical simulation, considering the clamp material as API 5L Gr. X65 steel, which has a minimum yield strength of 448 MPa and a minimum tensile strength of 531 MPa. In this simulation, the shell thickness was set at 19 mm (3/4"). Based on the hoop stress equation for thin-walled pressure vessels, it was verified that for an internal pressure of 17.12 MPa, the pipe would reach its yield strength, and for an internal pressure of 20.29 MPa, it would reach its ultimate tensile strength. It is worth noting that according to API 5L: Specification for Line Pipe (2004), the minimum test pressure for this type of pipe is 15.10 MPa (2190 psi).

Following the initial thickness definition test, an optimization was performed aiming to reduce the shell thickness in low-stress regions. The areas defined as non-critical were reduced to 15.88 mm (5/8"), while the critical regions maintained a thickness of approximately 19 mm, preserving the clamp's capacity to withstand a pressure condition of approximately 17 MPa. Within the project scope, two 20" clamps, referred to here as Clamp P1 and Clamp P2, were manufactured for delivery in a relevant environment to CREDUTO (Brazilian emergencial center of pipe repair), with the objective of field application. Prior to their practical application, both clamps were used for project-aligned activities: Clamp P1 was used to conduct an upskilling course for the plant maintenance teams, and Clamp P2 was used for bench testing.

For the clamp fabrication, a 5/8" (15.88 mm) ASTM A516 Gr. 70 plate was used, which has a Specified Minimum Yield Strength (SMYS) of 260 MPa and a Minimum Tensile Strength of 485 MPa. A reinforcement by additive manufacturing (AM) was planned for this component.

The additive manufacturing reinforcement was applied to the regions identified as critical in the numerical simulation step. The reinforced areas included the cap region, in the form of a collar or hyperbolic paraboloid, and the flange attachment area, as shown in the detail of Figure 2.

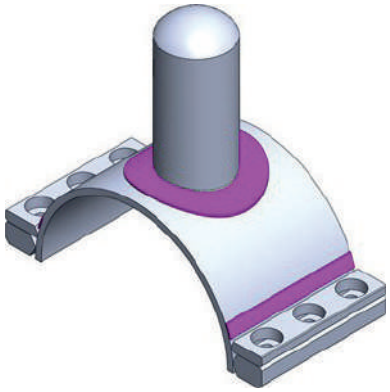

Figure 2 – Clamp with two channels for housing the dual O-ring sealing system.

In this specific case, the outputs of the parameter prediction algorithm were directly implemented on the DX100 controller of the Motoman HP20D robot and the MOTOPOS MPD250B positioner, without the use of any CAM software, using the Inform III programming language. This approach was adopted due to the geometric variations between the CAD model and the actual part, which remains one of the major challenges in wire and arc additive manufacturing (WAAM).

Initially, the welding process and its preliminary parameterization were defined. In this case, due to the size of the part, a process with high deposition rate and good bead geometry control was selected. Thus, the chosen process was CMT Pulse, a hybrid variant of the GMAW process with dynamic wire feeding, combining pulsed arc and Cold Metal Transfer (CMT) characteristics. The material used for deposition was a carbon steel wire ER70S-6, 1.2 mm in diameter, along with a gas mixture of 8% CO_2 and 92% argon. The parameters used included a wire feed speed of 6.5 m/min and a travel speed of 60 cm/min, resulting in a bead approximately 7 mm wide and 3 mm high.

For the reinforcement collar, a complex trajectory planning study was required due to the shape of the part. The trajectory programming was performed online, directly on the robot controller, through synchronized motion programming between the robotic arm and the positioner table. The programming was organized into five steps, as shown in the flowchart in Figure 3.

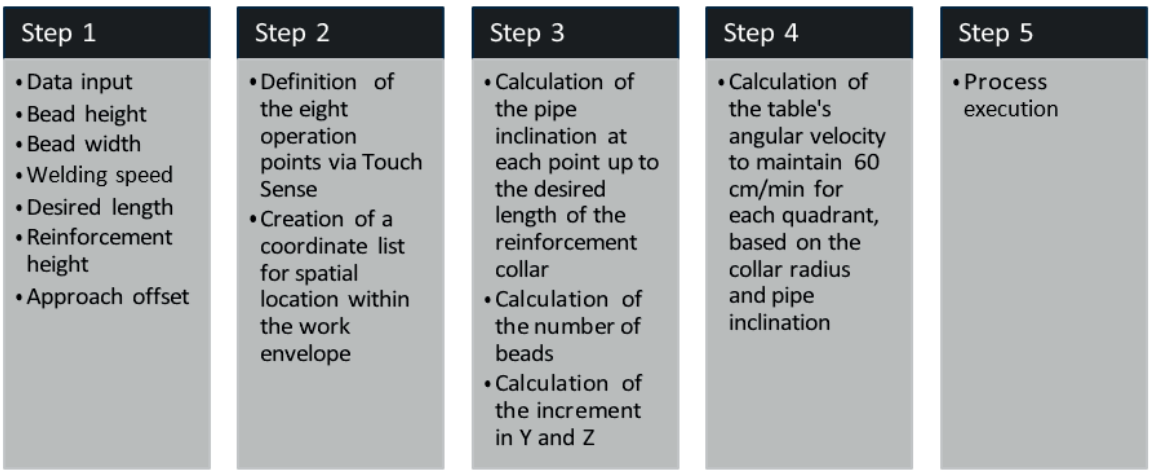

Figure 3 – Flowchart of the trajectory planning used for the reinforcement collar deposition.

For the flange reinforcement, a linear bead trajectory was used, with alternating beads overlapped at a center-to-center distance equivalent to 67% of the bead width, or 4.2 mm. Additionally, using the MOTOPOS positioner, the clamp was tilted to position the flange reinforcement operation in the flat position.

For validation and inspection of the clamp, visual inspection, penetrant testing, measurements, and finally a hydrostatic test were performed to validate the prototype. It is worth noting that four identical clamps were built for testing and validation of the created model. For the hydrostatic tests, a test bench was set up with a 20" external diameter balloon made of API 5L steel, and an automated hydraulic pump made of AISI 316L, with a maximum pressure capacity of 300 Kgf/cm², as shown in Figures 4a and 4b.

Figure 4 – a) Balloon for testing; b) Hydrostatic pump.

A hydrostatic test was performed on each of the clamps, and the main criterion used was resistance to pressure of at least 155 Kgf/cm², equivalent to 1.5 times the operating pressure, which is the target value for the qualification of repairs for class #600. In addition to this criterion, as per the design specifications for the clamps, a torque of 600 Nm was defined for tightening each bolt.

3 Results and Discussion

As described in the methodology, the reinforcement by AM was performed in critical regions, including the area near the capote and the flange area. Although the project initially aimed at reducing thickness to decrease mass, the expected loads in these regions required localized reinforcement to compensate for the thickness reduction in these areas. This was done while maintaining the premise of structural optimization and mechanical strength.

For better understanding of the process, the following Figure 4 contains QR codes linking to demonstration videos of the touch-sense operations, the reinforcement collar fabrication, and the reinforcement of the flange.

Touch-sense

Reinforcement of the Collar

Reinforcement of the Flange

Figure 4 – QR-Codes for examples of the main operations performed in the additive manufacturing reinforcement process of the clamp.

The result of the reinforcement applied to the clamp can be seen in Figure 5. Figure 5A illustrates the deposition stage of the collar around the capote, while Figure 5B presents the deposition stage of the reinforcement on the flange. It is important to note that the reinforcement of the flange was carried out on both sides of the clamp.

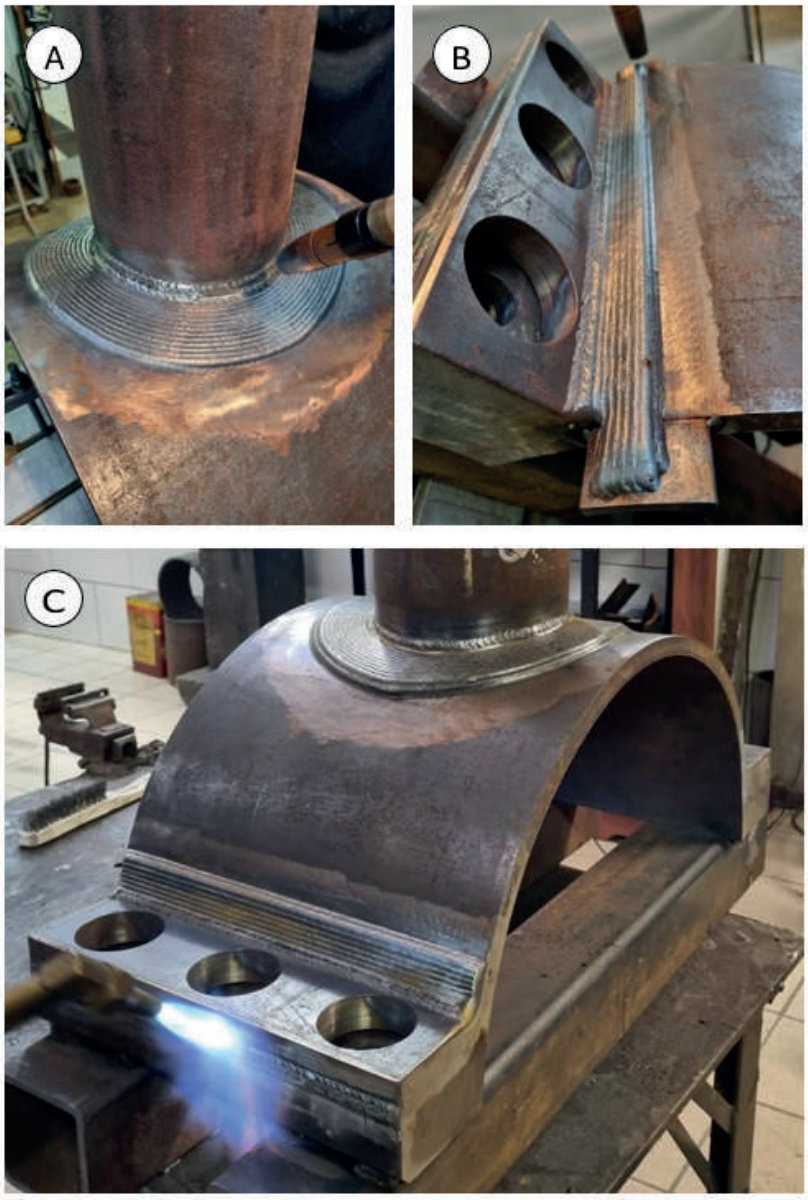

The measurements performed on the clamp focused on the diameter of the flat section, width, and thickness of the reinforcements. The results of these measurements are detailed in Table 1. It was found that all measurements were within the initially defined tolerances, with a low standard deviation.

Feature	Section A			Section B		
	Nominal (mm)	Mean (mm)	Std. Dev. (mm)	Nominal (mm)	Mean (mm)	Std. Dev. (mm)
Diameter / Width	278 ± 3	280.3	0.4	32	32.3	0.4
Thicknesses	Min 5	6.4	0.3	Min 5	6.3	0.3

Table 1 – Measurement of the clamp reinforcement

The clamp was tested in the same test balloon previously mentioned, with a diameter of 511.99 mm, using rubber seals with a cross-sectional height of 14 mm and thickness of 15 mm, and a torque of 600 N/m/bolt. The clamp withstood a pressure of 160 Kgf/cm². Additionally, this clamp exhibited a final gap between the flanges of approximately 10 mm with a variation of +1 and -1 mm.

Regarding the first experiment conducted with this clamp at CREDUTO, as shown in Figure 6a, Viton sealing gaskets with a shore hardness of 60, a height of 10 mm, and a width of 15 mm were used. The bolts were tightened in the required sequence, progressing from 200 Nm up to 600 Nm per bolt. The gap measured between the flanges was around 3 mm with a tolerance of -1 and +1 mm, as shown in Figure 6b. The hydrostatic test was conducted, and the pressure achieved was 160 Kgf/cm², as shown in Figure 6c, a value sufficient for the validation of class #600 repairs.

Figure 6 – a) Installed clamp; b) Recording of the flange gap; c) Recording of the achieved pressure.

This same clamp was tested for the second time at CREDUTO, under a condition that differed from the first only in the torque applied to the bolts, which was 400 Nm per bolt. The result of this second test showed that, even with a lower torque, the sealing rubber withstood a pressure of 160 Kgf/cm$_2$.

5 Conclusion

The offline programming method adopted, using the touch-sense feature and velocity calculations based on the sample's tilt, proved effective for achieving the goal of constructing a collar around the capote through additive manufacturing. Furthermore, the welding process adopted demonstrated high stability in terms of both process and geometry, producing a defect-free weld with low standard deviation.

The clamps produced are the first prototypes tested at CREDUTO, featuring two sealing channels and the application of a reinforcement collar via additive manufacturing. Additionally, the use of sealing rings with a prismatic cross-section proved more efficient in the tests conducted. However, it is important to emphasize the need to follow the installation instructions for the clamp.

In conclusion, the team involved in the test noted the ease of clamp installation due to its lighter weight compared to commercial clamps, a significant improvement that has been mentioned in other reports.

6 Acknowledgments

The authors would like to thank the Welding and Mechatronics Laboratory – LABSOLDA and GRANTE at the Federal University of Santa Catarina (UFSC) for the technical support and infrastructure provided during the development of this work. They also extend their gratitude to Petrobras for the financial support and encouragement of applied research in welding and additive manufacturing processes.

Referências

Scientific Journal

Ali, Y., Henckell, P., Hildebrand, J., Reimann, J., Bergmann, J.P., Barnikol-Oettler, S. Wire arc additive manufacturing of hot work tool steel with CMT process. J Mater Process Technol. 269, 109–116 (2019). https://doi.org/10.1016/j.jmatprotec.2019.01.034

Bai, X., Colegrove, P., Ding, J., Zhou, X., Diao, C., Bridgeman, P., roman Hönnige, J., Zhang, H., Williams, S. Numerical analysis of heat transfer and fluid flow in multilayer deposition of PAW-based wire and arc additive manufacturing. Int J Heat Mass Transf. 124, 504–516 (2018). https://doi.org/10.1016/j.ijheatmasstransfer.2018.03.085

Ding, D., Pan, Z., Cuiuri, D., Li, H. A tool-path generation strategy for wire and arc additive manufacturing. International Journal of Advanced Manufacturing Technology. 73, 173–183 (2014). https://doi.org/10.1007/s00170-014-5808-5

Ding, D., Pan, Z., Cuiuri, D., Li, H. A practical path planning methodology for wire and arc additive manufacturing of thin-walled structures. Robot Comput Integr Manuf. 34, 8–19 (2015). https://doi.org/10.1016/j.rcim.2015.01.003

Ding, D., Pan, Z., Cuiuri, D., Li, H. A multi-bead overlapping model for robotic wire and arc additive manufacturing (WAAM). Robot Comput Integr Manuf. 31, 101–110 (2015). https://doi.org/10.1016/j.rcim.2014.08.008

Ding, D., Pan, Z., Cuiuri, D., Li, H. Wire-feed additive manufacturing of metal components: technologies, developments and future interests, (2015)

Ding, D., Pan, Z., Cuiuri, D., Li, H., van Duin, S., Larkin, N. Bead modelling and implementation of adaptive MAT path in wire and arc additive manufacturing. Robot Comput Integr Manuf. 39, 32–42 (2016). https://doi.org/10.1016/j.rcim.2015.12.004

Frazier, W.E. Metal Additive Manufacturing: A Review. J Mater Eng Perform. 23, 1917–1928 (2014). https://doi.org/10.1007/s11665-014-0958-z

Furukawa, K. New CMT arc welding process – welding of steel to aluminium dissimilar metals and welding of super-thin aluminium sheets. Welding International. 20, 440–445 (2006). https://doi.org/10.1533/wint.2006.3598

Mehnen, J., Ding, J., Lockett, H., Kazanas, P. Design for Wire and Arc Additive Layer Manufacture. In: Global Product Development. pp. 721–727. Springer Berlin Heidelberg, Berlin, Heidelberg (2011)

Mvola, B., Kah, P., Layus, P. Review of current waveform control effects on weld geometry in gas metal arc welding process. The International Journal of Advanced Manufacturing Technology. 96, 4243–4265 (2018). https://doi.org/10.1007/s00170-018-1879-z

Posch, G., Chladil, K., Chladil, H. Material properties of CMT—metal additive manufactured duplex stainless steel blade-like geometries. Welding in the World. 61, 873–882 (2017). https://doi.org/10.1007/s40194-017-0474-5

Doctoral Dissertation

Galeazzi, D. Desenvolvimento de um sistema integrado de manufatura aditiva por deposição a arco usando a variante GMAW com alimentação dinâmica CMT, (2024)

TAG's Social Commitment: Social Action in Local Communities

Narelly Matos[1], Tais Carneiro Ferreira de Castro[2], Edielen Pereira Matos[3], Isvani Pinheiro[4], Rafaela Carvalho[6], Taissa Bonguardo[7], Michelle Vasconcelos[5]

Abstract

TAG operates an extensive network of 4,500 km of natural gas pipelines in Brazil, crossing more than 200 municipalities in 10 states and covering nearly 400 communities within its area of influence. Recognizing the importance of strengthening ties with the communities near its infrastructure, TAG promotes initiatives that contribute to local development, income generation, and improved quality of life through social projects. Many of these communities face challenges such as limited access to essential health, education, and infrastructure services. As part of its social commitment, TAG is developing a pilot project to be implemented in the community of Bom Pastor, in Espírito Santo. The initiative includes the establishment of a pedagogical garden in a municipal school, encouraging environmental education and food security, as well as the organization of a health and wellness event for students and their families. These actions not only promote local development and safety awareness but also strengthen the bond between the company and the community, creating a relationship of trust and cooperation. This work presents the implementation strategy of the initiative, its social and environmental impacts, and the feasibility of replicating the model in other locations

Keywords: Social Responsability; Community; Social Project

1 TAG - TRANSPORTADORA ASSOCIADA DO GÁS. Brazil. E-mail: narelly.matos@ntag.com.br (https://orcid.org/0009-0005-3152-678X).

2 TAG - TRANSPORTADORA ASSOCIADA DO GÁS. Brazil. E-mail: tais.carneiro.castro@poli.ufrj.br (https://orcid.org/0009-0009-7262-959X).

3 TAG - TRANSPORTADORA ASSOCIADA DO GÁS. Brazil. E-mail: edielen.matos@ntag.com.br.

4 ENGIE BRASIL E ENERGIA. Brazil. E-mail: isvani.pinheiro@engie.com.

6 TAG - TRANSPORTADORA ASSOCIADA DO GÁS. Brazil. E-mail: rafaela.carvalho@ntag.com.br.

7 Engie Soluções de Operação e Manutenção - ESOM. Brazil. E-mail: taissa.bonguardo@engie.com.

5 TAG - TRANSPORTADORA ASSOCIADA DO GÁS. Brazil. E-mail: michelle.vasconcelos@ntag.com.br (https://orcid.org/0000-0002-3948-5346)

1 Introduction

TAG is a national gas transportation company in Brazil and it has the most extensive network of gas transportation pipelines in the country, with over 4,500 km, crossing nearly 200 municipalities in ten Brazilian states and covering nearly 400 communities within its area of influence. There are more than 3,700 km in the coastal region of Brazil – in the states of Ceará, Rio Grande do Norte, Paraíba, Pernambuco, Alagoas, Sergipe, Bahia, Espírito Santo, and Rio de Janeiro – and about 800 km in Amazonas, as shown in Figure 1.

Figure 01 – TAG's natural gas transportation pipeline network.
Produced by the author)

The company invests in social projects around its assets, benefiting populations in situations of social and economic vulnerability. Thus, it contributes to social transformation, community empowerment, and local development. Social investment is aligned with the values and expectations of the business, creating value for the territories where it operates. Through humanitarian actions, support for culture, and encouragement of sports, it promotes respect for interculturality and human rights.

Additionally, TAG strengthens its competitive edge through the attraction, selection, and mobility of employees aligned with its organizational culture. To achieve this, the company has developed programs such as the Trainee Program, in partnership with Engie, one of its shareholders. As a challenge of this program, a group of six trainees was responsible for developing a social project for TAG.

The goal is to create a comprehensive and sustainable social project for a community selected from the municipalities of São Mateus or Viana, both located in the State of Espírito Santo. The project aims not only to address the difficulties identified in the diagnosis but also to promote long-term solutions and generate a significant impact on the quality of life. It will involve an integrated and strategic approach.

The result of this challenge is the project "Cultivating Health with TAG" developed based on a previous study, with a strategic approach that addresses not only the difficulties identified in the diagnosis but also promotes a long-term solution and generates a significant impact on the community. The goal is to create a sustainable social project to mitigate vulnerabilities in the community of Bom Pastor, located in Viana, Espírito Santo. The project aims to improve the quality of life and promote long-term solutions, so as strengthen the relationship with TAG.

2 Methodology

The project structure relied on a social diagnosis conducted in the proposed region by a non-profit organization that acts as a social manager, promoting the connection between companies, people, and social projects. For the mapping of the communities, the company studied the regions and sent a team to interview the residents and understand their quality of living. It was possible to analyze the perception of different aspects of quality of living in that community, in order to assess the social vulnerability of the area. The interviewed residents qualitatively reported their perception of education, health, sports, leisure, and other aspects offered in the community, rating them as poor, fair, medium, good, and very good. In addition, they expressed their opinions on aspects they considered as strengths and vulnerabilities, as well as on infrastructure conditions such as access to electricity, water supply, waste disposal, sewage system, climatic effects, among others. Therefore, it was possible to understand the main needs of the community residents to define a project scope that would bring significant improvements to the population.

Another important part of the diagnosis is the communities' perception of TAG. Since these communities are located along the pipeline right of way and other assets, understanding the community's perception is essential to creating a bond between the company and the community. A pipeline right of way presents a risk, and therefore, the community must understand the risks and the necessary behaviors to mitigate them. The social diagnosis assessed whether the residents knew TAG, Engie, felt safe in the localities, and were aware of the call center number 168. This survey was done for the following communities: Perobas (Viana/ES), Bom Pastor (Viana/ES), São Jorge (São Mateus/ES), Barra Seca / Urussuquara (São Mateus/ES), Estiva (São Mateus/ES) and Aroeira (São Mateus/ES).

The proposed challenge was to develop a pilot project in one of the communities that could, in the future, be expanded to other locations. The first step was to select one of the locations to develop the project based on the social diagnosis. Then, it was necessary to define the scope of the project

and choose to meet the needs of the selected community. The main criteria used to narrow the priorities was the knowledge and relationship with TAG and ENGIE and knowledge of the call center number 168[1]. It is crucial to determine whether the community is aware of the emergency telephone number, the guidelines for use and prohibitions related to the gas pipeline right of way, if it was trained on these guidelines, if there are any concerns or if there are occurrences in relation to the gas pipeline.

Among all the evaluated communities, Bom Pastor, community located in the municipality of Viana, had the highest rate of residents without knowledge about TAG, ENGIE, the call center, or the risk of the pipeline right of way. These were the main criteria for choosing the Bom Pastor community to receive the pilot Project.

Once the community was selected, the next step was to develop the scope of the project. The region shows potential such as sports, culture and agriculture. In addition, considering the stakeholders presented in the social diagnosis, it was identified that schools are receptive and willing to receive extra activities.

Also, a survey of internal initiatives related to the Engie group was conducted. The project "From Garbage to Energy: Education for the Energy Transition" donates and installs biodigesters to schools and institutions, providing a sustainable alternative for the disposal of organic waste in the vicinity of ENGIE group companies across Brazil. This project is conducted in cooperation with Energy Assistance France (EAF), an international volunteer organization formed by ENGIE employees and former employees. In addition to EAF, ENGIE Foundation, Abiogás and Biomovement-Homebiogás are partners in this project. In this context, one of the biodigesters donated were at an elementary school in Viana, near TAG's assets.

As for the need to create ties with the company, it was observed that the community is located near Viana City Gate, which is a TAG's asset, and Cabiúnas-Vitória pipeline right of way, as shown in Figure 02.

Figure 02 – Bom Pastor Community, Viana/ES.
Source: TAG's Geographic Information System.

1. The 168 is the call center in case of emergencies, doubts, complaints and problems in the surroundings of the units and pipelines. The service by 168 is free and available 24 hours a day throughout the week, being a means of communication between local communities and pipeline companies.

After careful consideration of the needs and resources available, the project "Cultivating Health with TAG" was created. That way, the social project scope is to build a pedagogical garden at a community's school, adding value to the existing project "From Garbage to Energy: Education for the Energy Transition", which had implemented a biodigester at the school. The garden will be inaugurated by the students, and to increase the target audience, a health-related event covering various aspects will be held for the family members.

Once the project scope was defined, the structure of other project aspects, such as costs, deadlines, expectations, metrics, and other aspects, were carried out. For the next phases, alignment of details with the school, contracting relevant companies, and implementation will be evaluated.

3 Scope

Thus, the social project has two main pillars: the implementation of a pedagogical garden at a school in the community of Bom Pastor in Viana and the organization of a health-themed event for the students and their family members. The goal of the project is to leave a functional garden as a legacy, which can be used both in educational activities and using the planted vegetables and fruits to prepare meals at the school. In this way, it will be possible to utilize the biofertilizer generated by the biodigester installed by the "From Garbage to Energy" project, facilitating the maintenance of the garden. The pedagogical aspect of the garden is directly related to the event of the garden's inauguration, highlighting the educational importance of the project from its inception. Additionally, it is expected that the health-themed event promotes a legacy of encouraging healthy practices in the daily lives of the participants.

"Cultivating Health with TAG" is a project proposal that involves organizing a three-day event. The first two days will focus on environmental activities, including the implementation of a garden with the participation of volunteers and students. On the third day, a health and environmental awareness event will be held for the students and their families.

Before the event, the proposal includes the installation of five of 3m x 1m beds for the educational garden, totaling a planting area of 15m². Additionally, a storage area for maintenance materials, called "Green Space," will be constructed. During the first two days of the event, students and volunteers will collaborate on setting up the garden beds and the Green Space. Activities will include filling the beds with soil, planting seedlings, and decorating the Green Space, all conducted through workshops. For this part of the activity, the estimation is that 50 volunteers will participate in the event, and the expected attendance will be up to 240 students from the school.

The health-themed event will feature simultaneous activities for children and adults, covering three main themes: "Oral Hygiene," "Nutrition," and "Body Care". The event would be structured for over 70 families of the students, promoting an environment of integration and awareness about the environment and health. The participants will be divided into three groups to ensure everyone can participate in all activities.

For children, the nutrition theme will include a sensory food workshop and the "Food Twist" game, while adults will attend a lecture on healthy diet and best practices for reduce waste. In the oral hygiene area, children will have a dental brushing workshop, and adults will attend a lecture on the importance of oral hygiene and other care practices.

Regarding body care, both children and adults will participate in a functional training session. This activity will use everyday materials to demonstrate how to maintain an exercise routine practically and accessibly, utilizing resources available at home.

Additionally, part of the event's scope includes promoting TAG's business and the 168 call center to strengthen the company's ties with the community. One of the objectives is for participants to leave the event with knowledge about the gas transportation business, the role of TAG in the natural gas supply chain, the necessary precautions near pipeline areas, awareness of the call center for emergency reports, and a positive view of TAG.

The preliminary budget for the pedagogical garden scope considered construction of the Green Space, garden beds, rainwater harvesting structure, maintenance of the garden for three months and two days of activities, and it is an approximate value of R$100,000.00. The preliminary budget for the health-themed event is R$ 45,000.00, which consists of registration and confirmation management, one day of activities, the logistics and the team.

4 Insights and Future Perspectives

The diagnosis identified social vulnerabilities, such as the lack of access to quality medical services, inadequate basic sanitation, and an absence of a history of health education. Based on this information, the project aims to mitigate these difficulties through the implementation of a pedagogical garden and the promotion of a health event. It is expected that the garden will contribute to the improvement of students' nutrition and quality of life, that way is expected to generate savings of approximately R$ 1,250.00 per year on food (based on the production and estimate productivity of lettuce, tomato and carrot). The saving from the existing biodigester will be approximately R$ 300.00 per month on fertilizer. The health themed event aims to reduce costs with dental treatments and encourage physical exercise, potentially generating annual savings of up to approximately R$ 98,000.00 for the community. The need for sustainable projects, such as pedagogical gardens and health events, is fundamental to promoting social inclusion and improving the quality of life of communities.

The issue of vandalism and the use of the 168 call center were also relevant to the development of the project. The history of complaints reveals a lack of knowledge of the community about the gas transportation process and related safety protocols, highlighting the need for greater clarification and awareness within the community. Furthermore, the project emphasizes the importance of preventive measures to address episodes of theft and vandalism, making asset security a challenge for the company. The post-project expectation is that the dissemination of TAG business and the 168 call center during the event will strengthen ties with the community and contribute to the reduction of vandalism cases.

Based on this, performance indicators to measure the effectiveness of the project's execution were discussed, including the number of registrations and attendance on event days, increased knowledge about TAG and the 168 call center, and the reduction of theft and vandalism cases. These indicators will allow for the evaluation of public adherence and engagement, as well as the project's impact on the security and integrity of TAG's facilities. The expectation is that the project will not only promote the company but also contribute to the positive and lasting transformation of the community, creating opportunities and improving living conditions.

5 Final Remarks

TAG has the most extensive pipeline network in the country and passes through more than 400 communities in its area of influence and there is a concern to positively impact the communities near its pipeline network. In order to contribute to social transformation, community empowerment, and local development of communities directly affected by TAG's assets, the "Cultivating Health

with TAG" project was proposed, with a strategic approach that addresses not only the difficulties identified in the diagnosis but also promotes a long-term solution and generates a significant impact on the community. The work presented in this paper, shows the development of the pilot project applied at the community of Bom Pastor, located in Viana, Espírito Santo. The project scope consists of an event at a public school, featuring environmental and health activities, as well as the implementation of a pedagogical garden for use in meals and school activities. The goal is to leave a legacy of healthy practices and awareness about TAG, promoting a fairer and more sustainable environment for the community. In addition to developing the local community, an important goal of the project is to strengthen the bond between TAG and the population. The events planned in the project serve as a platform to disseminate information about TAG, the natural gas transportation business, usage and prohibitions related to the pipeline corridor, and the emergency call center 168.

6 Acknowledgments

It is important to highlight that this work was carried out in partnership between the Trainee group of the Engie's Trainee Program 2024 and TAG's Social Responsibility team. Through this collaboration, we were able to develop a social event proposal that will bring significant benefits to the chosen community. We would like to express our gratitude to TAG, ESOM (Engie Soluções de Operação e Manutenção), and everyone involved for their valuable contributions, expertise, and support throughout the development of the project.

Lastly, we thank the organizers of the Rio Pipeline Congress for providing a platform to share our findings and innovations.

Referências

Transportadora Associada do Gás. (2025, April 30). Sustainability. Responsabilidade Social. https://ntag.com.br/

ENGIE. (2023, October 20). From Garbage to Energy: Education for the Energy Transition. https://www.engie.com.br/en/imprensa/press-releases/engie-foundation-and-abiogas- install-18-biodigesters-in-schools-and-communities/

Transportadora Associada do Gás. (2025, April 30). TAG Viewer: TAG's Transport Pipeline Network. https://gis-tag.ntag.com.br/portal/apps/sites/?#/tag-malha-gasodutos

Use of Finite Element Analysis and Burst Testing as a Tools for Optimizing the Integrity Management of Slurry Pipelines

Demétrio Marques Pereira Junior[1], José Luiz de França Freire[5], Rafael Correa Lima[6], Rafael Terzi Araujo[7], Rodrigo Márcio S. Oliveira[8], Ronaldo D. Vieira[9], Eduardo Campos de Oliveira[3], George Soares Almeida[4], Bernardo Pessoa[2]

Abstract

A leak in a slurry pipeline is a catastrophic event with significant impacts on the safety of people and the environment, directly compromising the operation of ore transport systems and potentially leading to the suspension of the owner's activities. Despite the scarcity of specific studies on slurry pipelines in the technical literature, it is widely recognized that threats such as erosion and corrosion are common in this type of asset. Managing the integrity of a slurry pipeline requires the development of a structured inspection and repair plan to ensure the operational continuity of the asset. In this context, this study, conducted in partnership with a laboratory, proposes optimizing the repair strategy based on burst testing by internal pressure performed on six tubular specimens extracted from an operational pipeline. The experimental results were analyzed and compared with finite element simulations and analytical models, using widely recognized standards such as ASME B31.4, ASME B31G, DNV RP-F101, and PCORRC. As expected, the findings confirmed that internal erosion was the main contributing factor to the ruptures. However, the study also identified the analytical model that best represented the experimental results, providing valuable insights for the company to improve asset integrity management and optimize planned interventions.

Keywords: Burst testing; Slurry Pipeline; Integrity Management; ASME B31G

[1] Universiade Federal de Goiás - UFG. Brazil. E-mail: alcindop@transpetro.com.br (https://orcid.org/0000-0001-6012-2817).

[2] Transpetro S/A. Brazil. E-mail: paulocesarjr@transpetro.com.br.

[3] Universiade Federal de Goiás - UFG. Brazil. E-mail: thyago@ufg.br

1 Introduction

Slurry pipelines play a critical role in the transportation of mineral ores over long distances, providing a cost-effective and efficient solution for mining operations. However, the nature of the transported material introduces unique integrity challenges, especially because of internal erosion and corrosion, which are commonly observed in this type of asset. These mechanisms, if not properly managed, can lead to failures, compromising safety, environmental, and the continuity of operations, with results that can impact the mining operation.

Despite the widespread use of slurry pipelines in mining operations, the availability of specific technical studies and practical methodologies aimed at their integrity assessment remains limited in the literature. Traditionally, the integrity management of slurry pipelines has relied on standards and models developed for oil and gas transmission systems, which may not adequately address the particularities of slurry transport.

In this context, the present study proposes a structured evaluation methodology combining experimental burst testing and finite element analysis (FEA) to better understand the failure behavior of eroded pipes from an operational slurry pipeline. Pipe segments were extracted from the field and subjected to internal pressure tests until its rupture. The results were compared against predictions from well-established analytical models, such as ASME B31G, B31Gmod, Tresca, von Mises, Zhu-Leis, PCORRC, Barlow, DNV RP-F101, with the objective of identifying the most reliable approach for assessing residual strength in this scenario.

By integrating experimental and computational techniques, this work aims to provide practical insights into optimizing repair strategies and enhancing the integrity management of slurry pipelines, ultimately contributing to increased safety, reduced downtime, and more efficient maintenance planning.

2 Methodology

The methodology employed to obtain the results presented in this paper involved conducting mechanical and chemical tests on pipe samples extracted from the bauxite slurry pipeline operated by Hydro Paragominas Bauxite Mine. The process began with the logistical coordination for the extraction, transportation, and delivery of the pipe segments to the testing facilities. Following this step, the preparation of the technical team and laboratory infrastructure was carried out.

A total of twelve pipe segments fabricated from API 5L X70 PSL2 steel, each with a nominal diameter of 24 inches, were received. These segments were extracted from Hydro's bauxite slurry pipeline, which had been in operation for 15 years. These segments had shown indications of internal erosion and external corrosion, as identified through inline inspection (PIG) data. Among the specimens received, six segments measured approximately one meter in length and were designated for laboratory mechanical and chemical tests, while the remaining six segments measured approximately five meters were prepared for internal pressure burst testing. The overall scope of work also included computational modeling through finite element analysis.

The activities occurred within a period of 6 months, table 1.

2.1. Material Composition

Six samples (CP2, CP2A, CP3, CP3A, CP5, and CP5A) were subjected to chemical analysis using optical emission spectrometry, in accordance with ASTM A751. The results were compared against the requirements of the API 5L X70 PSL2 standard, including the calculation of the carbon equivalent (CE).

Activities	Month 1	Month 2	Month 3	Month 4	Month 5	Month 6
Material Composition: iIncludes sample cutting and preparation, analyses, and reporting						
Mechanical Testing: Includes cutting, specimen preparation, testing, and reporting						
Burst Tests: Includes analytical predictions, inspections, specimen preparation, testing, and reporting						
Finite Element Modeling: Includes level 3 finite element modeling for each individual specimen, result comparison, and reporting						

2.2. Mechanical Testing

Tensile Test: A total of 24 tensile specimens were manufactured from the same segments, with 4 specimens per pipe (2 longitudinal and 2 transverse or circumferential per CP). Specimen extraction was performed at 180° from the longitudinal weld, following API 5L X70 PSL2 requirements. The tensile tests also adhered to ASTM A370/2020 and were executed using clip-gages for direct strain measurement. Stress-strain diagrams were obtained to determine the yield strength (0.2% offset method), tensile strength, and elongation at rupture over a gauge length of 50 mm.

Charpy Impact Test: A total of 72 Charpy V-notch specimens were fabricated, with 12 specimens per tube segment (6 longitudinal and 6 transverse for each CP). The specimens had 5 mm thickness due to the original pipe wall dimensions and a standard V-notch at 45°, 2 mm deep, oriented radially. Impact tests were conducted at two temperatures: 0°C and 23°C. Specimen preparation

and testing followed ASTM A370/2020 and ASTM E23 standards. The positioning of the Charpy specimens was in accordance with API 5L X70 PSL2, requiring samples to be removed at 90° relative to the longitudinal weld seam.

2.3. Internal Pressure Burst Tests

Tubular specimens approximately 5.3 meters in length were tested until its rupture under controlled internal pressure. The procedures involved were:

- → Seal the pipe and fill it with water.
- → Gradual increase of pressure using a water hydraulic pump.
- → Pressure and deformation data register using the LYNX AQDados system.
- → Burst pressure recording and photographic documentation of the event.

The procedure was validated through ambient temperature measurement and calibration of the pressure transducer used.

2.4. Finite Element Computational Modeling

Finite element computational models were developed to simulate the structural behavior of the tubular specimens under internal pressure loading until failure. Numerical analyses were performed using ANSYS software, version 18.1.

For each specimen, seven different models were developed, each aiming to represent different approaches to evaluating structural integrity:

- → **Type 1 – Realistic Pipe Geometry Based on Ultrasonic Measurements:** Full three-dimensional reconstruction of the pipe geometry, incorporating all thickness measurement points obtained by ultrasonic inspection.
- → **Type 2 – Critical Section with Minimum Thickness:** Modeling based on the minimum thickness measured at the most critical transverse section, applied uniformly across the model.
- → **Type 3 – Average Thickness Section:** Modeling based on the average thickness measured circumferentially at each axial position.
- → **Type 4 – Longitudinal Profile with Variable Thickness:** Modeling using multiple longitudinal sections, assigning the minimum measured thickness to each section along the specimen's length.
- → **Type 5 – Global Minimum Thickness:** Modeling using a uniform thickness equal to the minimum measured wall thickness across the entire specimen.
- → **Type 6 – Modal Thickness Profile with Longitudinal Defect:** Modeling based on the most frequently measured thickness (mode), incorporating a longitudinal defect region simulating critical thinning.
- → **Type 7 – Geometry Incorporating Localized External Corrosion:** Advanced modeling for specimens with circumferential welds and external corrosion (specifically CP4 and CP4A), explicitly incorporating localized loss of thickness due to corrosion pits, based on manual pit depth mapping.

All models assumed elastoplastic material behavior, adopting true stress-strain curves derived from tensile testing results. The boundary conditions simulated progressive internal pressure loading until structural collapse.

The solid element SOLID187 was used to simulate the tubular specimens. The main characteristic of this 3D solid element is its ability to withstand large deformations.

Two numerical criteria were established to represent failure by rupture of models caused by internal pressure. The first, the Lower-Bound (LB) criterion, considers that failure occurs when the first point on the internal surface of the model reaches the true tensile strength of the material, whether considering the Tresca or von Mises criteria. The second criterion, called Upper-Bound (UB), considers that failure occurs when the point located on the external surface and positioned radially along the thickness with reference to the first point to reach the LB reaches the true tensile strength, meaning that all points along the thickness reach the tensile strength of the material.

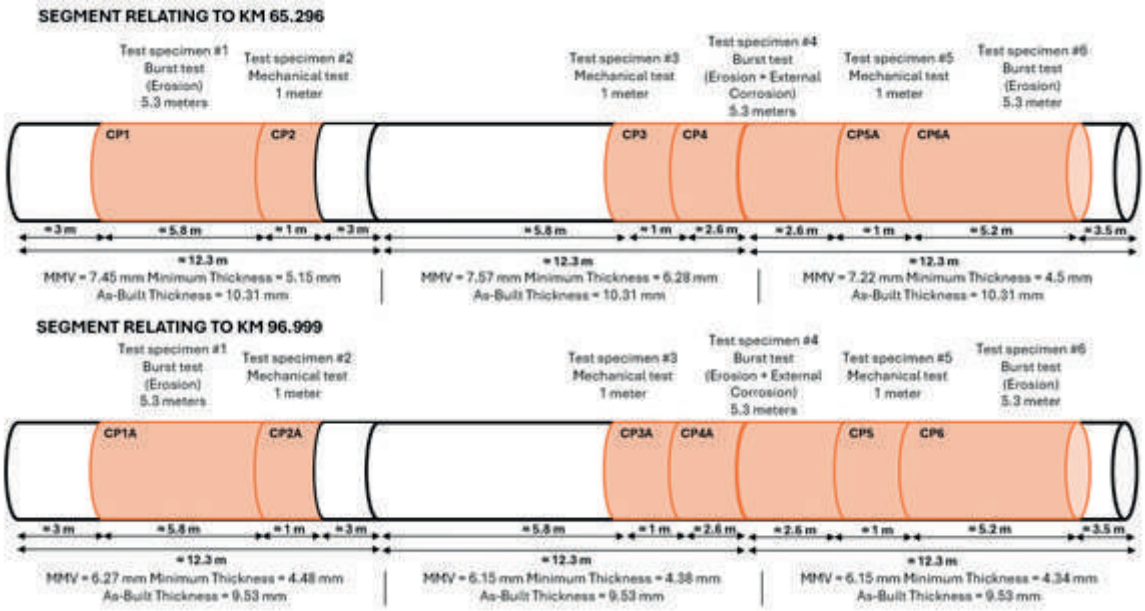

Table 1 – Segmentation of Pipe Specimens Extracted from Hydro's 24-inch Slurry Pipeline.
Prepared by the author (2025)

2.5. Analytical Evaluation

In addition to finite element modeling, an analytical evaluation of the burst pressure of the tubular specimens was conducted to complement and validate the experimental and numerical results. The evaluation followed internationally recognized engineering standards and specific methodologies for assessing defects in pressurized pipelines. The analytical formulations applied included:

- → ASME B31G 2012 – Level 1
- → Modified ASME B31G 2012 – Level 1
- → Tresca Flow Criterion
- → Von Mises Flow Criterion
- → Zhu-Leis (ZL) Model
- → PCORRC Method
- → Barlow Formula
- → DNV-RP-F101

This analytical development was structured to enable confidently select the evaluation method that best reflects the actual condition of assets, balancing technical rigor with operational efficiency.

3 Results

Initial dimensional inspections revealed an irregular loss of wall thickness in the pipe segments. This asymmetric wear pattern was particularly evident in the bottom of the pipes due to continuous abrasion caused by the erosion. Figure 2 present's clearly highlight the non-uniform erosion patterns that have developed over 15 years of service.

The observed wall thickness variations were decisive in planning the subsequent testing campaign. The specimens were extracted considering both angular and longitudinal positions of the most degraded regions, ensuring a critical representation of the pipeline's real operational condition.

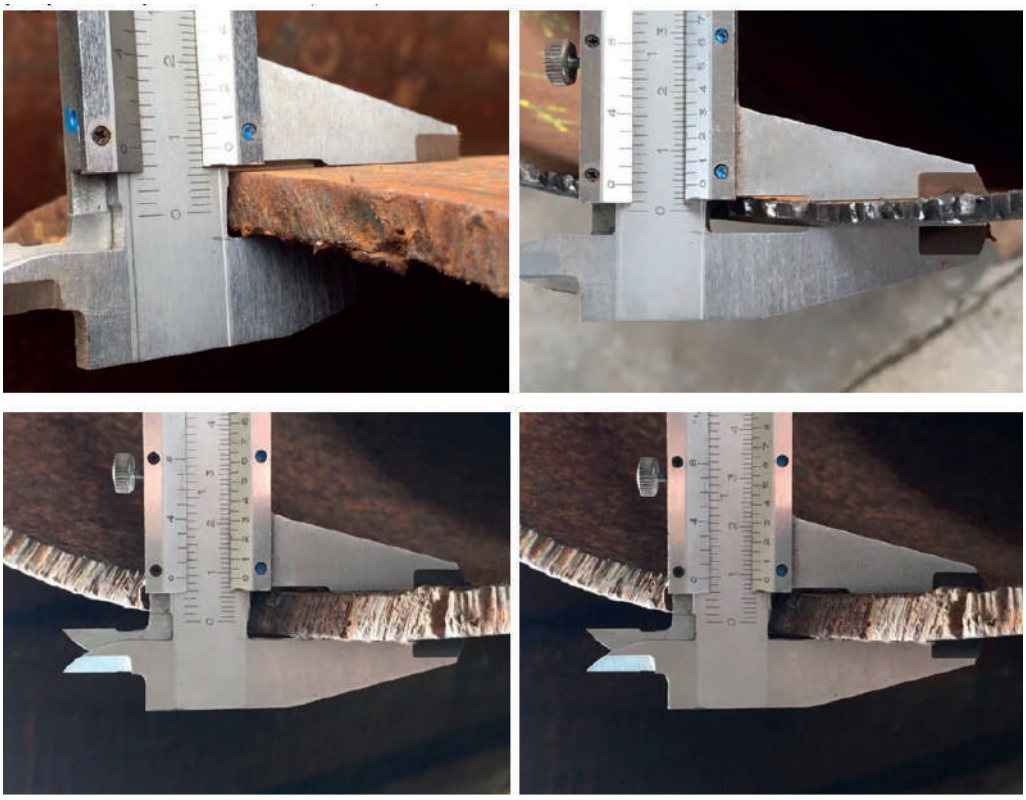

Figure 2 - Wall Thickness Profiles at Clock Positions 12h, 6h, 9h, and 3h.
Prepared by the author (2025)

3.1. Material Composition Results

All results met the chemical composition limits established by the API 5L X70 PSL2 standard. The carbon equivalent (CE) values, calculated according to the Pcm formula from the API 5L standard, were also within the specified limits, ensuring the material's weldability and mechanical strength.

Element	(%)	CP2	CP2A	CP3	CP3A	CP5	CP5A	Max. Limit API 5L X70 PSL2
Carbon	(C)	0.114	0.062	0.109	0.046	0.065	0.119	0.12
Silicon	(Si)	0.245	0.264	0.259	0.272	0.276	0.221	0.45
Manganese	(Mn)	1.37	1.44	1.39	1.46	1.47	1.38	1.7
Phosphorus	(P)	0.016	0.012	0.013	0.016	0.0099	0.015	0.025
Sulfur	(S)	0.0044	0.0042	0.0065	0.0042	0.0051	0.0047	0.015
Chromium	(Cr)	0.016	0.025	0.029	0.02	0.018	0.018	0.5
Nickel	(Ni)	0.027	0.037	0.029	0.036	0.04	0.029	0.5
Molybdenum	(Mo)	<0.0020	<0.0020	<0.0020	<0.0020	<0.0020	<0.0020	0.5
Aluminum	(Al)	0.035	0.046	0.044	0.036	0.047	0.042	-
Copper	(Cu)	0.0068	0.012	0.015	0.01	0.011	0.0082	0.5
Cobalt	(Co)	0.0041	0.014	0.0055	0.014	0.014	0.0048	-
Titanium	(Ti)	0.0087	0.015	0.012	0.013	0.014	0.012	a
Niobium	(Nb)	0.031	0.044	0.052	0.043	0.043	0.04	a
Vanadium	(V)	0.022	0.044	0.024	0.051	0.045	0.022	a
Tungsten	(W)	<0.010	<0.010	0.012	<0.010	<0.010	<0.010	-
Lead	(Pb)	<0.0030	<0.0030	<0.0030	<0.0030	<0.0030	<0.0030	-
Boron	(B)	<0.0005	<0.0005	<0.0005	<0.0005	<0.0005	<0.0005	-
Tin	(Sn)	<0.0010	0.0014	<0.0010	<0.0010	0.0016	<0.0010	-
Zinc	(Zn)	<0.0020	<0.0020	0.0022	<0.0020	<0.0020	<0.0020	-
Arsenic	(As)	0.012	0.012	0.011	0.011	0.012	0.011	-
Bismuth	(Bi)	<0.0010	<0.0010	<0.0010	<0.0010	<0.0010	<0.0010	-
Calcium	(Ca)	0.0025	0.0025	0.0024	0.0026	0.0032	0.0019	-
Cerium	(Ce)	<0.0030	<0.0030	<0.0030	<0.0030	<0.0030	<0.0030	-
Zirconium	(Zr)	<0.0015	0.0017	0.0018	0.0016	0.0017	<0.0015	-
Lanthanum	(La)	<0.0010	<0.0010	<0.0010	<0.0010	<0.0010	<0.0010	-
Iron	(Fe)	98.1	98	98	98	97.9	98.1	-
CE Pcm	(%)	0.197	0.152	0.195	0.138	0.157	0.202	0.25

[a] The sum of the concentrations between niobium, vanadium and titanium must be less than 0.15%.

Table 2 - Composition results.
Prepared by the author (2025)

3.2. Mechanical Testing Results

The specimens showed average yield strength and ultimate tensile strength values consistent with the API 5L X70 PSL2 standard, confirming that the material retained its strength properties after prolonged operation.

All Charpy impact test specimens, tested at 0°C and 23°C, exhibited absorbed energies greater than the minimum requirement of 27 Joules, as specified for API 5L X70 PSL2 pipe material with a 24-inch diameter. Furthermore, all 72 fractured specimens showed a fully ductile fracture appearance after failure, confirming the material's high toughness even after 15 years of operational exposure.

Test Temperature	Test Specimens	Absorbed Energies [J]					
		CP2	CP2A	CP3	CP3A	CP5	CP5A
0 °C	1	62	54	54	60	81	71
	2	61	51	49	56	94	72
	3	60	52	55	63	82	76
	Average	61	52	53	60	86	73
	[1]CP 10x10	122	104	106	120	172	146
23 °C	1	61	51	46	58	85	76
	2	64	58	47	63	86	72
	3	60	57	55	61	90	70
	Average	61	55	49	61	87	73
	[1]CP 10x10	122	110	98	122	174	146

[1] Line CP10x10 in Table 3 shows the energy absorbed in Joules if the test specimen had a standard cross-section of 10 x 10 mm

Table 3 - Charpy impact test results – Transverse and Longitudinal Test Specimens.
Prepared by the author (2025)

Test Specimens	Specified Ultimate Tensile Strenght [S_{UT}]	Specified Yield Strength 0.2% [S_{YT} 0.2%]	Specified Yield Strength 0.5% [S_{YT} 0.5%]	Stretching by 50 mm
CP3L1	647	600	600	18
CP3L2	644	572	578	19.6
CP3T1	615	582	579	16.2
CP3T2	614	563	562	16.8
CP3AL1	648	558	557	22.2
CP3AL2	652	560	559	21.8
CP3AT1	665	606	601	17.8
CP3AT2	671	575	574	20.4
CP5L1	614	551	552	19.6
CP5L2	620	653	566	23.4
CP5T1	631	553	557	23
CP5T2	623	554	556	18
CP5AL1	592	502	507	18
CP5AL2	653	566	566	19.4
CP5AT1	604	515	521	20
CP5AT2	606	526	526	18.2

[L] longitudinal test specimen; [T] transverse or circumferential test specimen

Table 4 - Tensile test results. Source: prepared by the author (2025).
Prepared by the author (2025)

3.3. Internal Pressure Burst Test Results

Burst tests were performed on tubular specimens CP1, CP1A, CP4, CP4A, CP6 and CP6A. Burst pressures varied depending on the tube wall thickness. All specimens, including CP4 and CP4A, with indications of external corrosion around the circumferential welds, had their failures occurring predominantly in regions of minimum wall thickness, outside the externally corroded region near the welds. Each rupture event was recorded, and the fracture locations were mapped and characterized.

Figure 3 - Fracture surfaces and rupture locations in specimens after internal pressure burst test. Prepared by the author (2025)

3.4. Finite Element Modeling Results

The models accurately predicted the locations of highest stress concentration and potential failure points, matching experimental rupture pressures with good correlation. The models were also effective in capturing the influence of external corrosion on structural integrity.

For specimens CP4 and CP4A, additional modeling was performed to simulate external corrosion pits near circumferential welds, significantly affecting the predicted burst pressure.

Test Specimens	Test Specimens					
	CP1	CP1A	CP6	CP6A	CP4	CP4A
Axial distance [mm]	600	2805	1800	2870	3602	4140
Circumferential distance [mm]*	1200	800	700	1300	690	1185
Burst pressure measured in tests [Mpa]	12.65	10.02	9.11	9.73	9.78	9.2
Thickness where failure occurs [mm]	5.96	4.62	4.30	3.92	4.26	4.61
Failure in internal erosion	Yes	Yes	Yes	Yes	Yes	Yes
Test temperature [°C]	24.8	26.1	27.8	26.9	27.8	30.8
Volume increase [L]	22.6	26.4	14.5	20.8	20.7	14.8
3	60	57	55	61	90	70
Average	61	55	49	61	87	73
'CP 10x10	122	110	98	122	174	146

* In reference to longitudinal seam welding

Table 5 - Pressure Test Rupture Location Values. Prepared by the author (2025)

Test Specimens	Test Specimens					
	CP1	CP1A	CP6	CP6A	CP4	CP4A
Axial distance [mm]	1700	2600	300	400	3700	4600
Circumferential distance [mm]*	1200	800	700	1300	700	1200
Finite element burst pressure with smallest difference to the test pressure [Mpa]	12.64	10.01	9.07	9.64	9.63	9.15
Pressure failure criterion with smallest difference to test pressure	Model 5 Tresca UB	Model 6 Tresca LB	Model 4 Tresca UB	Model 4 Tresca UB	Model 4 Tresca UB	Model 4 Tresca UB

* In reference to longitudinal seam welding

Table 5 - Pressure Test Rupture Location Values.
Prepared by the author (2025)

3.5. Analytical Development Results

Both the Modified B31G and Zhu-Leis (ZL) models showed the best correlation with the experimental burst pressures, presenting root mean square errors (RMSE) below 5%, especially when using true tensile strength values.

The Barlow equation, although widely used for design purposes, proved to be overly conservative for integrity assessments, underestimating the actual burst pressure by more than 25% in some cases. The von Mises criterion, particularly when applied with engineering stress, tended to overestimate burst pressures, while Tresca, PCORRC, and DNV-RP-F101 produced intermediate results.

For 4 out of the 6 evaluated specimens, the Zhu-Leis model with true tensile strength provided the lowest deviations from actual burst pressures. However, considering the balance between accuracy, and practical applicability, the Modified ASME B31G (2012 – Level 1) method was determined to be the most appropriate analytical alternative for preliminary assessments by Hydro's integrity engineering team.

4 Discussion

The integrated results of this study offer a detailed assessment of the residual integrity of pipe segments extracted from Hydro Paragominas Bauxite Mine 24-inch bauxite slurry pipeline after 15 years of continuous operation. The initial dimensional inspection revealed pronounced asymmetrical wall loss, particularly in the 6 o'clock position of the pipe cross-section, characteristic of long-term slurry erosion mechanisms.

Chemical composition analyses confirmed that the material remained compliant with API 5L X70 PSL2 requirements, with all six samples maintaining low levels of phosphorus, sulfur, and carbon equivalent—ensuring both weldability and structural soundness. Mechanical tests, including Charpy impact and tensile strength, revealed that the steel's ductility and toughness were preserved. All impact specimens exceeded the 27 J minimum absorbed energy requirement, with fully ductile fracture surfaces observed under both test temperatures.

Burst tests revealed that failures consistently occurred in regions of minimum remaining wall thickness, caused by internal erosion from prolonged slurry flow. In all specimens, rupture was initiated away from circumferential welds, confirming that localized internal thinning—rather than external corrosion or weld proximity—was the dominant factor in reducing structural capacity. These results emphasize the importance of incorporating asymmetric wall loss and erosive wear patterns into the integrity assessment of long-distance slurry pipelines.

Finite element modeling proved essential in validating experimental rupture behavior. The Type 4 model (Critical Longitudinal Profile with Variable Thickness) consistently provided the best alignment with experimental results across all six specimens, with root mean square errors below 3%.

Analytical predictions using industry-standard formulations complemented the experimental and numerical approaches. Among the eight analytical methods evaluated, the Modified ASME B31G (2012 – Level 1) method demonstrated the best balance of accuracy and practicality. While the Zhu-Leis model presented slightly lower error margins in select cases, the B31Gmod formulation consistently offered reliable predictions with easier field implementation, reinforcing its value as a primary assessment tool for Hydro's integrity engineering workflows.

5 Conclusion

This study presents a comprehensive and validated methodology for assessing the structural integrity of eroded slurry pipeline segments through an integrated approach involving chemical and mechanical testing, full-scale internal pressure burst tests, finite element modeling, and analytical predictions.

Key findings include:

- → The base material from Hydro's bauxite pipeline remains chemically and mechanically sound after 15 years of operation.
- → Severe metal loss was detected at the 6 o'clock position, aligning with expected slurry erosion patterns.
- → Rupture tests confirmed that corrosion near circumferential welds significantly reduces structural capacity, even in otherwise intact pipe sections.
- → Finite element models based on critical geometry and real wall thickness profiles provided accurate predictions of failure location and burst pressure.
- → Among the analytical formulations tested, Modified ASME B31G (2012 – Level 1) was the most effective in aligning with experimental results while maintaining operational feasibility.

As a result of this comprehensive investigation, Hydro adopted the proposed methodology as its new strategy for integrity management of the asset, replacing previous practices based solely on design-code equations such as Barlow. This transition has already led to measurable financial benefits, including reduced maintenance costs and more precise repair prioritization, while significantly improving the reliability of decision-making processes within the company's asset integrity program.

6 Acknowledgments

The authors would like to thank Hydro Paragominas Bauxite Mine for providing the pipe samples and supporting the development of this research. Special thanks are extended to the integrity engineering team and laboratory staff involved in the specimen preparation, testing, and modeling stages. The authors also acknowledge the technical contributions from Simpipe Engenharia e Soluções Computacionais Ltda., particularly in the execution of the finite element simulations and analytical assessments.

Referências

American Petroleum Institute (API). (2018). API 5L – Specification for Line Pipe. 46th ed. Washington, DC.

American Society for Testing and Materials (ASTM). (2020). ASTM A370-20 – Standard Test Methods and Definitions for Mechanical Testing of Steel Products.

American Society for Testing and Materials (ASTM). (2018). ASTM E23-18 – Standard Test Methods for Notched Bar Impact Testing of Metallic Materials.

American Society for Testing and Materials (ASTM). (2014). ASTM A751-14 – Standard Test Methods, Practices, and Terminology for Chemical Analysis of Steel Products.

American Society of Mechanical Engineers (ASME). (2012). ASME B31G-2012 – Manual for Determining the Remaining Strength of Corroded Pipelines.

Det Norske Veritas (DNV). (2010). DNV-RP-F101:2010 – Corroded Pipelines. Recommended Practice.

Zhu, X. K.; Leis, B. N. (2005). "Evaluation and Modification of the RSTRENG Model for Corroded Pipeline Assessment." Corrosion 2005, Paper No. 05522.

Leis, B. N.; Stephens, D. R. (1997). "An Alternative Criterion for Residual Strength of Corroded Line Pipe." Proc. of the 3rd International Pipeline Conference (IPC).

Tresca, H. (1864). "Mémoire sur l'écoulement des corps solides soumis à de fortes pressions." Comptes Rendus de l'Académie des Sciences.

von Mises, R. (1913). "Mechanik der festen Körper im plastisch deformablen Zustand." Göttinger Nachrichten, Math. Phys. Klasse.

Barlow, P. (1836). "On the Strength and Stress of Materials." Treatise on the Strength of Materials.

Entrevista

Byron Souza, a experiência no parecer

Na edição de 2025 da Rio Pipeline & Logistics 2025, a curadoria técnica reafirma seu papel estratégico na promoção do conhecimento aplicado ao setor de dutos. Neste processo, destaca-se o trabalho de avaliadores experientes e comprometidos com a excelência técnica. Byron Souza Filho é Diretor Executivo no CTDUT (Centro de Tecnologias em Dutos e Terminais), com mais de 30 anos de experiência no setor de óleo&gás, contribui como membro ativo de comitês e associações técnicas no Brasil e no exterior. Nesta entrevista à Think Energy, ele compartilha sua visão sobre o processo de avaliação técnica do congresso, os temas que emergem como prioridade para a indústria de dutos e a importância do voluntariado qualificado na construção de um evento de classe internacional.

> *O sucesso progressivo do Rio Pipeline contribuiu na melhoria de resultados para a indústria, trazendo mais capacitação de pessoal, segurança dos processos e confiabilidade operaciona."*

EXPERIÊNCIA E PAPEL NO CONGRESSO

Você já participou como avaliador técnico em diversas edições da Rio Pipeline. Conta para gente como foi sua primeira participação como avaliador e como a vivência acumulada influencia seu olhar sobre os desafios do setor de dutos?

Minha primeira participação no Rio Pipeline foi em 2001 como Autor apresentador, e para a edição seguinte, de 2003, já fui convidado pelo IBP a integrar o Comitê Técnico que tem entre algumas atribuições a avaliação dos artigos técnicos submetidos. Naquela época já contávamos com uma indústria bem integrada com academia e muitos trabalhos de altíssimo nível precisavam ser avaliados, e eu particularmente atuava no Tema de Integridade de Dutos. Nesta época estávamos, a nível Brasil, implementando e consolidando boas práticas internacionais na nossa indústria dutoviária, o que enriquecia ainda mais a qualidade dos artigos submetidos. Isso também trazia uma maior responsabilidade para o Comite Técnico, para entregar uma justa avaliação daqueles artigos.

Como atuar de forma contínua em um papel técnico estratégico dentro de um congresso com a relevância da Rio Pipeline contribuiu para o seu desenvolvimento profissional e consolidação como referência no setor?

Excelente pergunta, e começo fazendo menção aos meus Mentores da época que comecei a atuar como voluntario no processo de organização temático do congresso Rio Pipeline, e também como avaliador técnico. Essa atividade requer habilitação técnica e dedicação. E por ser um trabalho voluntario você tem que se desdobrar para não deixar suas tarefas corriqueiras, de sua ocupação principal, ficarem para trás. Aí veio o empurrãozinho dos meus Mentores mostrando exatamente como essa atividade poderia contribuir para o meu desenvolvimento pessoal, mas ▸

também o quanto o sucesso progressivo do Rio Pipeline contribuiu na melhoria de resultados para a indústria, trazendo mais capacitação de pessoal, segurança dos processos e confiabilidade operacional do segmento de dutos no Brasil. Eu deixo aqui meu testemunho de como essa atividade me projetou, nacional e internacionalmente, me colocando em um patamar de especialista reconhecido mundialmente. Um ponto a destacar na trajetória desta atuação continuada como avaliador do Rio Pipeline foi uma decisão do IBP exigir artigos técnicos escritos em inglês que contribuiu sobremaneira com a internacionalização do Congresso. E para demonstrar meu agradecimento aos meus Mentores, acabei podendo atuar como Mentor também, e tenho indicado e incentivados novos profissionais a trilharem esta mesma trajetória de sucesso pessoal

O PROCESSO DE AVALIAÇÃO

Como funciona, na prática, o processo de avaliação de trabalhos submetidos ao congresso? Há algum aspecto do processo que você destacaria como fundamental para garantir a qualidade do conteúdo técnico?

Como já venho atuando neste processo há muito tempo, consigo identificar as melhorias que o IBP implantou desde suas primeiras edições. O processo sempre contou com valores importantes como priorização de assuntos técnicos, estímulo a inovação, pioneirismo, aderência com a temática do congresso, qualidade e clareza do conteúdo avaliado. Nesse sentido o Comite Técnico tem que ser composto por uma equipe de especialistas reconhecidos pela comunidade e estabelecer um elenco de avaliadores com perfil adequado para realizar o processo de avaliação de forma competente, confidencial e isenta. Além destas qualidades, o elenco de avaliadores deve ainda ser nivelado e minimamente equilibrado para garantir o mesmo rigor no processo de avaliação, atendendo ao regramento divulgado pela organização do evento. Eu enfatizo que este nivelamento contribui em muito para o resultado final das avaliações, que vem conquistando progressivamente o reconhecimento pela comunidade industrial e acadêmica sobre a qualidade do processo de julgamento dos artigos técnicos.

Quais são, na sua visão, os critérios-chave para identificar um trabalho técnico relevante e com potencial de impacto no setor?

Dois pontos usualmente antagônicos são fundamentais para a caracterização de um artigo técnico de alta relevância, a inovação e a prontidão para seu emprego na indústria. Se o(s) autor(es) conseguirem transmitir esses dois pontos vai ser um enorme diferencial dentro do processo de julgamento. Entretanto não se deve ignorar o ineditismo que pode requerer um processo mais longo de amadurecimento para se tornar um produto comercial. Em ambos os casos fica o destaque para os autores não perderem a visão de implantação da solução associada com seu trabalho técnico, o que vai refletir em impacto naquele setor da indústria.

"O processo sempre contou com valores importantes como priorização de assuntos técnicos, estímulo a inovação, pioneirismo, aderência com a temática do congresso, qualidade e clareza do conteúdo avaliado."

QUALIDADE TÉCNICA E FORMAÇÃO

A avaliação técnica também envolve um papel formativo, e orientador, ao oferecer direcionamentos e comentários que contribuem para o amadurecimento dos trabalhos submetidos. Como você enxerga esse aspecto de mentoria presente na atividade de avaliação?

O processo de avaliação técnica de artigos requer um aprofundamento de conhecimento significativo para a tarefa. Esse grau de conhecimento e competência vai sendo conquistado na maioria das vezes com a figura do mentor ou orientador. O avaliador tem que ser um exímio redator de textos técnicos, desde conhecimentos básicos de gramática e ortografia, a domínio de idioma Inglês e produção de textos científicos, que o torne referência no setor, conseguindo também a legitimidade na execução desta tarefa. Ou seja, o avaliador contribui para o desenvolvimento profissional dos Autores avaliados, na medida que ele consegue transferir o seu conhecimento na forma de crítica construtiva via seus comentários e sugestões de melhoria.

TEMAS EMERGENTES E TENDÊNCIAS

A partir dos trabalhos que você avaliou nesta edição, quais temas ou abordagens técnicas se destacaram como tendência ou prioridade para a comunidade de dutos

Dentre os trabalhos técnicos que avaliei nesta edição, destaco que todos estão um elevado grau de qualidade técnica e bem aderentes com a expectativa de implantação, mas destaco a inserção das tecnologias associadas a Transformação Digital que estamos experimentando mundialmente, desde o final dos anos 60, época da chamada 3ª Revolução Industrial, baseada em controles computadorizados. Muito inserida na atual 4ª Revolução Industrial, baseada na digitalização, a Inteligência Artificial é a principal abordagem técnica presente na maioria dos trabalhos técnicos por mim avaliados.

Há alguma solução, metodologia ou abordagem específica que tenha chamado sua atenção pela inovação, aplicabilidade ou potencial de transformação?

Acabei tendo oportunidade de avaliar artigos de assuntos variados dentro da temática proposta pelo IBP para esta edição do congresso. Não desassociado com a realidade mundial os temas de eficiência energética e descarbonização me chamaram a atenção pela relevância e impacto de sustentabilidade das atividades que hoje são tão questionadas, mostrando como a indústria, a academia e a sociedade de dutos estão engajadas em conceitos de ASG (Ambiental, Social e Governança).

> *O IBP é reconhecido internacionalmente pelo histórico de organização de eventos no segmento de O&G, e principalmente pela sua conexão com os temas mais atuais."*

INTEGRAÇÃO COM A COMUNIDADE TÉCNICA

Você atua também em comissões técnicas da ABNT, ASME e outras instituições. Como essa integração entre diferentes fóruns técnicos impacta na sua visão sobre o conteúdo técnico da comunidade brasileira de dutos?

Sim, além de participar como avaliador no Congresso Rio Pipeline, eu sou membro da Comissão de Transporte Dutoviário do IBP e de sua equivalente nos Estados Unidos, a Pipeline System Division, da ASME. E venho, ao longo de minha carreira, atuado como voluntário em diversas entidades como a ABNT/CB-50, "Comitê Brasileiro de Materiais, Equipamentos e Estruturas Oceânicas para a indústria de Petróleo e Gás Natural", na elaboração e revisão de Normas Técnicas. E pela ABNT também contribuo, nas mesmas atividades, para o ISO/TC 67, "Oil and gas industries including lower carbon energy". Essas atividades como voluntário, me serviram e ainda me servem como grande fonte de capacitação, e me permite auxiliar na integração de competências de diversos núcleos tecnológicos no Brasil e no exterior, divulgando e compartilhando conhecimentos, para o fortalecimento da comunidade Brasileira de Dutos.

Como você vê o papel do IBP - Instituto Brasileiro de Petróleo, Gás e Biocombustíveis, e da Rio Pipeline em particular, no cenário técnico internacional do setor de dutos?

O IBP é reconhecido internacionalmente pelo histórico de organização de eventos no segmento de O&G, e principalmente pela sua conexão com os temais mais atuais dos segmentos, hábil e prontamente adaptando sua estrutura organizacional para incorporar as tendencias dos diversos setores industriais por ele coberto. Isso contribuiu sobremaneira para o sucesso de muitas de suas atividades no brasil, não só em eventos, mas também em treinamento, certificação, e posicionamento como entidade setorial. Nesta esteira, e com a colaboração de muitos voluntários, nasceu, cresceu e frutificou a Rio Pipeline. Mesmo em um cenário internacional bastante competitivo por representatividade internacional pretendida por diversos países, o Rio Pipeline se consagrou como um marco relevante para profissionais e pesquisadores a nível internacional.

ENCERRAMENTO E LEGADO

Ser reconhecido como avaliador destaque da Rio Pipeline 2025 é também um reconhecimento entre pares. O que esse destaque representa para você?

Este reconhecimento por parte do time do IBP me enche de orgulho, me traz uma ótima sensação de missão cumprida, mas ao mesmo tempo me estimula a me aprimorar e me atualizar para continuar produzindo este resultado e contribuindo para o desenvolvimento do País, que muito depende deste segmento industrial, mesmo imaginando cenários de transição energética. O mundo sempre precisou de dutos e vai continuar precisando. Então não podemos esmorecer e achar que já esgotamos oque precisávamos aprender. Já estamos acompanhando o surgir de dutos de Hidrogênio e de Gás Carbônico em torno do mundo. Aqui no Brasil vimos surgir os dutos de Etanol e estamos vendo a integração do nosso Agro Negócio com a indústria de dutos no transporte de Biometano e óleo de soja. E vem muito mais por aí...

> ***"O mundo sempre precisou de dutos e vai continuar precisando. Então não podemos esmorecer e achar que já esgotamos oque precisávamos aprender."***

Que conselho você daria a profissionais que desejam se envolver mais ativamente na produção técnica e no ecossistema de conhecimento do setor?

Vou listar alguns conselhos aos entrantes na atividade dutoviária, para incentivar o crescimento profissional em sintonia com a Comunidade Internacional de Dutos;

- *Moderadamente participe de comitês e grupos de trabalho para gerar resultados para a indústria de Dutos;*
- *Contribua com publicações técnicas, sonhe com patentes e premiações;*
- *Estude Inglês e Programação de Computador;*
- *Utilize plataformas digitais de compartilhamento de conhecimento;*
- *Seja um mentor ou instrutor para incentivar novos profissionais a crescer em suas carreiras;*
- *Não se deixe vencer por timidez, pensamentos ou comentários negativos, acredite e invista na sua trajetória e na sua capacitação.*

Não é exaustivo, mas é um começo. ■

Expediente

Régis Henrique Gonçalves e Silva
Rodrigo Márcio S. Oliveira
Ronaldo D. Vieira
Sergio Luis Gonzalez Assias
Tais Carneiro Ferreira de Castro
Taissa Bonguardo
Tatiana Das Chagas Almeida
Victor Zoratti Ferreira

PROJETO DE COMUNICAÇÃO

Gerência Responsável
Gerência de Comunicação e Marketing

Coordenadora de Imprensa e Conteúdo
Tatiana Campos

Coordenadora de Comunicação e Marketing
Vanessa Rangel

Design gráfico e diagramação
Luis Felipe Costa